Universidade de Aveiro Departamento de Física
2012

Leandro Alves Vaz

Estudo hidrodinâmico do efeito da ondulação na embocadura de Aveiro

Hydrodynamic study of the wave effect in the Aveiro inlet

Universidade de Aveiro Departamento de Física
2012

Leandro Alves Vaz

Estudo hidrodinâmico do efeito da ondulação na embocadura de Aveiro

Hydrodynamic study of the wave effect in the Aveiro inlet

Dissertação apresentada à Universidade de Aveiro para cumprimento dos requisitos necessários à obtenção do grau de Mestre em Ciências do Mar e das Zonas Costeiras, realizada sob a orientação científica do Doutor João Miguel Sequeira Silva Dias, Professor Auxiliar do Departamento de Física da Universidade de Aveiro e co-orientação da Doutora Sandra Marta Nobre Plecha, Pós-Doutorada do Departamento de Física da Universidade de Aveiro.

Este trabalho foi desenvolvido no âmbito do projeto PAC:MAN (PTDC/AAC-AMB/113469/2009) com o apoio financeiro da Fundação para a Ciência e Tecnologia - FCT

o júri

presidente

Prof.ª Doutora Filomena Maria Cardoso Pedrosa Ferreira Martins
Professora Associada do Departamento de Ambiente e Ordenamento da Universidade de Aveiro

Doutor Nuno Alexandre Firmino Vaz
Investigador auxiliar do CESAM e Departamento de Física da Universidade de Aveiro

Prof. Doutor João Miguel Sequeira Silva Dias
Professor auxiliar do Departamento de Física da Universidade de Aveiro

Doutora Sandra Marta Nobre Plecha
Pós-Doutorada do Departamento de Física da Universidade de Aveiro

acknowledgements

This work was been supported by FCT and by European Union (COMPETE, QREN, FEDER) in the framework of the research project PTDC/AAC-AMB/113469/2009 - PAC:MAN - Pollution accidents in coastal areas: a Risk management system.

In first place, a special thank to my supervisor, Prof. Doctor João Miguel Dias, for his scientific supervision. Most important, thank you for all your support, help, patience, trust and friendship in the last years.

To my supervisor, Doctor Sandra Plecha, for her scientific supervision, patience and trust.

I also wish to thank to Anabela Oliveira, André Fortunato and Alberto Azevedo from the Portuguese National Laboratory of Civil Engineering (LNEC) for adapting and making available the numerical codes used.

Thanks to all my friends and colleagues of NMEC (Estuarine and Coastal Modeling Division) for the exchange of knowledge and ideas throughout my work. A special thanks to Renato Mendes, Juliana Valentim and Ana Azevedo by support in all the moments in 'lab'.

Thanks to my all friends and my incredible family who was always present in my studies and in my life at every moment.

Thanks Raquel for your help, support and comprehension in these last months.

palavras-chave

Modelação hidrodinâmica, maré, ondas, ELCIRC, SWAN, Ria de Aveiro, embocadura

resumo

A hidrodinâmica da Ria de Aveiro tem sido extensamente analisada através de vários estudos observacionais e de modelação numérica, sendo concluído que a maré constitui o principal forçamento hidrodinâmico da laguna. Contudo, a costa adjacente à Ria de Aveiro está a sujeita a um clima de agitação marítima bastante intenso, com um regime de agitação anual médio caracterizado por ondas com altura significativa entre 2 e 2.5 m e períodos entre 9 e 11 s, tipicamente provenientes de WNW-NNW. Assim, é expectável que a hidrodinâmica da embocadura dependa simultaneamente da maré e da acção das ondas.

Apesar dos vários estudos hidrodinâmicos realizados anteriormente sobre este sistema, o impacto das ondas na hidrodinâmica da embocadura nunca foi avaliado. Assim sendo, o principal objectivo deste estudo consiste em avaliar a influência do efeito da ondulação na dinâmica da embocadura, quer por análise de dados observados, quer por modelação numérica

Na análise numérica foi utlizado o sistema de modelação MORSYS2D, que integra o modelo hidrodinâmico ELCIRC acoplado com o modelo de ondas SWAN. O modelo hidrodinâmico foi calibrado com sucesso, apresentando valores de RMS e Skill que reflectem o bom desempenho do modelo.

A metodologia utilizada para atingir os objectivos definidos consiste em forçar os modelos numéricos com os constituintes harmónicos locais de maré e com diferentes cenários de ondas típicas do litoral norte Português: um cenário normal e outro de elevada actividade de ondas (regime de temporal). Foi igualmente definido um cenário de referência que consiste na ausência do forçamento das ondas. Os cenários foram simulados para três tipos distintos de maré: maré viva, intermédia e morta.

Os resultados mostram que para o cenário normal de agitação marítima, a hidrodinâmica da embocadura é essencialmente dominada pela maré. Para o cenário de temporal, são encontradas sobre-elevações do nível do mar quando comparado com o cenário de normal actividade das ondas e com o cenário sem ondas. De facto, os resultados do modelo mostram que durante períodos de tempestade o nível do mar da laguna permanece acima do nível do mar observado ao largo.

A análise do campo de correntes mostrou que as correntes induzidas pelas ondas interagem com as correntes de maré, alterando as suas características, quer em magnitude, quer em direcção do fluxo predominante. Assim, devido à sobre-elevação, a profundidade da coluna de água aumenta causando um ligeiro aumento da velocidade da corrente na zona da embocadura.

Conclui-se que embora o forçamento principal da Ria de Aveiro seja a maré, o nível do mar e as flutuações de velocidade na embocadura da Ria de Aveiro também dependem do regime de agitação. Consequentemente, os eventos de tempestade podem alterar a sua hidrodinâmica, justificando que o acoplamento entre as ondas e marés deva ser considerado de modo a representar com precisão os processos que dependem da dinâmica de embocadura.

keywords Hydrodynamic modelling, tide, waves, ELCIRC, SWAN, Ria de Aveiro, inlet

abstract

The hydrodynamics of the Ria de Aveiro lagoon has been extensively analysed through previous observational and numerical studies, being concluded that the tide is the main forcing of the lagoon's hydrodynamic. However, the adjacent coastal zone of Ria de Aveiro is subjected to a highly energetic wave climate, with a yearly mean significant wave height of 2 - 2.5 m and wave periods of 9 - 11 s, corresponding to WNW to NNW swell. Consequently, it should be expected that the lagoon inlet hydrodynamic depends simultaneously on both tidal and wave regime forcing.

Despite the several hydrodynamic studies previously performed about this system, the impact of the coastal waves in the inlet hydrodynamic has never been evaluated. Thus, the main goal of this study is to assess the influence of the coastal wave regime at the inlet channel dynamics, either by observational data as by numerical modeling.

The numerical analysis was performed through the modeling system MORSYS2D, which comprises the hydrodynamic model ELCIRC coupled with the wave model SWAN. The hydrodynamic model was successfully calibrated and the RMS errors and Skill values determined reflect the good performance of the model.

The methodology used consists in forcing the numerical models with local tidal harmonic constituents and with different constant regular wave scenarios typical of the northern Portuguese coast: a normal and a high (storm condition) wave activity. A scenario with waves absence was also defined. These three scenarios were simulated for spring, intermediate and neap tidal conditions.

The results found under the wage regime forcing show that for the low wave activity scenario (normal regime) the inlet hydrodynamics is mainly dominated by the tidal forcing. For the highest wave regime higher sea surface elevations at the inlet when compared with simulations performed only with tidal forcing or with the normal regime are found, induced by the wave set-up. In fact, the modelling results show that the lagoon sea level remains above offshore sea level during storm wave periods.

The currents field analysis shows that the currents induced by the waves interact with the tidal currents, modifying its characteristics such as the magnitude and the direction of the predominant flow. In summary, due to wave set-up, the water depth increases, causing a slight increase of the current velocity in the inlet area.

Is concluded that despite the tide constitute the dominant forcing of the Ria de Aveiro inlet hydrodynamics, the sea level and current velocity fluctuations at the Ria de Aveiro inlet also depend on the wave regime. Consequently, the storm events induce important waves set-up that change the inlet hydrodynamics, requiring that the coupling between waves and tides should be considered in order to accurately represent the processes dependent on the inlet dynamics.

Contents

Acknowledgements i
Resumo ii
Abstract iii
LIST OF FIGURES vi
LIST OF TABLES viii
1. INTRODUCTION 1
1.1. MOTIVATION AND AIMS 1
1.2. STATE OF THE ART 2
1.3. WORK STRUCTURE 4
2. STUDY AREA 5
2.1. GENERAL DESCRIPTION 5
2.2. PHYSICAL AND HYDRODYNAMIC DESCRIPTION 6
2.3. WAVE AND WIND CHARACTERIZATION 7
2.3.1. WAVE CHARACTERIZATION 7
2.3.2. WIND CHARACTERIZATION 9
3. NUMERICAL MODELS AND METHODOLOGY 11
3.1. HYDRODYNAMIC NUMERICAL MODEL (ELCIRC) 11
3.2. WAVE MODEL (SWAN) 13
3.2.1. WAVE MODEL SETUP 13
3.3. MODEL ESTABLISHMENT AND HYDRODYNAMIC MODEL CALIBRATION 14
3.3.1. RESULTS 19
3.4. ANALYSES OF FIELD DATA OF SSE, HS AND ATMOSPHERIC PRESSURE 24
3.5. ESTABLISHMENT OF SCENARIOS 24
4. WAVE EFFECT IN RIA DE AVEIRO INLET 27
4.1. ANALYSIS OF FIELD DATA OF SSE, *HS* AND ATMOSPHERIC PRESSURE 27
4.2. MODELING RESULTS 31
4.2.1. SEA SURFACE ELEVATION 31
4.2.1.1. SPRING TIDE 31
4.2.1.2. INTERMEDIATE TIDE 35
4.2.1.3. NEAP TIDE 39
4.2.2. CURRENT VELOCITY 44
4.2.2.1. SPRING TIDE 44
4.2.2.2. INTERMEDIATE TIDE 48
4.2.2.3. NEAP TIDE 52
5. CONCLUSIONS AND FUTURE IMPROVEMENTS 57
6. REFERENCES 59

List of Figures

1.The Ria de Aveiro lagoon. **5**

2. Wave directions and heights (meters) at Figueira da Foz buoy. **8**

3. Frequency of occurrence (%) of each class of significant wave height. **8**

4. Frequency of occurrence (%) of each class of wave period. **8**

5. Wind direction and velocity at Casal do Rato station. **9**

6. Wind direction and velocity at Casal do Rato station for each season. **10**

7. Map with the identification of field works. **14**

8. Numerical bathymetries for 2002 (left panel) and 2011 (right panel) of Ria de Aveiro. The A and B correspond to a zoom in the inlet area for bathymetries of 2002 and 2011, respectively. The station used to study the hydrodynamic changes induced by the waves is represented with the number 1. **15**

9. Scheme illustrating the grids integration, with the representation of the final grid. **16**

10. Stations used in hydrodynamic model calibration. **18**

11. Comparison between observations and model results of SSE time series from station A until F, used in the hydrodynamic calibration procedure. **20**

12. Comparison between observations and model results of SSE time series from station I until R, used in the hydrodynamic calibration procedure. **21**

13. Comparison between model predicted and observed amplitude and phase for the major semi-diurnal and diurnal constituents (M_2 – 12.42 h; S_2 – 12 h; O_1 – 25.82 h; K_1 – 23.93 h) and for the shallow water overtide of the principal lunar constituent, M_4 (6.21 h). The black and white bars represent the observed and predicted values, respectively. **23**

14. Figure representing the scenarios established in the hydrodynamic model simulations. **26**

15. Atmospheric pressure data between 1/12/1985 and 31/12/1985 (upper panel) and between 1/1/1996 and 15/1/1996 (lower panel). **27**

16. Low and high frequency signal of SSE, and Hs (upper panel), between 1/12/1985 and 31/12/1985. The comparison between low frequency signal and the effect of atmospheric pressure is represented in the middle panel. In low panel is represented the difference between the lines represented in the middle panel (wave induced residual). **29**

17. Low and high frequency signal of SSE, and Hs (upper panel), between 1/1/1996 and 15/1/1996. The comparison between low frequency signal and the effect of atmospheric pressure id represented in the middle panel. In low panel is represented the difference between the lines represented in the middle panel (wave induced residual). **30**

18. Comparison between normal and storm regimes as well as the reference scenario, for spring tide condition (upper panel). The vertical lines correspond to instants chosen to illustrate horizontal sea surface elevation fields. In the lower panel is represented the differences between all the scenarios. **31**

19. Horizontal fields of differences of sea surface elevation between scenarios 0 and 1 for spring tide condition, in meters. The letters correspond to the instants chosen to compute the horizontal fields, represented in Figure 18. **33**

20. Horizontal fields of differences of sea surface elevation between scenarios 1 and 2 for spring tide condition, in meters. The letters correspond to the instants chosen to compute the horizontal fields, represented in Figure 18. **34**

21. Comparison between normal and storm regimes as well as the reference scenario, for intermediate tide condition (upper panel). The vertical lines correspond to instants chosen to illustrate horizontal sea surface elevation fields. In the lower panel is represented the differences between all the scenarios. **35**

22. Horizontal fields of differences of sea surface elevation between scenarios 0 and 1 for intermediate tide condition, in meters. The letters correspond to the instants chosen to compute the horizontal fields, represented in Figure 21. **37**

23. Horizontal fields of differences of sea surface elevation between scenarios 1 and 2 for intermediate tide condition, in meters. The letters correspond to the instants chosen to compute the horizontal fields, represented in Figure 21. **38**

24. Comparison between normal and storm regimes as well as the reference scenario, for neap tide condition (upper panel). The vertical lines correspond to instants chosen to illustrate horizontal sea surface elevation fields. In the lower panel is represented the differences between all the scenarios **39**

25. Horizontal fields of differences of sea surface elevation between scenarios 0 and 1 for neap tide condition, in meters. The letters correspond to the instants chosen to compute the horizontal fields, represented in Figure 24. **41**

26. Horizontal fields of differences of sea surface elevation between scenarios 1 and 2 for neap tide condition, in meters. The letters correspond to the instants chosen to compute the horizontal fields, represented in Figure 24. **42**

27. Representation of the velocity intensity in spring tide condition for the three scenarios, in m/s. The letters correspond to the instants chosen (presented in Figure 18) to represent the horizontal fields. **45**

28. Horizontal fields of differences of the current velocity between scenarios 1 and 2 in spring tide condition, in m/s. The letters correspond to the instants chosen to represent the horizontal fields. **47**

29. Representation of the velocity intensity in intermediate tide condition for the three scenarios, in m/s. The letters correspond to the instants chosen (presented in Figure 21) to represent the horizontal fields. **49**

30. Horizontal fields of differences of the current velocity between scenarios 1 and 2 in intermediate tide condition, in m/s. The letters correspond to the instants chosen (presented in Figure 21) to represent the horizontal fields. **51**

31. Representation of the velocity intensity in neap tide condition for the three scenarios, in m/s. The letters correspond to the instants chosen (presented in Figure 24) to represent the horizontal fields. **53**

32. Horizontal fields of differences of the current velocity between scenarios 1 and 2 in neap tide condition, in m/s. The letters correspond to the instants chosen to represent the horizontal fields. **55**

List of Tables

1. Bottom friction coefficients. **17**

2. RMS and Skill for all the calibration stations. **19**

1. Introduction

1.1. Motivation and Aims

Estuaries and the adjacent coastal areas are very complex and extremely dynamic regions exposed to vast natural and anthropic pressure. The Ria de Aveiro lagoon is an evident example of this, since it is inserted in highly populated region, harbouring important commercial and fishing ports.

The coastal shoreline includes a considerable extension of lagoons and estuaries, often characterized by dynamic tidal inlets. These environments are normally sheltered and the wave action is minimal when compared with exposed coasts [Short, 2007; Vila-Concejo *et al*., 2010].

Coastal systems of this type are quite dynamic and strongly influenced by tidal action. The physics and hydrodynamics in these systems play a major role in the development of several processes, including ecological, biological and sediment transport. The importance of coastal systems has been recognized over the years, not only by the scientific community but also by the people who live around these areas. The freshwater discharge, the entry of sea water and transport of suspended sediment and of organic and inorganic nutrients are processes that have a great importance for urban and social-economic development of surrounding estuarine regions [Miranda *et al*., 2002].

The scientific knowledge about these systems can be used to develop solutions to several problems such as the hydrographic basin's changes, the identification of sedimentation areas that can affect navigation, the computation of the residence time of substances within these areas, the study of water properties patterns to support aquaculture projects, among others [Vaz, 2007]. In terms of estuarine hydrodynamics, tidal currents structure analysis is essential to understand problems such as dispersion, rate of pollutants, sediment transport and erosion processes [Prandle, 1982]. Moreover, tidal asymmetries and residual circulation have an influence on nutrient balances, sediment loads, particles and pollutants transportations [Aldridge, 1997]. Therefore, understanding the central processes induced by the tidal wave is crucial to obtain an overview concerning the different uses of the coastal systems.

Talking further about the tidal inlets, where this work is focused, is clear that its economic and environmental importance has been growing worldwide. The management of these systems is no longer restricted to the maintenance of navigation channels, but also addresses new challenges, such as the adjacent shoreline stability or the water renewal in the inner part of the system, for instance in the back barrier lagoons which are used for aquaculture. Portuguese lagoons illustrate very well this phenomenon, since many social and economic activities are concentrated in these coastal areas and include [Bertin *et al*., 2009]:

- habitation and construction development on the barrier islands, despite the shoreline threat hazard;
- aquaculture and fishing;
- commercial maritime traffic;
- recreational activities.

According to Fitzgerald [1996], among the different types of tidal inlets, wave-dominated inlets rather occur in micro to mesotidal environments subjected to moderate to severe wave regimes. Because of the combination of wave, tides and shallow waters, wave dominated inlets are frequently extremely dynamic, with fast and considerable morphological changes. This strongly dynamic behaviour is particularly true for several Portuguese tidal inlets, where the combination of a severe wave climate, a mesotidal range and shallow channels may result in channel migration which can reach 200 meters within a few months [Oliveira *et al*., 2006a].

In this type of inlets, changes in the sea level may be related to the tide, but also with the action of wind and waves, and with meteorological events. Therefore, direct and indirect atmospheric and marine (tide and waves) forces cause large differences and rapid changes in the physical characteristics of coastal lagoons [Troussellier and Gattuso, 2007].

The presence of waves can cause large differences in terms of sea-level variations [Nielsen and Apelt, 2003]; their relative importance depends upon the morphology of the lagoon entrance, as well as the local wave regime. In shallow and narrow entrances, the sea-level elevation caused by wave motion, such as wave breaking, is an important mechanism. This rise in sea level, or set-up, induced by waves is commonly termed as ‘‘wave set-up’’ [Angwenyi and Rydberg, 2005].

Thus, the main goal of this work is to study the influence of the wave regime on the hydrodynamics of Ria de Aveiro inlet through the analysis of field data and numerical model results. Combined with this primary aim, there are other specific goals such as: improve a previous implementation to Ria de Aveiro of the hydrodynamic numerical model ELCIRC, updating the lagoon bathymetry using the most recent bathymetry data sets and consequently recalibrating the model; use MORSYS2D to couple the wave model SWAN to ELCIRC, to make the study of the combined effects of tidal and wave regime.

Consequently, this work was driven not only by the need to improve and develop the numerical tools available to study Ria de Aveiro dynamics, but also to research the influence of the coastal waves in the lagoon hydrodynamic that has never been the subject of study in this coastal system.

1.2. State of the Art

The importance of coastal environments is recognized worldwide by the scientific community, being published several studies on coastal lagoons focusing its hydrology, biology, physical and chemical processes, among others.

The Ria de Aveiro lagoon was largely studied from a biological and chemical perspective and several publications regarding to bacterioplancton, zooplankton, benthic biodiversity, pollution impacts, fisheries, among several others issues were performed [e.g. Morgado *et al*., 2003; Lopes *et al*., 2010; Pereira *et al*., 2011; Ahmad *et al*., in press; Anjum *et al*., 2012; Pires *et al*., in press]. Also the physical processes in the lagoon have been studied in the last decades. One of the first steps in this task is the study made by Dias *et al*. [1999]. The authors concluded that the tide in the Ria de Aveiro is semi-diurnal and is the main forcing agent, and M_2 and S_2 are the most important constituents in the lagoon, representing approximately 90% of the tidal energy in Ria de Aveiro. They also showed that the lagoon should be considered vertically homogenous, with exception to periods of important rainfalls. These hydrological characteristics may also be found in Vaz and Dias [2008] which verified that, during the winter (wet season), the stratification caused by Vouga river flow can be extended up to the inlet.

The tide in the entire lagoon was simulated by Dias *et al*. [2000] using a two-dimensional depth integrated mathematical model with the aim to predict the water level and depth mean current. These authors showed that tides propagate from the inlet and are present in the entire lagoon, decreasing its amplitude with the distance to the mouth while the phase lag increases.

Another relevant study in order to understand the changes of tidal characteristics was performed by Araújo [2005]. The author compared two different surveys (1987/8 and 2002/3) in order to analyse sea level changes and the amplitude and phase of the main harmonic constituents. The data showed that the amplitude of the main harmonic constituents in the lagoon increased and its phase decreased. The tidal asymmetry also showed modifications over the past years. During 1987/8, the majority of the lagoon was

flood-dominant and, since then, the central section of the Ria de Aveiro has become ebb-dominant whereas the northern and southern sections are flood-dominant.

Several studies based on numerical modelling were performed to investigate subjects such as the tidal propagation in the lagoon [Dias and Fernandes, 2006; Dias and Picado, 2011], the Lagrangian transport of particles [Picado *et al*., 2011] and the sediment transport [Lopes *et al*., 2006; Lopes *et al*., 2011b; Plecha *et al*., 2011; Plecha *et al*., 2012;].

An important numerical study were performed by Mendes *et al*. [2011], that included, for the first time in the numerical models, the low lying areas adjacent to Ria de Aveiro. The goal of this work is to evaluate if the inclusion of the low lying coastal adjacent flooded areas in the models' numerical bathymetry induce changes in model predicted hydrodynamics for the Ria de Aveiro. They found minor differences for the Ria de Aveiro numerically predicted general circulation when including the low lying coastal adjacent flooded areas.

Recently, Dias and Mariano [2011] evaluated the hydrodynamic response of Ria de Aveiro to an alteration on the present geometry of its inlet. It was studied the impact of the extension by 200 meters of the north jetty of the lagoon inlet. This study shows a slightly change of the local hydrodynamic patterns, and that may induce modifications in the overall lagoon circulation related with the tidal prism decrease found for the main channels.

The Ria de Aveiro lagoon is also source of concern when discussing climate changes impacts. Silva and Duck [2001] analysed the historical modifications of bottom topography and tidal amplitude in the lagoon since the construction of the articial inlet and presented tendencies for future evolutions. These authors concluded that any future increase of the mean sea level will contribute to an increase of both area and volume of water mass, increasing the speed of tidal propagation. Lopes *et al.* [2011a] estimated the impact of sea level rise in lagoon hydrodynamics performing projections of SLR for the end of this century and found an increase of 20% of the lagoon tidal prism for a sea level rise of 0.42 m.

The tidal prism, as well as the tidal asymmetry were also analysed by Picado *et al*. [2010] when explored possible tidal changes induced by local geomorphologic changes, specially the flood caused by salt pans walls collapse. These authors concluded that the increase of the lagoon total area (5.6% for extreme destruction) also results in an increase of 5% of the tidal prism as well as in the tidal asymmetry, with the higher variations found close to the flooded area and in neap tide.

As previously mentioned, the influence of waves on the Ria de Aveiro hydrodynamics was never studied. However its influence in morphodynamics has already been studied. As example, Plecha *et al*. [2011], performed the evaluation of single waves effects on the morphologic evolution of a Ria de Aveiro lagoon inlet, concluding that the wave induced residual sediment fluxes in the cross sections upstream the lagoon mouth are smaller in magnitude than at the inlet, restricting the influence of the waves to the lagoon mouth and adjacent coastline.

In fact, the influence of waves has been weakly studied, however, there are some works studying this subject in other Portuguese estuaries or rivers entrances. For instance, Malhadas *et al.* [2009] analysed the effect of the coastal waves on sea level in Óbidos lagoon and they found a correlation between wave height and sea-level elevation only during high wave activity periods, and the occurrence of a significant super-elevation on lagoon sea level during storm wave periods. This super-elevation is explained, not only by wave set-up or radiation stresses due to waves, but also by tidal inlet morphology.

Additionally, this subject has relevance in some systems outside Portugal. Factors governing the relative magnitude of wave set-up at tidal inlets and river entrances have been addressed by Guza and Thorton [1981], Hanslow and Nielsen [1992], Hanslow *et al*. [1996], Dunn *et al*. [2000], Tanaka *et al*. [2000, 2003], Dunn [2001], Oshiyama *et al*. [2001] and Nguyen *et al*. [2007]. These authors found a wave

set-up at tidal inlets or river entrances with its magnitude dependent on the coastal system characteristics, being the morphology of the inlet a determinant factor to be taken into account on the wave set-up generation.

The most recent and consequently most importantly studies mentioned above, was the work performed by Nguyen *et al*. [2007], based upon data collected in seven different morphological river entrances and one inlet, showed that the set-up, or sea-level elevation, depends not only upon offshore wave height but also on the different morphological river entrances or tidal inlets. These authors found a correlation between wave set-up height and water depth of the entrance, concluding that the wave set-up height is inversely proportional to the average water depth, at a river entrance or inlet.

Different numerical models have been used to study the Ria de Aveiro hydrodynamics. The first numerical used to study the physical characteristics of Ria de Aveiro lagoon was SYMSYS2D model [Leendertse and Gritton, 1971]. Dias *et al*. [2000] used this numerical model to study the tidal propagation in Ria de Aveiro. Thenceforward, this model was used by several authors to study the Ria de Aveiro lagoon [Dias *et al*. 2003; Dias and Mariano, 2011]. More recently the lagoon has been characterized with other numerical models. As example, Vaz *et al*. [2005] and Vaz *et al*. [2007] used a 3D baroclinic model, Mohid [www.mohid.com], to study the importance of the river flow in the establishment of thermohaline horizontal patterns. Other numerical model usually used to study the lagoon hydrodynamics is ELCIRC model. Oliveira *et al*. [2006b] resorted to this model to analyse the tidal propagation in Ria de Aveiro lagoon and the variability of tidal asymmetry in the upper and lower lagoon. Posteriorly, several authors applied this numerical model in Ria de Aveiro [Picado 2008; Lopes 2009; Picado *et al*. 2010].

In this study, it was used the 2DH morphodynamic modeling system MORSYS2D. This modelling system integrates the hydrodynamic model ELCIRC [Zang *et al*., 2004], the wave model SWAN [Booij *et al.*, 1999], and the model SAND2D [Fortunato and Oliveira, 2004]. In this study, the module SAND2D was not activated. This modeling system has been already successfully applied in some previous studies in Ria de Aveiro. As example, Lopes *et al*. [2011a] used this numerical tool to study the local sea level change scenarios for the end of the 21st century and potential physical impacts in the lower Ria de Aveiro. [Plecha *et al.* 2011, 2012] also used this modeling system to study the Ria de Aveiro morphodynamics.

1.3. Work Structure

For an overall understanding of the items studied and mentioned in this work, some of the main characteristics of estuaries and lagoons were previously presented, as well as some important studies concerning the Ria de Aveiro and the effect of the coastal waves propagation inside the tidal inlets and river entrances.

The second chapter includes the description of the main characteristics of the study area (Ria de Aveiro) in order to understand their principal morphologic and hydrodynamic features. A characterization of the wave and wind climate is also present in this chapter. The chapter three contains the description of the numerical models used in this work, ELCIRC and SWAN. The methodology adopted in this study and the results of the hydrodynamic model calibration are also present.

In the chapter four are presented the results of this work, that includes the analyses of field data and the analysis of the results of the numerical model simulations. Finally, in chapter five are presented the most important ideas discussed in this work, as well as the main conclusions.

2. Study Area

2.1. General Description

The Ria de Aveiro (Figure 1) is the most extensive in Portugal [Teixeira, 1994] shallow coastal lagoon located on the northwest coast of Portugal, being separated from the Atlantic Ocean by a sand dune barrier. It has an irregular geometry, and its only connection with Atlantic Ocean is through an artificial channel, constructed in 1808 [Dias, 2001, Dias and Mariano, 2011]. The lagoon has a maximum width of 8.5 km and a length of 45 km, being constituted by four main channels: Mira, São Jacinto, Ílhavo and Espinheiro channels. The Mira channel is an elongated shallow arm, with 14 km length. S. Jacinto channel is about 29 km long, and Ílhavo and Espinheiro are 15 and 17 km, respectively [Dias, 2001].

The system is also characterized by a large number of channels between which lie significant intertidal areas, essentially mudflats, salt marshes and old salt pans [Picado *et al*., 2010].

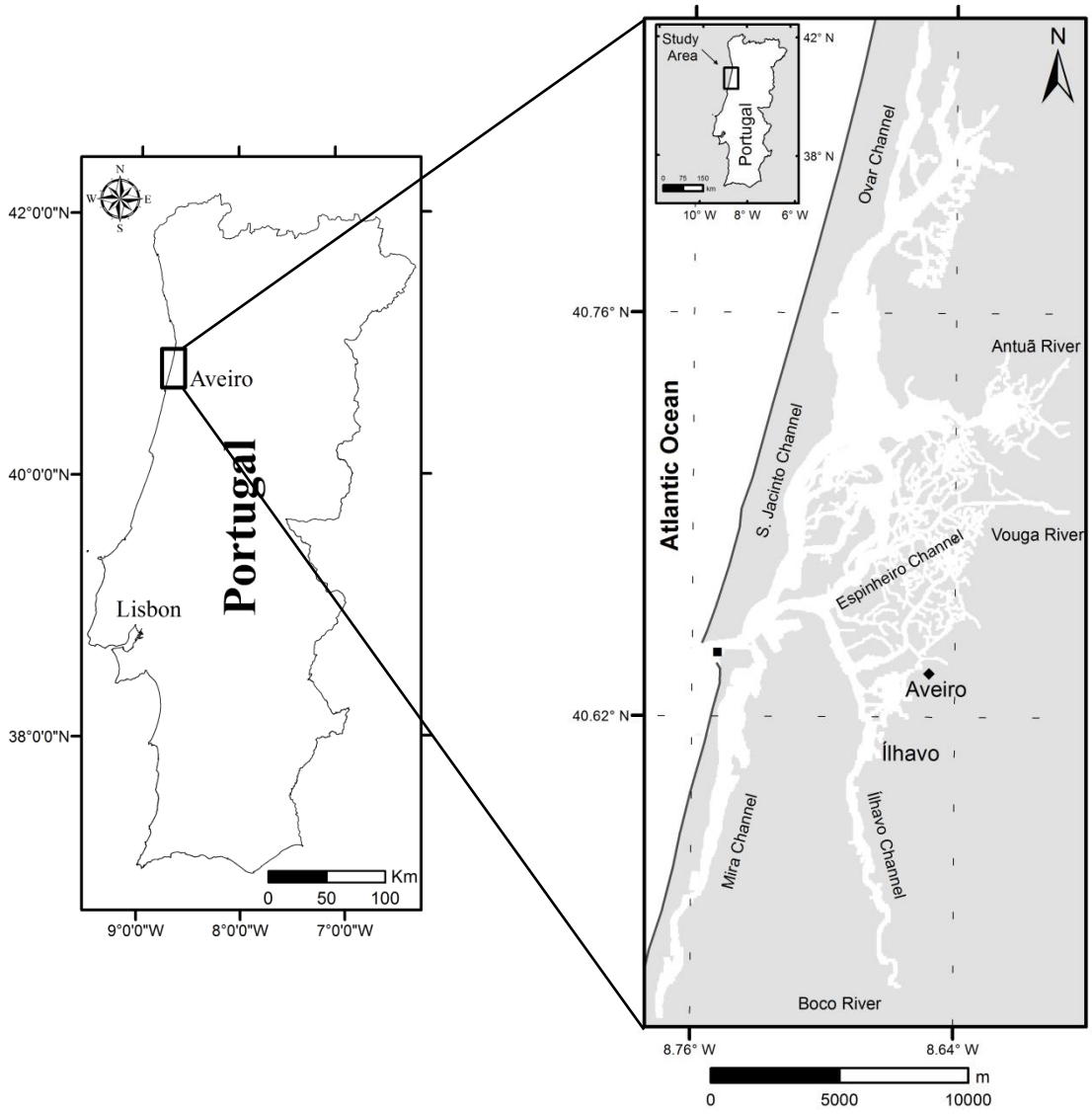

Figure 1. The Ria de Aveiro lagoon

The Ria de Aveiro is a very important ecosystem to the local economy and to the environment. It acts as keystone to the local agriculture, holds a large number of small traditional fishing ports, houses the Aveiro's Harbour, has aquaculture activities, it is an important place for the tourism with a growing subsector in the water sports area and it's also related to the traditional salt production activities [Alves *et al*., 2011].

From the nature conservation and biodiversity point of view, it is a great value area, both locally and nationally. It has a rich fauna and flora housing a large number of species. Due to rich variety of species the Aveiro lagoon was classified as a Special Protected Area, a classification that comes from the application of the Birds Directive. It contains also an important protected area, the Natural Reserve of *'Dunas de São Jacinto'*. A well preserved dune barrier located in the seaside area of the lagoon with several ponds that present themselves as an essential habitat for numerous local and migratory birds. [Alves *et al*., 2011].

2.2. Physical and Hydrodynamic Description

As mentioned before, the Ria de Aveiro is the most extensive lagoon in Portugal and it has a very complex and irregular geometry, composed by long and narrow channels, with a large longitudinal development, characterized by extensive intertidal areas, essentially mudflats, salt marsh and old saltpans. Consequently, the physical processes that occur in the system are also quite complex.

The area of the lagoon has a large variability according with the tidal influence in its hydrodynamics. In spring tides the lagoon area reaches a maximum area of 83 km^2 at high tide, which decreases to a minimum of 66 km^2 at low tide. The average depth in Ria de Aveiro is about 1 meter, relative to local datum, although the inlet channel can exceed 30 meters deep, due to dredging operations that are frequently carried out to allow the navigation [Dias and Lopes, 2006a].

The main forcing agent driving water circulation in Ria de Aveiro is the tide, which is mesotidal, presenting an average tidal amplitude at the inlet of 2 meters, and amplitudes of 0.6 meters in neap tides and 3.2 meters in spring tides [Dias 2001; Araújo *et al*., 2008]. Several authors evaluated the tidal prism for the Ria de Aveiro lagoon through different numerical models (considering different bathymetries), and several values were obtained. For maximum spring tide Dias [2001] and Lopes *et al*. [2006] estimate 136.7×10^6 m^3, Picado *et al*. [2010] 86.3×10^6 m^3 and Lopes *et al*. [2010] 87.5×10^6 m^3 and for minimum neap tide Dias [2001] and Lopes *et al*. [2006] estimated 34.9×10^6 m^3, Picado *et al.* [2010] 31.0×10^6 m^3 and Lopes *et al*. [2010] 28.9×10^6 m^3. These values of tidal prism were computed in a flooding cycle, thus the flux related to these ranges are 3.87 to 6.12×10^3 m^3s^{-1} for spring tide and 1.30 to 1.56×10^3 m^3s^{-1} for neap tide. These values are much higher when compared with the total freshwater input in a tidal cycle. Moreira *et al*. [1993] projected an input of nearly 1.8×10^6 m^3. The tidal prism of each channel relative to it its value at the mouth is: 35.4% for S. Jacinto channel, 25.6% for Espinheiro channel, 10.0% for Mira channel and 13.5% for Ílhavo channel [Dias and Picado, 2011]. Likewise, the semidiurnal tides are the main factor influencing the hydrodynamics of the lagoon [Dias *et al*., 2000]. Thus, the most important harmonic constituents in Ria de Aveiro are M_2 and S_2, corresponding of about 88% and 10% of total tidal energy, respectively [Dias, 2001].

The lagoon has five main rivers, one for each channel: Vouga, Antuã, Caster, Boco and Ribeira dos Moinhos, being the most important the Vouga river. According with *Ria de Aveiro Polis Litoral program*, which considered the data present in the *Plano de Bacia Hidrográfica* (www.arhcentro.pt), the mean freshwater inflow for Vouga River is 60.0 m^3s^{-1}, 4.5 m^3s^{-1} for Antuã, 1.6 m^3s^{-1} for Caster, and 1.0 and 3.6 m^3s^{-1} for Boco and Ribeira dos Moinhos, respectively.

Additionally to the tidal forcing, and in extreme situations, also the wind and freshwater discharge (mainly the Vouga river) influence the Ria de Aveiro hydrodynamics. During strong freshwater flows, the lagoon is characterized as weakly stratified [Vaz and Dias, 2008]. Wind is very significant in Aveiro considering periods from a few hours to a few days, when can become an important influence on lagoon circulation. Extreme conditions of strong wind may induce particular circulation patterns mainly in shallow areas and wide channels [Dias, 2001].

2.3. Wave and Wind Characterization

The wave and wind characterization was based in two technical reports of *Plano de Ordenamento da Orla Costeira* [Dias *et al.,* 2011a; Dias *et al*., 2011b]. In summary, the analysis presented in this subsection is used to establish regimes of typical wind and wave climate, as well as the exceptional regimes (storms). Thus, this knowledge will allow the establishment of scenarios to perform the numerical simulations in the frame of the research topics to be developed in this study.

2.3.1. Wave Characterization

The characterization of the wave regime was performed by analysing records of the Figueira da Foz wave directional buoy (40°11.13' N; 9°8.73' W, depth 92m ZH). The data was collected by the Portuguese Hydrographic Institute (IH) and is available on the website. The station is located 50 km South of Aveiro, however it is possible to say that there are no important variations in the wave regime in this spatial difference [Coli, 2003]. Therefore, in this work, it will considered that the wave regime in Figueira da Foz is representative of the region of Aveiro. The buoy data are comprised between 1984 and 1996.

In more detail, through the buoy data analysis of the rose of directions shows that the waves have a predominance from the Northwest quadrant (Figure 2). The higher frequency of occurrence, corresponding to the sector NW, is equivalent to 41% of the percentage of records, and then the sectors WNW and NNW have a frequency of occurrence of 29% and 18%, respectively. The combination of frequency of occurrence of direction and *Hs*, also presented in Figure 2, illustrates that the highest waves occur at west-northwest direction, albeit with small percentage of occurrence.

The distribution in classes of the significant wave height (Figure 3) shows that the class of significant height between 0.5 - 1.0 meters is dominant in the Portuguese coast with 40% frequency of occurrence, followed by class 1.5 - 2.5 meters with 35%. In continuity with the downward trend are the following classes, 2.5 - 3.5 and 3.5 - 4.5 meters, with frequencies of occurrence of 16% and 6%, respectively. With frequencies lower than 1% are found classes of significant height smaller than 0.5 m and higher than 5.5 meters. The waves with *Hs* higher than 5.5 meters represent the storm events.

The analysis of the distribution of the wave period (Figure 4) reveals that the most frequent periods of the waves in the Portuguese coast lie between 5 and 9 seconds, occurring with 77% of frequency. Within this range, the dominant class, with 23% of the frequency of occurrence, is 6 - 7 seconds, followed by the class between 7 - 8 seconds with 20% of occurrences.

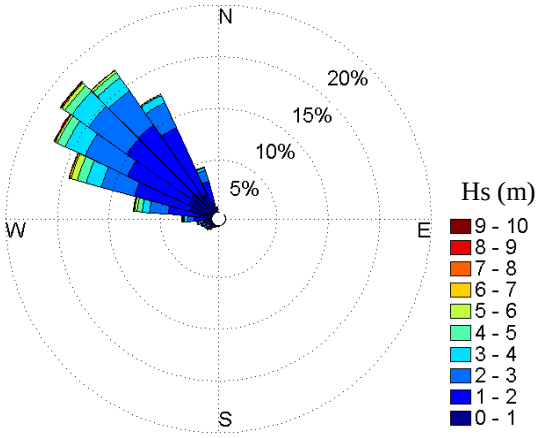

Figure 2. Wave directions and heights (meters) at Figueira da Foz buoy.

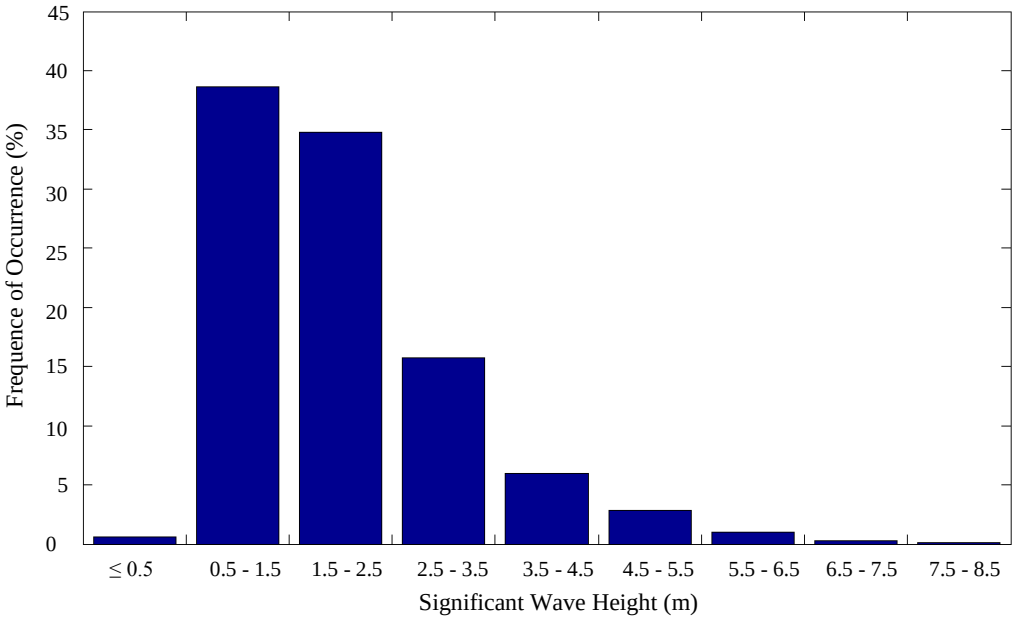

Figure 3. Frequency of occurrence (%) of each class of significant wave height.

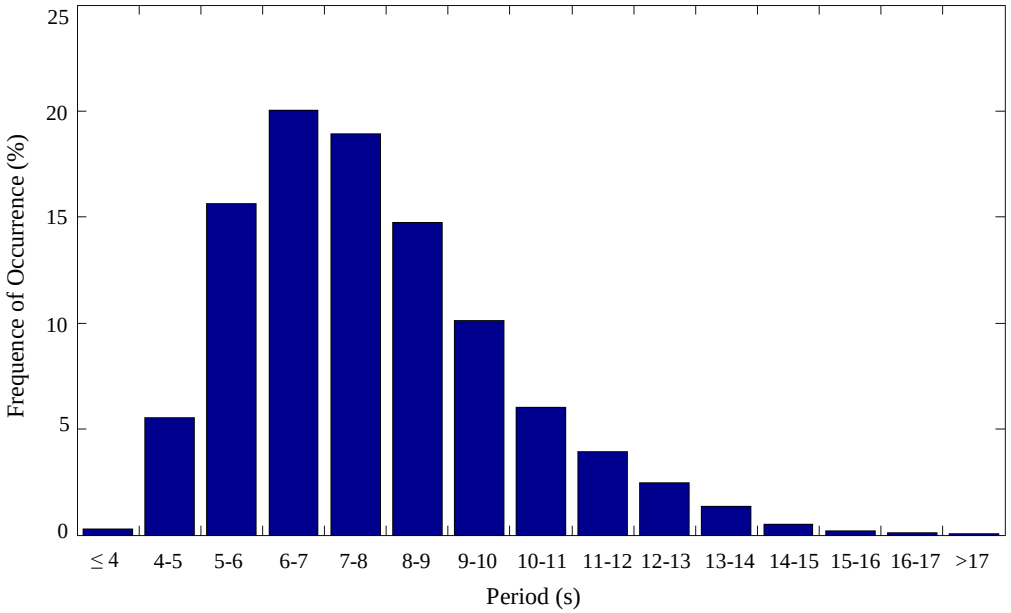

Figure 4. Frequency of occurrence (%) of each class of wave period.

Several storm events that were characterized by *Hs* higher than 5 meters and wave period higher than 10 seconds affects the study area during winter and transition periods. According to Pires [1985], there are two types of storm events. The first corresponds to exceptionally strong NW or SW swells that affected the area for one to two days. Several of these storm events are experienced each year, and are the most common types of storm that occur during the winter and transition periods of the western Iberian coast. The most severe of these storms can generate wave conditions with significant wave heights of up to 7.5 meters and wave peak periods of about 16.5 seconds. The second type of storm event is characterized by a succession of highly energetic storms that affect the western Iberian area for one to two weeks. These occur when the Azores anticyclone is situated at its most extreme southerly position (~30°N), allowing the transit of eastward-moving synoptic perturbations to the northern Iberian latitudes. These conditions, known as 'westerly storms', typically occur once per year and generate the most extreme wave conditions observed on the northern Portuguese shelf, mainly associated with a southerly wind regime [Pires, 1985].

In contrast to winter conditions, in the summer the wave regime is characterized by low energy conditions. From June to September, significant wave heights mean periods and peak periods are consistently smaller than 3 meters, 8 and 12 seconds, respectively. The monthly averages and standard deviations of the wave parameters are at their lowest values between June and August. In August, significant wave heights are smaller than 3 meters [Vitorino *et al.*, 2002].

2.3.2. Wind Characterization

The characterization of the wind field was performed through the analysis and representation of monitored data from the meteorological station 'Casal do Rato' (http://snirh.pt). The station is located in Figueira da Foz (40°09'12.52" N, 8°50'36.07" W), 50 km South of Aveiro. However in this study, the wind of the station 'Casal do Rato' is considered representative of the wind in the region of Aveiro. Wind intensity and the percentage of occurrence of each direction for all the records and seasonally (Spring, Summer, Autumn and Winter) are represented. The date of station data are between the years 2001 and 2009.

The most representative values of wind speed are between 0 and 8 ms^{-1}, while maximum values are around 18 ms^{-1}. Relatively to the prevailing wind direction, it should be noted that in the wind rose is shown the place where the wind blows. Thus, a typical North wind is represented in the wind roses in the lower quadrants. Therefore, the analysis of Figure 5 shows that the prevailing winds are from Northwest (NW) and Southeast (SE). In more detail, about 37% of the wind records are from NW quadrant, 27% comes from SE quadrant, 22% from NE quadrant, and finally, 15% from SW.

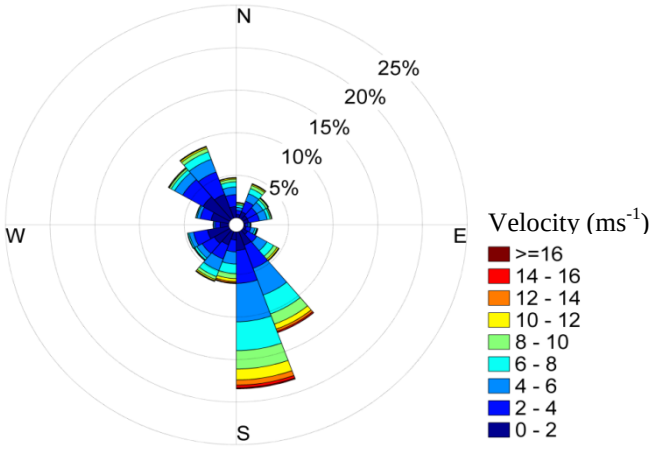

Figure 5. Wind direction and velocity at Casal do Rato

In Figure 6 is illustrated the seasonal variability of intensity and wind direction for Casal do Rato meteorological station. Note that the months of March, April and May are considered as Spring, June, July and August as Summer, September, October and November as Autumn, and finally, December, January and February as Winter.

In Spring about 60% of the wind records are northerly, with considerable speed, especially the winds coming from NW. These are most frequent (approximately 40%) and also the strongest, being usually referred as '*Nortada*'. This phenomenon is even more evident in the Summer months, with about 70% of wind records coming from the North, with maximum speeds of 18 ms^{-1}. During these months, the wind that comes from South is typically weaker, with maximum values of 8 ms^{-1}.

The patterns observed for Autumn and Winter are quite similar, showing higher frequency of wind records from the NW and SE quadrant. For the Autumn months, 35% of the winds are from the SE and 30% from NW. Already in the Winter months, 35% of the wind comes from the SE quadrant and 25% comes from NW. North winds are of higher intensity (almost always greater than 4 ms^{-1}), whereas the South winds have frequently intensity of 2 to 4 ms^{-1}.

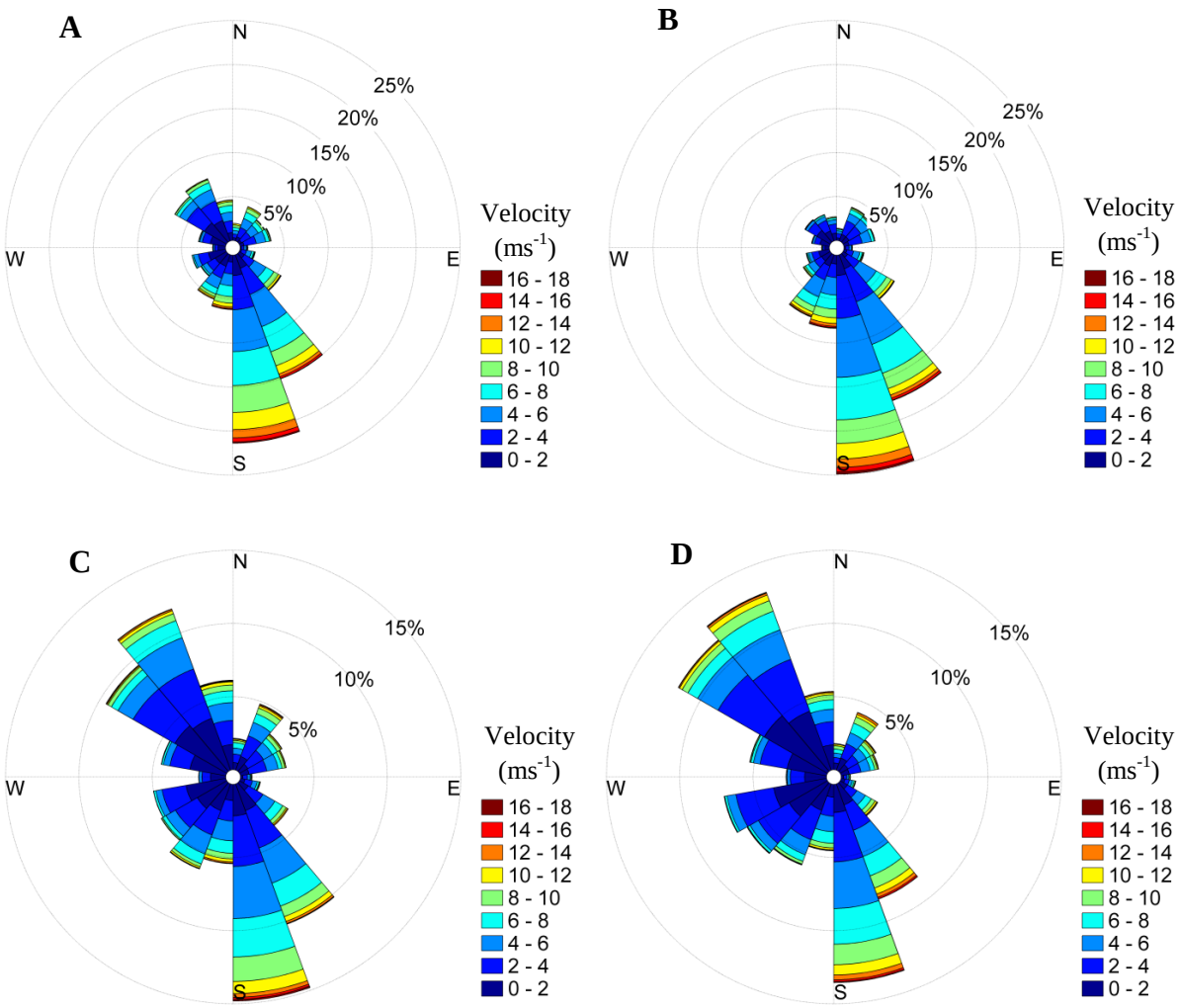

Figure 6. Wind direction and velocity at Casal do Rato station for each season: **A** - Spring; **B** – Summer; **C** – Autumn and **D** - Winter.

3. Numerical Models and Methodology

The numerical simulations were performed with the 2DH morphodynamic modeling system MORSYS2D [Fortunato and Oliveira, 2004]. This modelling system integrates the hydrodynamic model ELCIRC [Zang *et al*., 2004], which calculates tidal elevations and currents, the wave model SWAN [Booij *et al*., 1999], which computes wave propagation and the model SAND2D [Fortunato and Oliveira, 2004] that computes sand transports and updates the bottom topography. In this study, the module SAND2D was not activated. A brief description of each model component used in this study is presented in the following subsections.

3.1. Hydrodynamic Numerical Model (ELCIRC)

ELCIRC (www.stccmop.org/CORIE/modeling/elcirc/index.html) is a model developed for the effective simulation of three dimensional baroclinic circulation across river-to-ocean scales. The model ELCIRC uses a finite-volume/finite difference Eulerian-Lagrangian algorithm to solve the set of six hydrostatic equations based on the Boussinesq approximation: mass conservation, momentum conservation and conservation of salt and heat, addressing a wide range of physical processes and of atmospheric, ocean and river forcings [Zhang *et al.* 2004]. A finite volume technique conservation and natural treatment of wetting and drying are used to solve the model equations. The horizontal domain is discretized with a triangular mesh for flexibility. A semi-implicit time-stepping algorithm and the Lagrangean treatment of advective terms ensure stability at large time steps [Oliveira *et al*., 2006b].

Within MORSYS2D, the hydrodynamic model solves the equations in order to determine the free surface elevation, 3D water velocity, salinity and temperature. In Ria de Aveiro, a single layer is adopted, so the model reverts from 3 dimensions into 2 dimensions. The depth-integrated equations solved in this model express the conservation of mass and momentum:

$$\frac{\partial \zeta}{\partial t} + \frac{\partial (HU)}{\partial x} + \frac{\partial (HV)}{\partial y} = 0 \tag{1}$$

$$\frac{\partial U}{\partial t} + U\frac{\partial U}{\partial x} + V\frac{\partial U}{\partial y} = fV - g\frac{\partial \zeta}{\partial x} - \frac{\tau_{bx}}{\rho} + \frac{\tau_{sx}}{\rho} + \varepsilon\left(\frac{\partial^2 U}{\partial x^2} + \frac{\partial^2 U}{\partial y^2}\right) \tag{2}$$

$$\frac{\partial V}{\partial t} + U\frac{\partial V}{\partial x} + V\frac{\partial V}{\partial y} = -fU - g\frac{\partial \zeta}{\partial y} - \frac{\tau_{by}}{\rho} + \frac{\tau_{sy}}{\rho} + \varepsilon\left(\frac{\partial^2 V}{\partial x^2} + \frac{\partial^2 V}{\partial y^2}\right) \tag{3}$$

where H is the total depth, U and V are the depth averaged velocity components in the x (eastward) and y (northward) directions, τ_{bx}, τ_{by} are the bottom stress in x and y directions, τ_{sx}, τ_{sy} are the surface stress in x and y directions, t is the time, g is the acceleration of gravity, ρ is the water density, ε is the horizontal eddy viscosity.

There are several options of forcing agents in ELCIRC within MORSYS2D: tides, tidal potential, river flow and wind or waves-induced radiation stresses. Only the surface water elevation, wind and waves-induced radiation stresses are considered in this study. Under the action of tides only, the stress is defined at the bottom according to each horizontal direction:

$$\tau_{bx} = \rho C_D \sqrt{U^2 + V^2} U \quad (4)$$

$$\tau_{by} = \rho C_D \sqrt{U^2 + V^2} V \quad (5)$$

where C_D is the drag coefficient computed using the Manning law and given by:

$$C_D = g n^2 h^{-\frac{1}{3}} \quad (6)$$

where *n* is the Manning coefficient. The friction between the interface ocean-atmosphere was not considered in this work.

The earth rotation is represented through the *Coriolis* acceleration in the momentum equations. The *Coriolis* factor, *f*, is a known function of latitude ϕ :

$$f = 2\Omega \sin\phi \quad (7)$$

A semi-implicit scheme is used in the numerical algorithm of ELCIRC. The barotropic pressure gradient in the momentum equation and the flux term in the continuity are treated semi-implicitly, with implicitness factor 0.5 ≤ α ≤ 1. The vertical viscosity term and the bottom boundary condition for the momentum equation are treated fully implicit and all other terms are treated explicitly. According to Casulli and Cattani [1994] this ensures both stability and computational efficiency.

According to Longuet-Higgins and Stewart [1964] and Phillips [1977] the effect of short waves on the hydrodynamics is expressed through the forcing by the gradients of wave radiation stresses, which in this 2DH mode can be defined by:

$$\tau_{sx} = -\left(\frac{\partial S_{xx}}{\partial x} + \frac{\partial S_{yx}}{\partial y} \right) \quad (8)$$

$$\tau_{sy} = -\left(\frac{\partial S_{yy}}{\partial y} + \frac{\partial S_{xy}}{\partial x} \right) \quad (9)$$

and S_{xx}; S_{yy} ; S_{xy}; S_{yx} are wave radiation stress terms, given by:

$$S_{xx} = \frac{E}{2}\left(2\frac{C_g}{C}\left(\cos^2\alpha + 1\right) - 1 \right) \quad (10)$$

$$S_{yy} = \frac{E}{2}\left(2\frac{C_g}{C}\left(\sin^2\alpha + 1\right) - 1 \right) \quad (11)$$

$$S_{xy} = S_{yx} = E\frac{C_g}{C}\sin\alpha\cos\alpha \quad (12)$$

where $E = 1/8\rho g H_{rms}^2$ is the wave energy, α is the wave angle to the x axis, C_g is the wave group velocity and C the wave phase velocity.

3.2. Wave Model (SWAN)

SWAN is a third generation wave prediction model used to represent wave conditions in coastal and near-shore waters. This model has been extensively used for environmental impact assessment studies, sediment transport studies, near-shore wave prediction. The free surface elevation in SWAN is described in terms of action density (or energy density in the absence of currents). The energy balance equation gives a statistical description of the time evolution of surface gravity waves [Booij *et al*., 1999].

The wave model SWAN [Booij *et al*., 1999] computes the evolution of the wave spectrum by solving the spectral action balance equation adapted to near shore zones, given in Cartesian coordinates by Equation 13.

$$\frac{\partial}{\partial t}N+\frac{\partial}{\partial x}\left(c_x N\right)+\frac{\partial}{\partial y}\left(c_y N\right)+\frac{\partial}{\partial \sigma}\left(c_\sigma N\right)+\frac{\partial}{\partial \theta}\left(c_\theta N\right)=\frac{S}{N} \tag{13}$$

in which σ is the wave frequency (s^{-1}), θ the wave angle (radians), *N* the wave action density (m), c_x, c_y the wave propagation speeds in *x* and *y* directions (ms^{-1}) and *S* the energy source term (ms^{-2}).

The first term is the local rate of change of action density with respect to time. The second and third terms represent the propagation of the group velocity over a cartesian grid (c_x and c_y are the group velocity in *x* and *y* space). The fourth term accounts for the shifting of the relative frequency of waves due to variations in depth and currents. The fifth term is the refraction and propagation due to the depths and currents in the directional space (c_σ and c_θ are in spectral space). The right side of the equation incorporates *S*, which is the total of all source and sink terms in the form of energy density.

The model SWAN also accounts for depth-induced wave breaking and triad wave-wave interactions which is important for near-shore wave predictions. The inherent physical processes accounted in SWAN comprises the parameterization of wind input, non-linear wave-wave interaction, white-capping dissipation, bottom interaction, changes due to variation in water depth and effect of currents [Arora *et al*., 2012]. In this study, the white-capping dissipation was not taken into account.

3.2.1 Wave Model Setup

In the present study two nested grids are used in the wave model with different dimensions and characteristics, as reported in Plecha [2011] and Plecha *et al*., [2012]. The grid with higher dimensions extends from the offshore area with a coarser resolution. In this grid are imposed the waves boundary conditions: a regular monochromatic wave or a wave regime. The second grid encompassing the inlet area is curvilinear in space and with finer resolution. The calibration of SWAN was performed by Plecha [2011], by comparing model predictions with buoy records at Leixões (41°19'00"N, 8°59'00"W).

3.3. Model Establishment and Hydrodynamic Model Calibration

This study starts with the improvement of the previous implementation of the hydrodynamic model ELCIRC performed by Picado [2008], in order to understand the consequences of the partial salt pans walls destruction on the entire Ria de Aveiro lagoon hydrodynamics. The author used a bathymetry with topo-hydrographic data mainly from 1987/88 collected by Portuguese Hydrographic Institute (I.H). The exception is the inlet area where the bathymetry were updated with 2001 data, collected by the Administration of the Ria de Aveiro (A.P.A.).

Is known that the depth and the morphology of the main channels of the Ria de Aveiro changed considerably since 1987/88 until nowadays. For that reason and in order to represent the physical processes in the lagoon with more recent data, the bathymetry developed by Picado [2008] was updated, constituting the first step of this study.

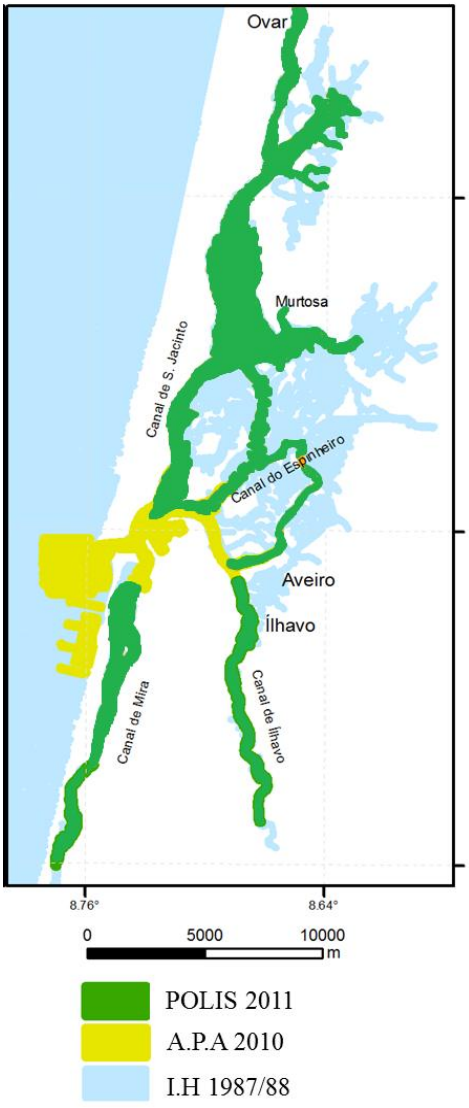

Figure 7. Map with the identification of field works.

Thus, the new bathymetry is composed by a compilation of 3 different topo-hydrographic data (POLIS 2011 collected by Ria de Aveiro Polis Litoral program; A.P.A 2010 data, collected by Administration of the Ria de Aveiro in the year 2010 and finally, the data of I.H 1987/88 also present in the bathymetry used by Picado [2008]). Thus, as illustrated in Figure 7, the bathymetry in the inlet area was updated with the data collected by A.P.A in 2010. The majority of the S.Jacinto channel was updated with POLIS 2011 data, however, in some channels in the upstream zone of the S.Jacinto channel, the bathymetry is from 1987/88.

In the downstream zone of Mira channel, the bathymetry was updated with A.P.A 2010 data, while in the remaining channel, the data used to update the bathymetry was POLIS 2011 data.

With the exception of the downstream area that was updated with A.P.A data, the Ílhavo channel was mainly updated with POLIS 2011 data.

Since the downstream area until the middle zone of the Espinheiro channel, the bathymetry was updated with POLIS recent data. The upstream zone of the channel keeps with the data of 1987/88.

The analysis of Figure 7 allows affirm that the principal zones of the main channels were updated with more recent data.

The two bathymetries (the bathymetry used by Picado [2008] and bathymetry created in this study) are represented in Figure 8, and the zoom of the inlet zone (study area) is also in the figure. The numerical bathymetries are referent to average mean sea level (2 m). The main difference between them is the deepening visible in the new bathymetry when compared with the bathymetry used by Picado [2008]. This is mainly

observed in the inlet zone, in the deeper zones of S.Jacinto channel and in the downstream region of Espinheiro channel. In the Ílhavo channel, the depth increase in the entire channel.

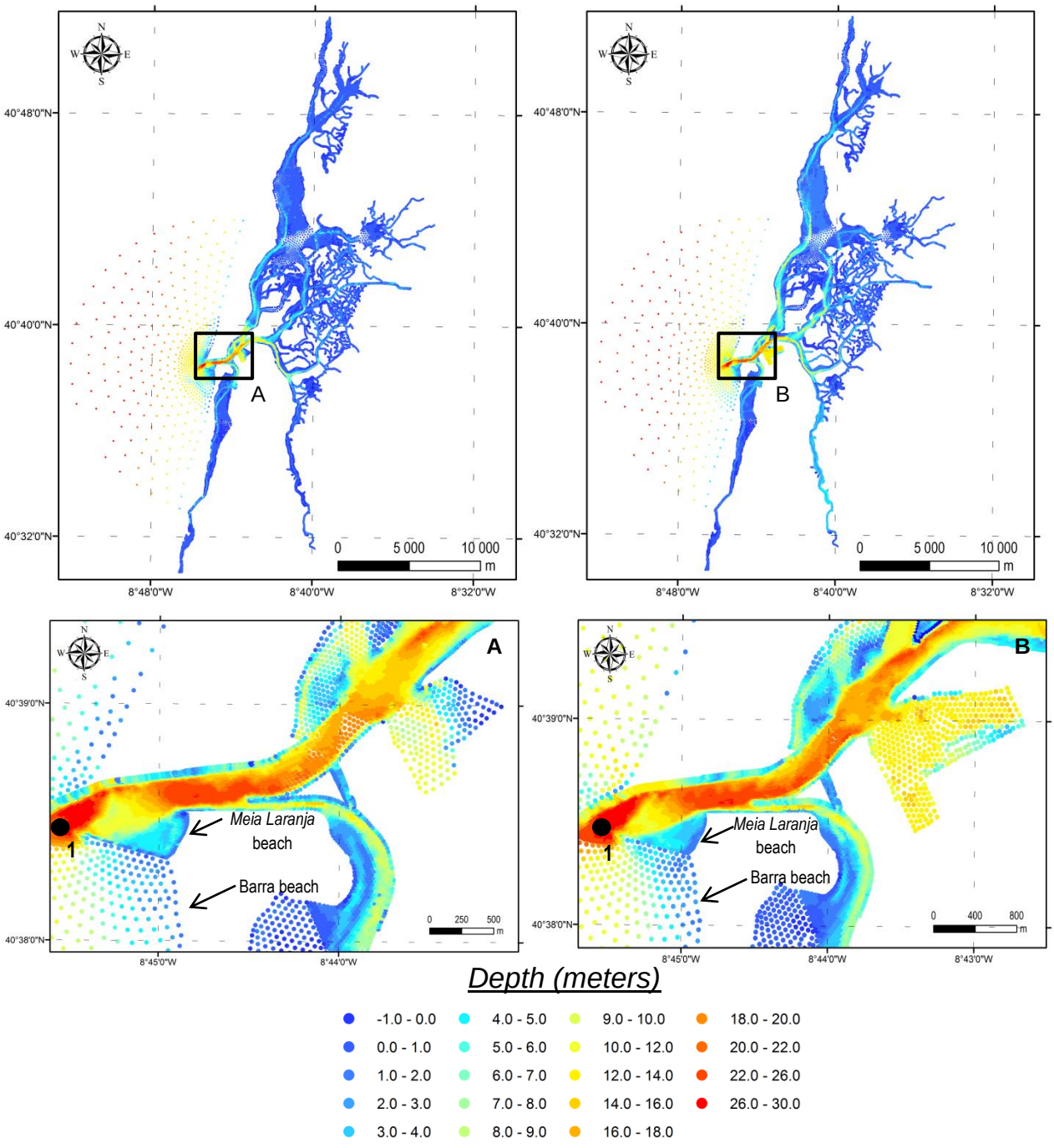

Figure 8. Numerical bathymetries for 2002 (left panel) and 2011 (right panel) of Ria de Aveiro. The A and B correspond to a zoom in the inlet area for bathymetries of 2002 and 2011, respectively. The station used to study the hydrodynamic changes induced by the waves is represented with the number 1.

The grid initially used in this study is the grid developed by Picado [2008] and represented in Figure 9 (B). It is numerical discretized with 87747 elements and 66092 nodes. This grid includes, with high resolution, all the channels in the interior of the lagoon, however without high resolution in offshore and inlet regions. Therefore, after some numerical runs, it was concluded that this grid has insufficient resolution in offshore zone to represent accurately the coastal waves propagation.

Therefore, it was necessary integrate the grid with higher resolution in the offshore and inlet areas developed by Plecha [2011] in order to study the morphodynamic in the Ria de Aveiro inlet. It is numerical discretized with 43169 elements and 25819 nodes. Due to the focus of the study (inlet area) performed by Plecha [2011], in this grid is excluded some interior channels of Ria de Aveiro. Thus, the final grid (C) is a merging of a grid with high resolution in the ocean area (A) with a grid with a high resolution in the lagoon area (B), as represented in Figure 9. Thus, this grid allows studying accurately the processes that occur in the inlet without neglecting the interiors channels of Ria de Aveiro. The final grid has 103515 elements and 74094 nodes, and is illustrated in the bottom panel of the figure (C).

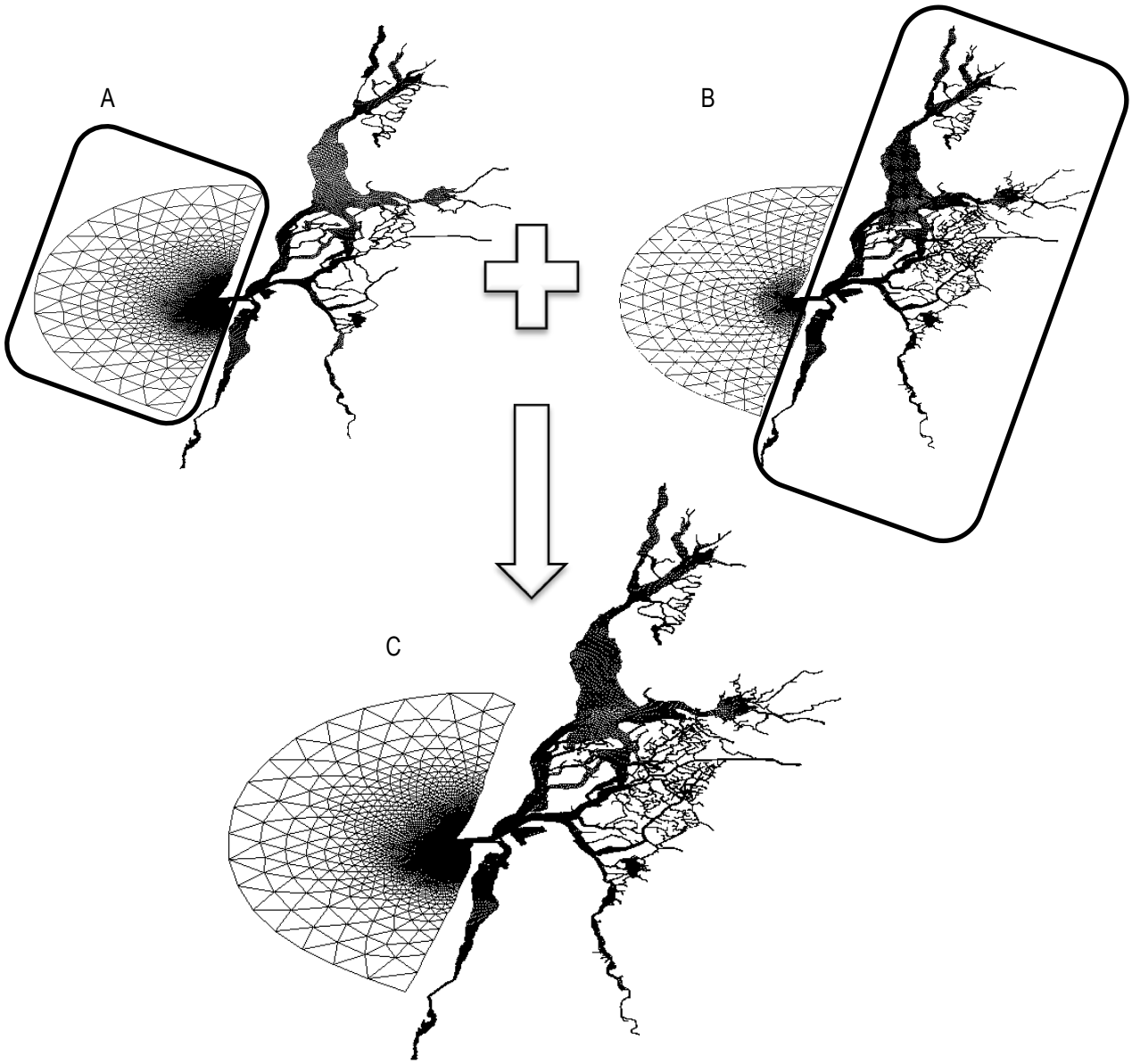

Figure 9. Scheme illustrating the grids integration, with the representation of the final grid.

Once completed this procedure, was performed the hydrodynamic model calibration. The hydrodynamic model ELCIRC was forced by eleven harmonic constituents (*MSF*, O_1, K_1, N_2, M_2, S_2, M_4, MN_4, MS_4, M_6 and $2MS_6$) obtained from the regional model of Fortunato *et al*. [2002]. The largest time step that prevents the appearance of oscillations was set to 90 seconds.

The calibration of the hydrodynamic model is based on the adjustments of parameters to which the model is most sensitive. According to Dias and Fernandes [2006], the magnitude of the bottom friction coefficient induces changes in the tidal wave propagation within the Ria de Aveiro. The water depth influences strongly the bottom stress. Therefore, based in previous works [Dias and Lopes, 2006a,b; Dias *et al.* 2009; Picado *et al*., 2011], it was decided to use the Manning coefficient dependent of the depth as calibration parameter. Several model runs were performed to calibrate the numerical model, by adjusting the bottom stress in order to reduce the differences between the available data and model results, reaching the relationship showed in Table 1. The Manning coefficients were adjusted using the guideline that an increase in the bottom friction will induce a decrease in the tidal wave amplitude in that zone, and vice-versa. Another principle used is that an increase in the bottom friction will lead an increase in the phase lag for high tide and a decrease for low tide [Fry and Aubrey, 1990].

Table 1. Bottom friction coefficients.

Depth (meters)	Manning *n* values
$h \leq -0.5$	0.029
$-0.5 \leq h \leq 0.0$	0.027
$0.0 \leq h \leq 0.5$	0.026
$0.5 \leq h \leq 1.0$	0.023
$1.0 \leq h \leq 3.0$	0.020
$3.0 \leq h \leq 6.0$	0.016
$6.0 \leq h \leq 10.0$	0.015
$h \geq 10.0$	0.014

The model was calibrated following the methodology proposed by Dias and Lopes (2006a), by initially comparing visually the observed sea surface elevation data with the hydrodynamic model results. For the model calibration, the data available are from field works carried out in Ria de Aveiro in the years 2003 and 2004. Field data were collected in the framework of the Araújo [2005] PhD Thesis and the measurements were performed every six minutes, with the exception of the Barra station, where the measurements were performed every hour. It is important to note that, in order to compare model results with measurements, the low frequency signal was removed from the data, considering a cut-off frequency of 0.0000093 Hz (30 h). This method has already been adopted in previous studies [Picado, 2008].

The hydrodynamic model calibration is performed at 18 stations within the lagoon (Figure 10). The predicted and observed time series of sea surface elevation comparison is shown in Figures 11 and 12. After comparing visually the observed sea surface elevation data with the hydrodynamic model results, the model performance was quantified by Root Mean Square (RMS) errors and Skill parameter (Table 2), given by:

$$RMS = \left\{ \frac{1}{N} \sum_{i=1}^{N} [\zeta_0(t_i) - \zeta_m(t_i)]^2 \right\}^{\frac{1}{2}} \quad (14)$$

$$Skill = 1 - \frac{\sum |\zeta_m - \zeta_0|^2}{\sum \left[|\zeta_m - \overline{\zeta_0}| + |\zeta_0 - \overline{\zeta_0}| \right]^2} \quad (15)$$

where $\zeta_0(t_i)$ and $\zeta_m(t_i)$ are the observed and computed SSE, respectively, N is the number of measurements in the time series and $\overline{\zeta_0}$ the time average of the observed SSE. Based in Dias *et al.* [2009], the RMS values should be compared with the local tidal amplitude and if those errors are lower than 5% of the local amplitude, the agreement between model results and observations should be considered excellent and if they range between 5% and 10% the agreement should be considered very good. The model predictive Skill, a method developed by Wilmott [1981] and used initially by Warner *et al.* [2005] and Li *et al.* [2005], yield a Skill of one for a perfect agreement between model results and observations and zero for a complete disagreement. Skill values higher than 0.95 should be considered representative of an excellent agreement between model results and observations [Dias *et al*., 2009].

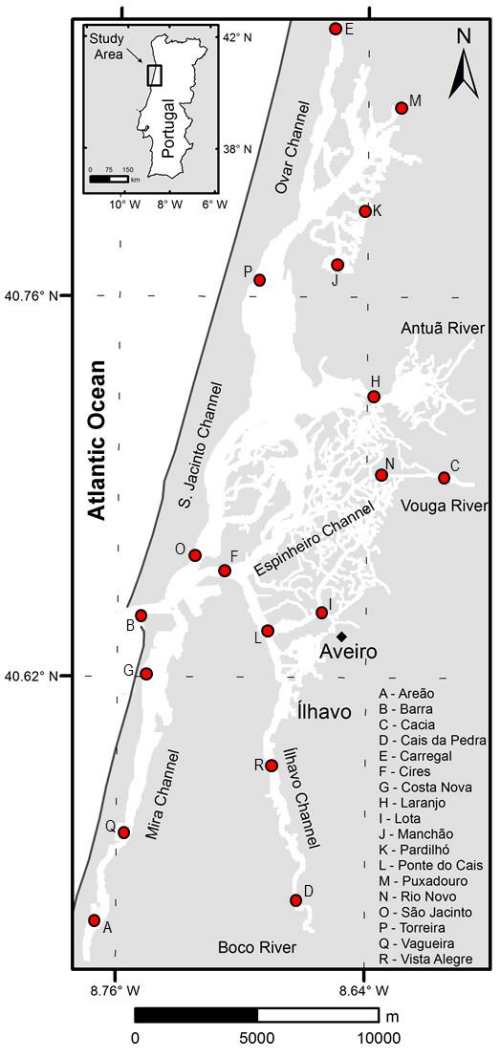

It was also performed the comparison between the observed and predicted amplitude and phase of the main tidal constituents determined from harmonic analysis is also performed, in order to quantify separately the amplitude and phase lags of the major tidal constituents for the all monitoring stations (Figure 13). In this work the harmonic analysis is performed using Pawlowicz *et al*. [2002] package.

Figure 10. Stations used in hydrodynamic model calibration.

3.3.1. Results

With the exception of the stations E, M, K and J, the RMS values ranges from 2.5% to 13.3% of the local amplitude in all stations. The stations B, F, G, H, I, L, N, O, P, Q and R have a RMS value between 0 and 10%. Thus, the agreement between predictions and observations, in the most of the stations, ranges from very well to excellent. For the stations E, M, K and J located on the North of the lagoon, the agreement between model and observations are lower comparing with other previous studies [Picado, 2008]. In the analysis of the calibration results, it is important to note that, in this study, is compared field data from 2003 with modelling results of the year 2011. Is known, through several publications, including Araújo *et al*., [2008], which over the years, the tidal range in the Ria de Aveiro has been increased, and the phase is decreasing. Thus, it is likely that these patterns will be visible in the time series of SSE, and in the comparison of the amplitude and phase of the main harmonics constituents. In these stations (E, M, K and J), the patterns identified by Araújo *et al*., [2008] are amplified, leading a highest disagreement between predictions and observations.

Table 2. RMS and Skill for all the calibration stations.

Station	RMS	Skill
A	0.1990	0.9252
B	0.0759	0.9905
C	0.2796	0.9470
D	0.3745	0.8866
E	0.3931	0.7625
F	0.1698	0.9873
G	0.0924	0.9962
H	0.2102	0.9719
I	0.1738	0.9859
J	0.3383	0.8167
K	0.5092	0.6521
L	0.1628	0.9879
M	0.4540	0.6960
N	0.2210	0.9724
O	0.1309	0.9911
P	0.1851	0.9756
Q	0.1528	0.9812
R	0.3150	0.9084

At station B (Barra), the most important for the aim of this study because is where this work is focused, the computed and observed data comparison should be perfect. The RMS is approximately 7 cm, which represents an error of 2.5% when compared with local tidal amplitude. This small error may partially explain the errors found in the other stations within the lagoon. In stations B, F, G, L and O the disagreement is lower than 5% of local tidal range. In general, the errors increase with the distance between the station and the lagoon mouth.

The time series represented in Figures 11 and 12 shows that the model results predicts a global increase of tidal amplitude since 2003 to 2011 and a slight phase lag between predictions and observations leading to an increase of the RMS. However, these patterns are in agreement with Araújo *et al*. [2008].

With the exception of the stations D, E, J, K and M, the skill values are always higher than 0.90. All of these stations are in the upstream zone of the channels, where the model has lower agreement with the observations. The stations B, F, G, H, I, L, N, O, P and Q have skill values greater than 0.95, thus it should be considered as an excellent agreement between model results and observations.

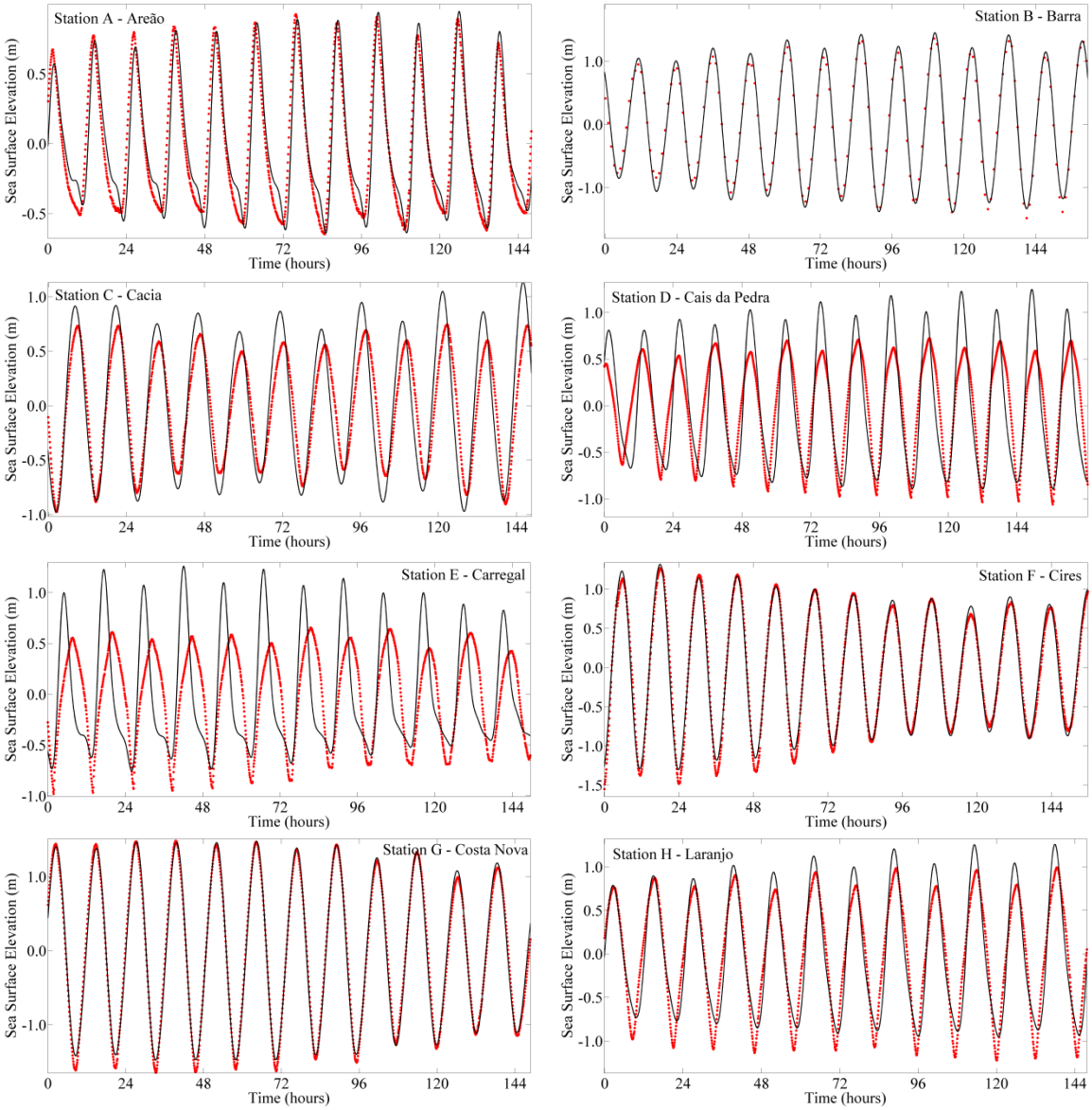

Figure 11. Comparison between observations and model results of SSE time series from station A until F, used in the hydrodynamic calibration procedure (● red circles: data; black solid line: model).

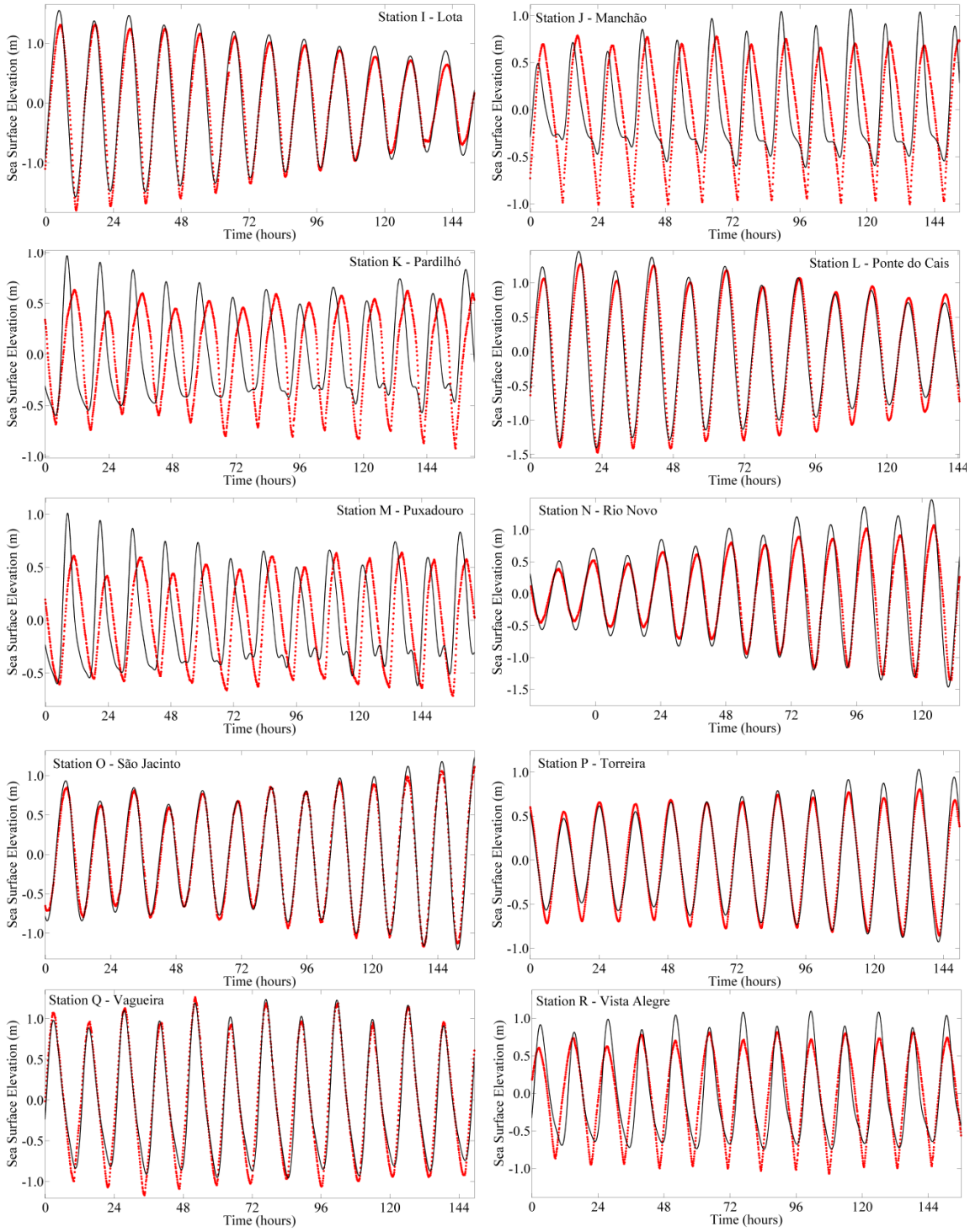

Figure 12. Comparison between observations and model results of SSE time series from station I until R, used in the hydrodynamic calibration procedure (● red circles: data; black solid line: model).

The analysis of the tidal constituents reveals that the M_2 and S_2 are the most important constituents in the lagoon, representing approximately 90% of the tidal energy in Ria de Aveiro lagoon in agreement with Dias *et al*. [1999]. The tidal constituent comparison shows major disagreement at the upstream stations.

The analysis of these results shows that the mean amplitude difference, in all stations, for the M_2 constituent is about 9 cm, and the mean phase difference is about 10º. This value corresponds to a difference of about 20 minutes in the arrival of tidal wave. In the station B, this difference is much smaller than the average value (less than 6 minutes in phase and 0.15 cm in amplitude). For the S_2 constituent, the mean amplitude difference is approximately 4 cm and phase difference is 10º, which means that the average delay is about 29 minutes. At station B, the difference in amplitude is 8 cm and in the phase is 1.8º, corresponding to 3.7 minutes.

For diurnal constituents (O_1 and K_1), the results are similar when compared with the semi-diurnal constituents, but with higher disagreement. The apparent error present in the O_1 phase at stations C, H and P is because of the adopted graphic scale. For the O_1 constituent, the mean amplitude difference corresponds to 0.79 cm and the mean phase difference is 48º, which means that the average delay is about 207 minutes. However, in Barra station it is observed a better agreement between model and observations, with an average of amplitude difference of about 0.26 cm and phase delay about 14 minutes. The mean amplitude difference for K_1 constituent is about 1.3 cm and the mean phase difference is approximately 60º, corresponding to 239 minutes. For station B (Barra), the amplitude difference is 0.25 cm and the phase difference is 6º, corresponding to a delay of 25 minutes.

The M_4 is a harmonic constituent which characterises a short-period harmonic term in order to take into account the change in the form of a tidal wave resulting from shallow water condition. In shallow waters the progression of a tidal wave is changed by numerous physical factors which depend on the square or higher powers of the tidal amplitudes [Pugh, 1996]. The mean amplitude difference, in all stations, for the M_4 constituent is about 6 cm while the mean phase difference is 69º, which corresponds to 71 minutes. In the most important station for this study, the difference in amplitude is 0.47 cm and the phase delay is about 30 minutes. The M_4 constituent amplitude and phase was not reproduced with the expected accuracy. The errors found in this constituent reproduction may be due to bathymetric errors that cannot be corrected by the adjustment of the bottom coefficient and because it was not considered the low lying areas adjacent to Ria de Aveiro.

According to the RMS and Skill results obtained, it may be considered that the model reproduces accurately the SSE data, and consequently the tidal processes in the lagoon. The numerical results obtained for the study area (inlet) should be considered in excellent agreement with the observed data. Relatively to the harmonic analysis, the observations and predictions has a good agreement, essentially in semi-diurnal constituents (the most important). In Barra station, area where this study is focused, the results are very good. Therefore it may be concluded that the hydrodynamic model is calibrated and able to reproduce the tidal processes in the area of interest for this study.

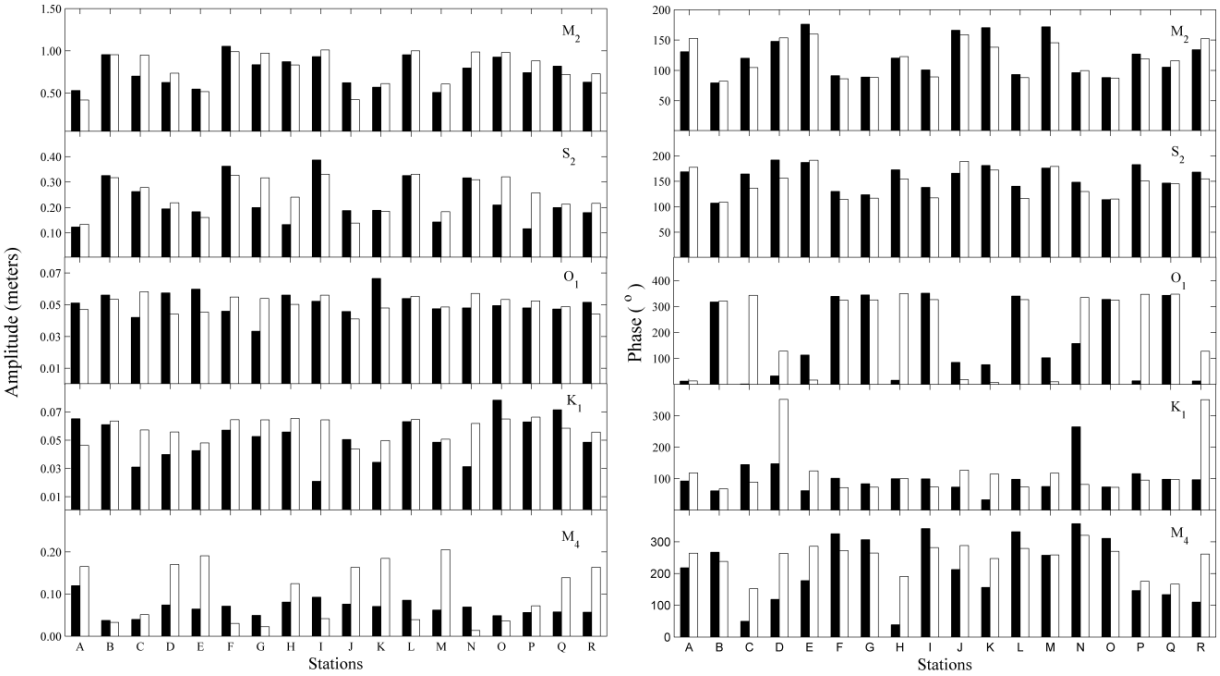

Figure 13. Comparison between model predicted and observed amplitude and phase for the major semi-diurnal and diurnal constituents (M_2 – 12.42 h; S_2 – 12 h; O_1 – 25.82 h; K_1 – 23.93 h) and for the shallow water overtide of the principal lunar constituent, M_4 (6.21 h). The black and white bars represent the observed and predicted values, respectively.

3.4. Analyses of Field Data of SSE, *Hs* and Atmospheric Pressure

In this subchapter, will be present the methodology used to relate the field data of *Hs* with over-elevations in Sea Surface Elevation (SSE), from the Barra tidal gauge (40°38.5'N, 8°44.92'W). The data available of *Hs* is from the Leixões Buoy comprised between 1984 and 1996. In this case, the analysis is done considering the Leixões wave directional buoy data, when previously was made with Figueira da Foz buoy data. This is possible because, according with Coli [2003], there is homogeneity of wave climate on the northern coast of Portugal.

Therefore, between 1984 and 1996, were searched events of high wave climate. Of the several found, will be studied the month of December of 1985 as well as the period between 1 and 15 of January of 1996.

In order to separate the high (tidal signal) and low frequencies signals of the tidal gauge data, was used a filter with a cut-off frequency of 0.0000093 Hz (30 h). Therefore, in the low frequency signal are included the meteorological events, mainly the atmospheric pressure variation, as well as the coastal waves effects. Thus, taking into account the goal of this work (study the influence of coastal waves in the inlet hydrodynamics), in order to represent only the effect of the waves in the low frequency signal, was remored the influence of atmospheric pressure in the SSE through the inverted barometer effect, given by:

$$\Delta\eta = -\frac{\Delta p_a}{\rho g} <=> \Delta\eta = -0.993\Delta p_a \quad (14)$$

where $\Delta\eta$ is the water level variation, ρ is the water density, g is the acceleration of gravity and Δp_a is the atmospheric pressure variation, given by $P_{measured}$ – 1013.25 hPa. The value of 1013.25 hPa corresponds to the normal atmospheric pressure at mean sea level.

The atmospheric pressure data used in this work for the Aveiro coast are available in the website of NOAA [http://www.esrl.noaa.gov/psd/data/gridded/data.ncep.reanalysis.html], corresponding to reanalysis data with a temporal resolution of 6 hours. In order to put in concordance the atmospheric pressure and tidal gauge data, an interpolation of the atmospheric pressure data was made, creating a new serie with a temporal resolution of 1 hour.

With this procedure is quantified the effect of the coastal waves in the SSE, through the analysis of field data, since a direct comparison between *Hs* data and the low frequency signal containing only the effect of the waves will be performed.

3.5. Establishment of Scenarios

After it has been demonstrated that the model simulates accurately the Ria de Aveiro hydrodynamics, will be defined the scenarios to simulate, in order to understand the influence of the waves in the lagoon hydrodynamics.

The SWAN model runs considering the wave and wind fields as driving forces, more specifically the significant wave height, period and direction of the waves and the velocity and direction of the wind. These inputs are defined and considered as constant for all the simulation period. As schematized in Figure 14, for each tidal range (Spring, Typical and Neap tide), it was simulated the normal and the storm wave action in the Portuguese coast, and a case with the absence of waves. The case with the absence of waves, therefore considering only the tidal forcing, is defined as scenario 0, constituting the reference scenario.

The normal and storm scenarios were defined taking into account the characterization of waves and wind presented in section 2.3. Thus, the normal regime has a typical WNW to NNW swell, with *Hs* between 2 and 2.5 meters and periods between 9 and 11 seconds, and moderate wind Northerly. In the storm events, the *Hs* may reach 8 meters, and the waves usually come from SW with a period of 12 seconds. In these events, the wind is stronger and has a provenience from SE.

Therefore, the normal regime named scenario 1 is characterized by:

- Significant wave height (*Hs*) = 2 meters
- Wave period = 9 seconds
- Wave direction = NW
- Wind speed = 4 ms^{-1}
- Wind direction = NW

For storm regime named scenario 2 it was considered:

- Significant wave height (*Hs*) = 8 meters
- Wave period = 12 seconds
- Wave direction = SW
- Wind speed = 16 ms^{-1}
- Wind direction = SE

The duration of the simulations is 8 days, and the spring, typical and neap tide were identified through the analyses of the tide at the inlet of the Ria de Aveiro during the year 2011. The event of maximum tidal amplitude (spring tide) was in March 20th 2011, the minimum amplitude (neap tides) in July 24th 2011 and intermediate tidal range in November 12th 2011.

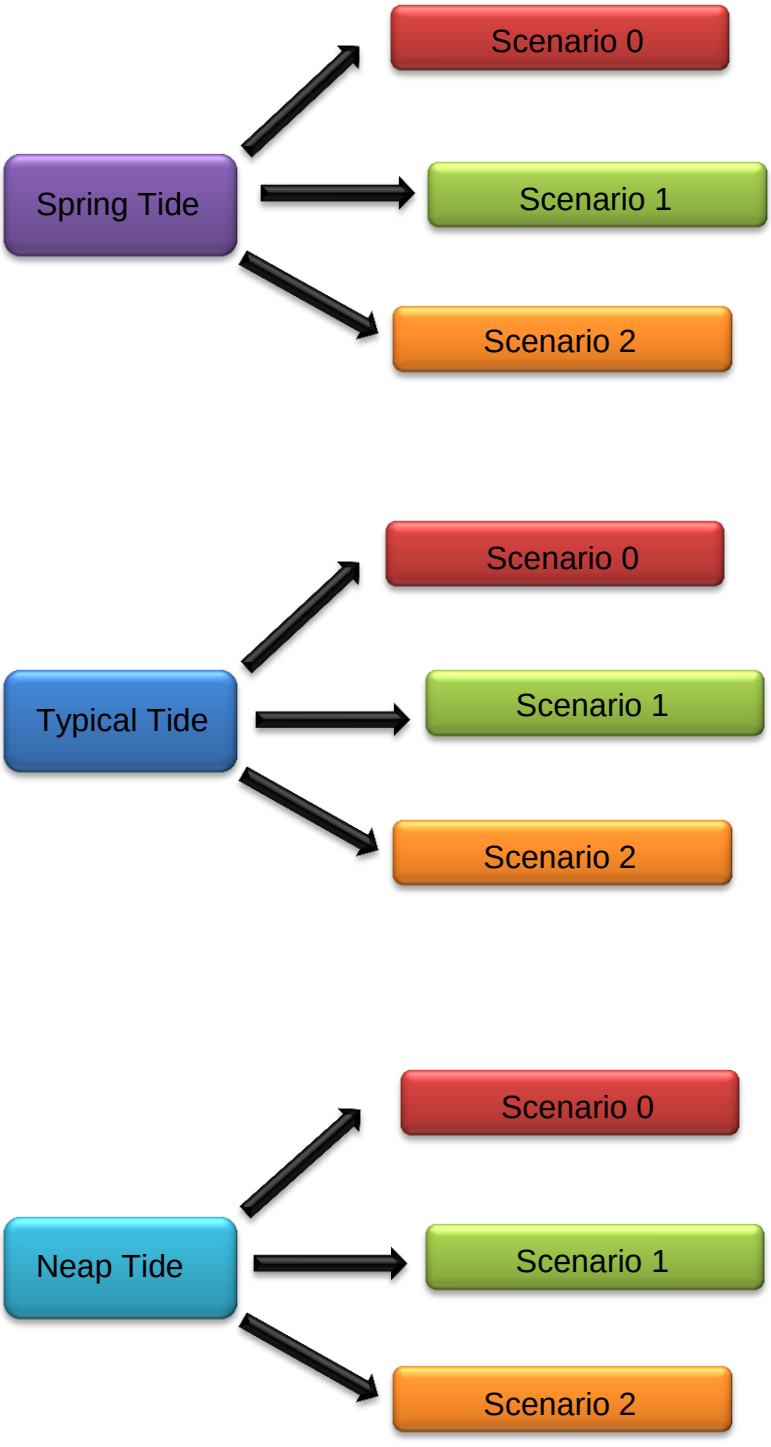

Figure 14. Figure representing the scenarios established in the hydrodynamic model simulations.

4. Wave Effect in the Aveiro Inlet

4.1. Analyses of Field Data of SSE, *Hs* and Atmospheric pressure

As mentioned in the methodology of the analyses of field data of SSE, *Hs* and Atmospheric pressure (section 3.4), the aim of this subsection is relate the *Hs* with over-elevations measured of the Barra tidal gauge and induced by coastal waves. Then, the SSE variations induced by atmospheric pressure were removed from the low frequency signal of SSE, in order to represent only the influence of waves in this signal.

Therefore, the atmospheric pressure data from December of 1985 (upper panel) and between 1 and 15 of January of 1996 (lower panel) is represented in Figure 15.

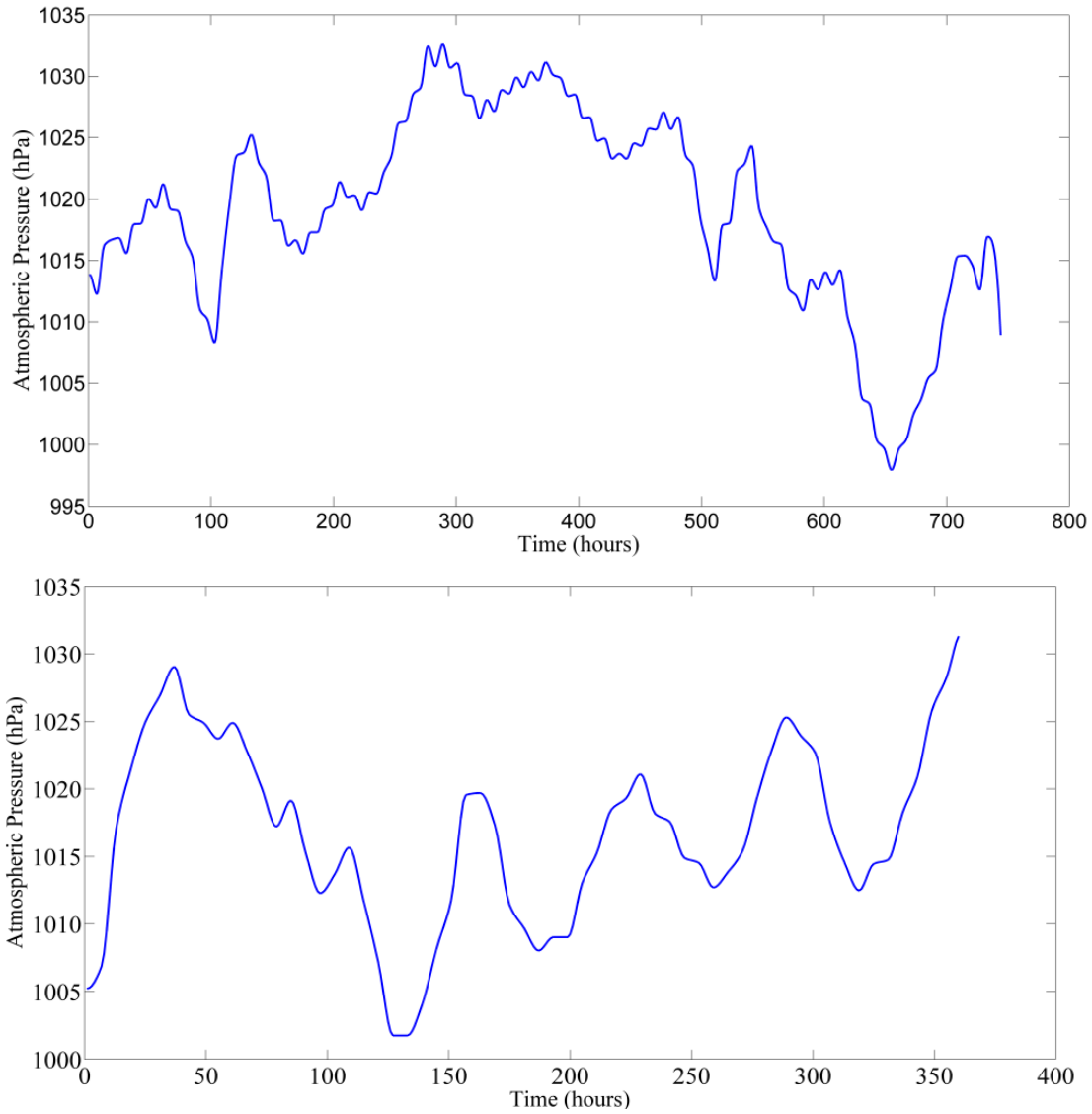

Figure 15. Atmospheric pressure data between 1/12/1985 and 31/12/1985 (upper panel) and between 1/1/1996 and 15/1/1996 (lower panel).

The atmospheric pressure has an important effect in SSE, wherein an increase of atmospheric pressure causes a compression in the water column leading to under-elevation in SSE. On the other hand, a decrease of atmospheric pressure causes an expansion of water column leading to over-elevation of SSE. Thus, a 1 mbar atmospheric pressure change corresponds to a linear response of the sea level of about 1 cm.

Therefore, in the upper panel of Figures 16 and 17 are illustrated the time series of the tidal signal (red line) and of the low frequency signal (blue line), which might be originated by meteorological action or 'wave set-up', collected from the Barra tidal gauge, for the periods in study.

The values of atmospheric pressure represented in Figure 15 were converted to values of low frequency water level through the expression of inverted barometer effect, constituting the red line of the middle panel of Figures 16 and 17. The blue line corresponds to the low frequency signal, also represented in the upper panel.

The analysis of the middle panel shows that the atmospheric pressure is related with the low frequency signal, because some over or under-elevations are mainly caused by the atmospheric pressure variation. However, there are some periods in the times series that the low frequency signal is not related with the atmospheric pressure, therefore, in the lower panel is represented the low frequency signal without the atmospheric pressure contribution. Thus, only the influence of coastal waves is represented.

Analysing the figures is observed that the tidal forcing is the most important forcing in the Ria de Aveiro, and the waves have a visible effect on SSE. In fact, some over-elevations observed in the figures are caused by the coastal waves. Some of these events are represented with a black bar in the figures. When *Hs* increases up to 4 meters, the mean sea level caused by wave set-up increases to a maximum of approximately 0.21 m. When the *Hs* decrease, the signal also tends to decrease. Indeed, only the waves higher than 4 meters have a considerable effect in SSE. The waves with a *Hs* lower than this value, has a maximum of over-elevation of 7 cm.

In most cases, the estimation of wave set-up at inlets is only based on observations. Numerical models, on the other hand, provide an approach to study the importance of simulating waves effect or other external forces (e.g., winds) upon the hydrodynamic behaviour. In addition, hydrodynamic model applications are useful in understanding the main physical processes [Malhadas *et al*., 2009].

Thus, these initial results through field data analyses could provide a starting point to understand, through the use of numerical modelling, the real effect of waves on the hydrodynamics of the Ria de Aveiro inlet.

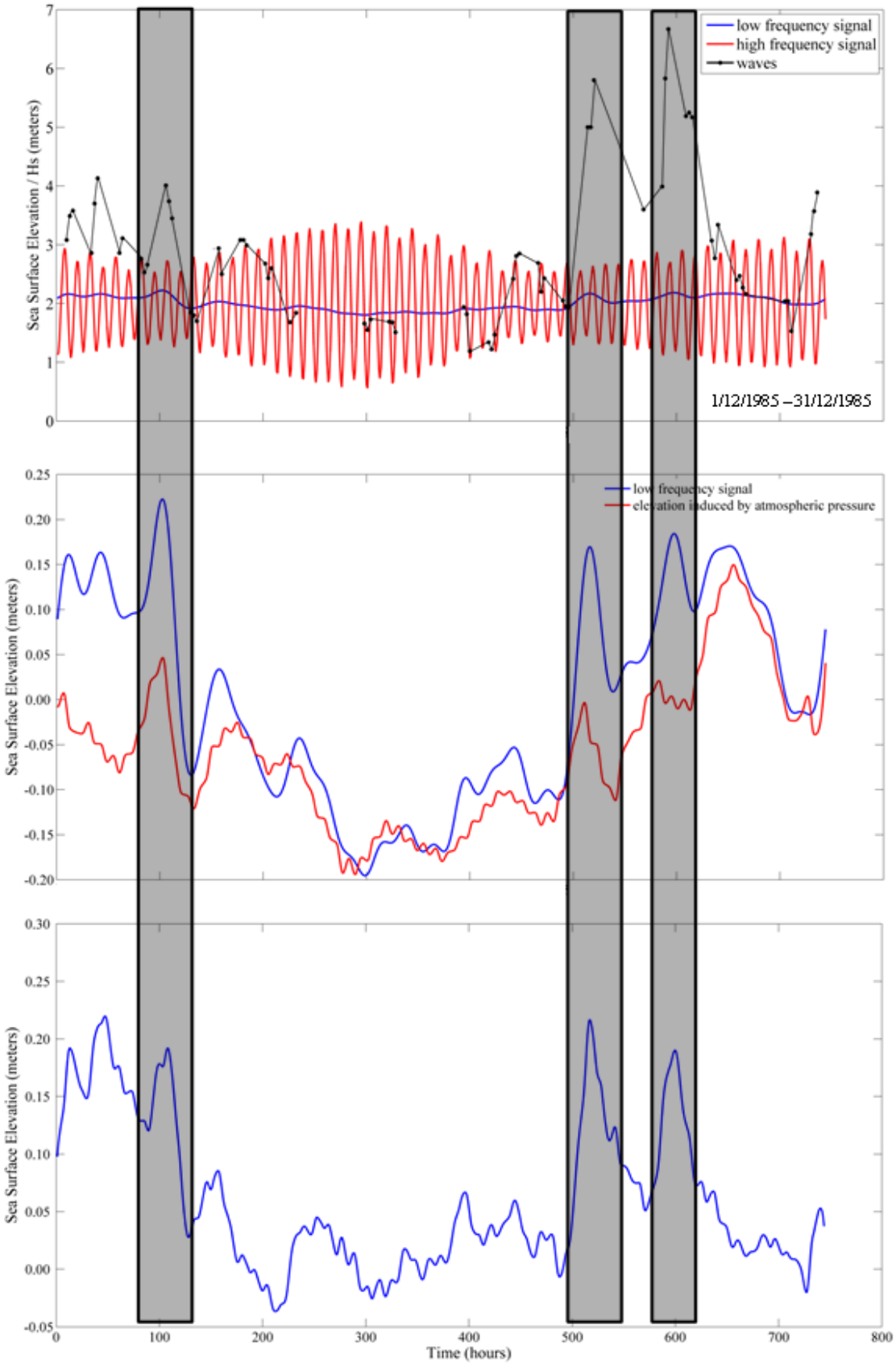

Figure 16. Low and high frequency signal of SSE, and *Hs* (upper panel), between 1/12/1985 and 31/12/1985. The comparison between low frequency signal and the effect of atmospheric pressure is represented in the middle panel. In low panel is represented the difference between the lines represented in the middle panel (wave induced residual).

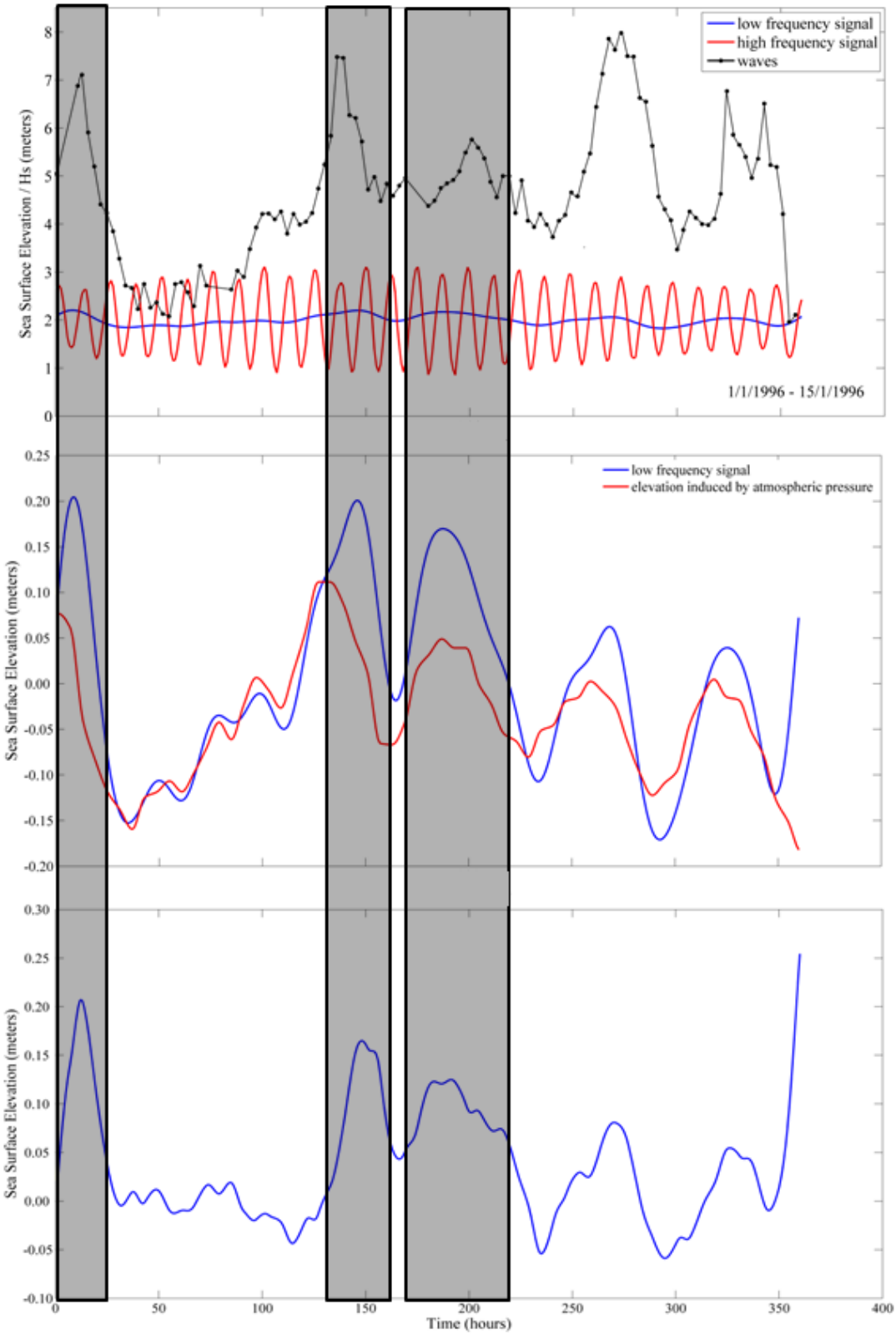

Figure 17. Low and high frequency signal of SSE, and *Hs* (upper panel), between 1/1/1996 and 15/1/1996. The comparison between low frequency signal and the effect of atmospheric pressure id represented in the middle panel. In low panel is represented the difference between the lines represented in the middle panel (wave induced residual).

4.2. Modelling Results

4.2.1. Sea Surface Elevation

Considering the scenarios defined in section 3.5, the results of the numerical simulations performed are present in this subsection. Additionally, the variations in sea surface elevation induced by the wave action are evaluated. First, the analysis of the time series of SSE at station 1 is performed, for each tidal range. The horizontal fields of the differences of SSE between scenarios 0 and 1 and between scenarios 1 and 2 for each tidal range are also shown in this subchapter.

4.2.1.1. Spring Tide

The time series for the three scenarios aforementioned for spring tide condition for station 1 (Figure 8) are illustrated in Figure 18, as well as the differences between all the scenarios.

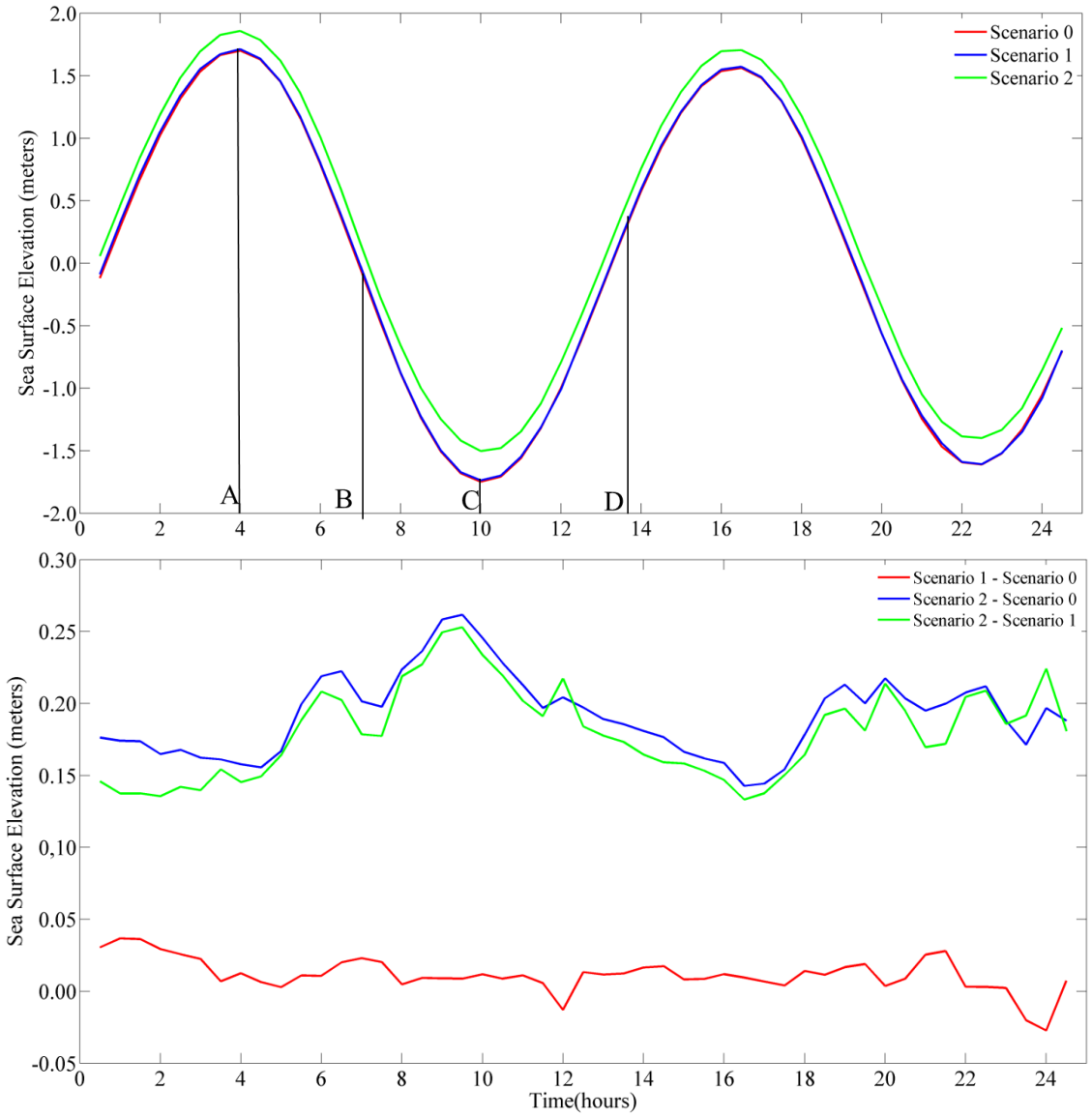

Figure 18. Comparison between normal and storm regimes as well as the reference scenario, for spring tide condition (upper panel). The vertical lines correspond to instants chosen to illustrate horizontal sea surface elevation fields. In the lower panel is represented the differences between all the scenarios.

The analysis of the SSE time series reveals that the normal wave climate (scenario 1) has no influence in the sea surface elevation, because there is an almost complete overlap of the lines of the scenario 1 and scenario 0. For the storm regime scenario (scenario 2) is found a clear over-elevation of the sea surface (wave set-up), and consequently the high and low tides have higher elevations. The differences between the numerical results are higher in low tide when compared with high tide (visible in the low panel of the figure). In the station analysed, the difference between scenarios 1 and 2 in the high tide is 14.5 cm, while in the low tide is about 25 cm. As mentioned before, the differences between the scenarios 0 and 1 are not substantial, however there is a slight over-elevation in scenario 1 not visible in the figure. In high tide, those differences are 1.3 cm, while in low tide are 1.2 cm. The analysis of the low panel of time series help to clarify that the differences between scenarios 0 and 1 (red line) are negligible. The highest difference between these scenarios is 3.6 cm. The figure also shows that the differences between blue and green lines corresponding to the differences between scenario 2 and 0, and between 2 and 1, respectively, never exceed 2.1 cm, therefore, for this station, only the storm waves (scenario 2) causes significant changes in SSE. In order to investigate if these differences are not significant for all the inlet area, the horizontal fields of the differences between SSE determined for scenarios 0 and 1 are performed and are presented in Figure 19. It is important to note that the vertical lines and correspondent letters, represented in Figure 18, correspond to instants chosen to illustrate the horizontal sea surface elevation fields. In order to analyse the time evolution of the spatial distribution of the SSE differences, the images A, B, C and D of Figure 19 corresponds to high tide, ebb condition, low tide and flood condition, respectively. Positive values mean that there is a wave set-up in the scenario 1 relatively to scenario 0.

The analysis of Figure 19 reveals that the differences between the scenarios 0 and 1 never exceed the 3 cm, being close to 0 for most of the area, therefore there are negligible. Thus, it is assumed that the SSE in scenarios 0 and 1 are equal. Taking this into account and to better visualize the effects of the wave characteristics, horizontal fields of the differences between scenarios 1 and 2 are performed and are presented in Figure 20. Positive values mean that there is a wave set-up in the scenario 2 relatively to scenario 1.

The patterns found in the illustration of the SSE time series (Figure 18) are also perceptible in the horizontal fields of SSE differences between scenarios 1 and 2 (Figure 20), verifying an over-elevation in scenario 2. Generally, the *Barra* beach (south to the inlet) is the most affected area by the coastal waves. In contrast, the *Meia Laranja* beach is the local where the wave set-up is smaller, because it is a sheltered zone.

Analysing the time evolution it is observed that at high tide (Figure 20 A) the differences between the scenarios are minimal, approximately 15 cm in whole inlet area. However, between the jetties there are areas where the differences are 17 cm. On the other hand, in the *Meia Laranja* beach the wave set-up is minimal (12 cm). In ebb condition (Figure 20 B), the differences increase to values around 19 cm in most of the inlet area. Close to the North jetty, the difference between the scenarios are lower (12 cm), while near to the South jetty, the difference is about 22 cm. In the low tide (image C), the differences reache a maximum of 21 cm in all the inlet area. In the flood condition (image D), the difference between the scenarios decrease to values about 13 cm.

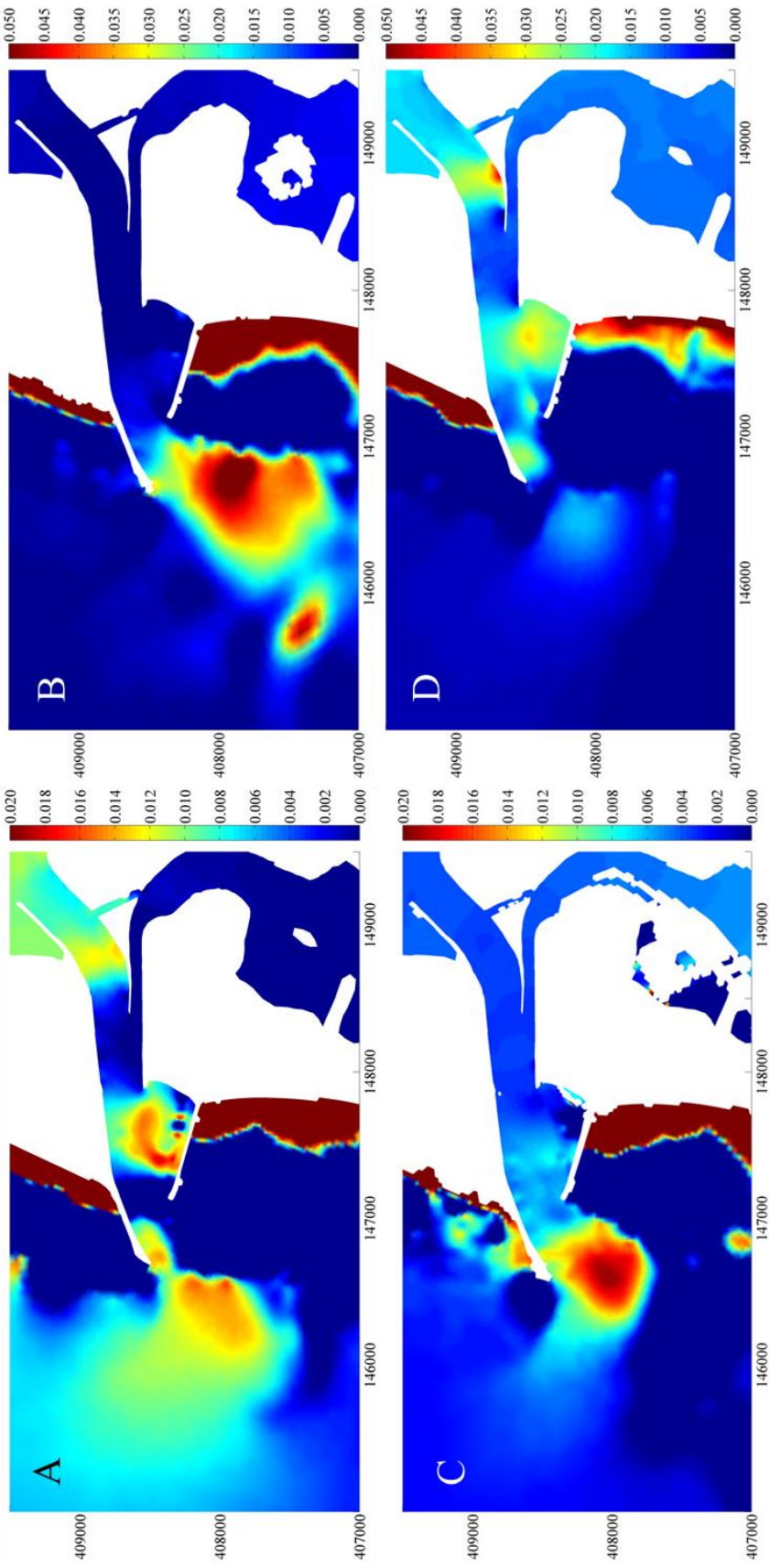

Figure 19. Horizontal fields of differences of sea surface elevation between scenarios 0 and 1 for spring tide condition, in meters. The letters correspond to the instants chosen to compute the horizontal fields, represented in Figure 18.

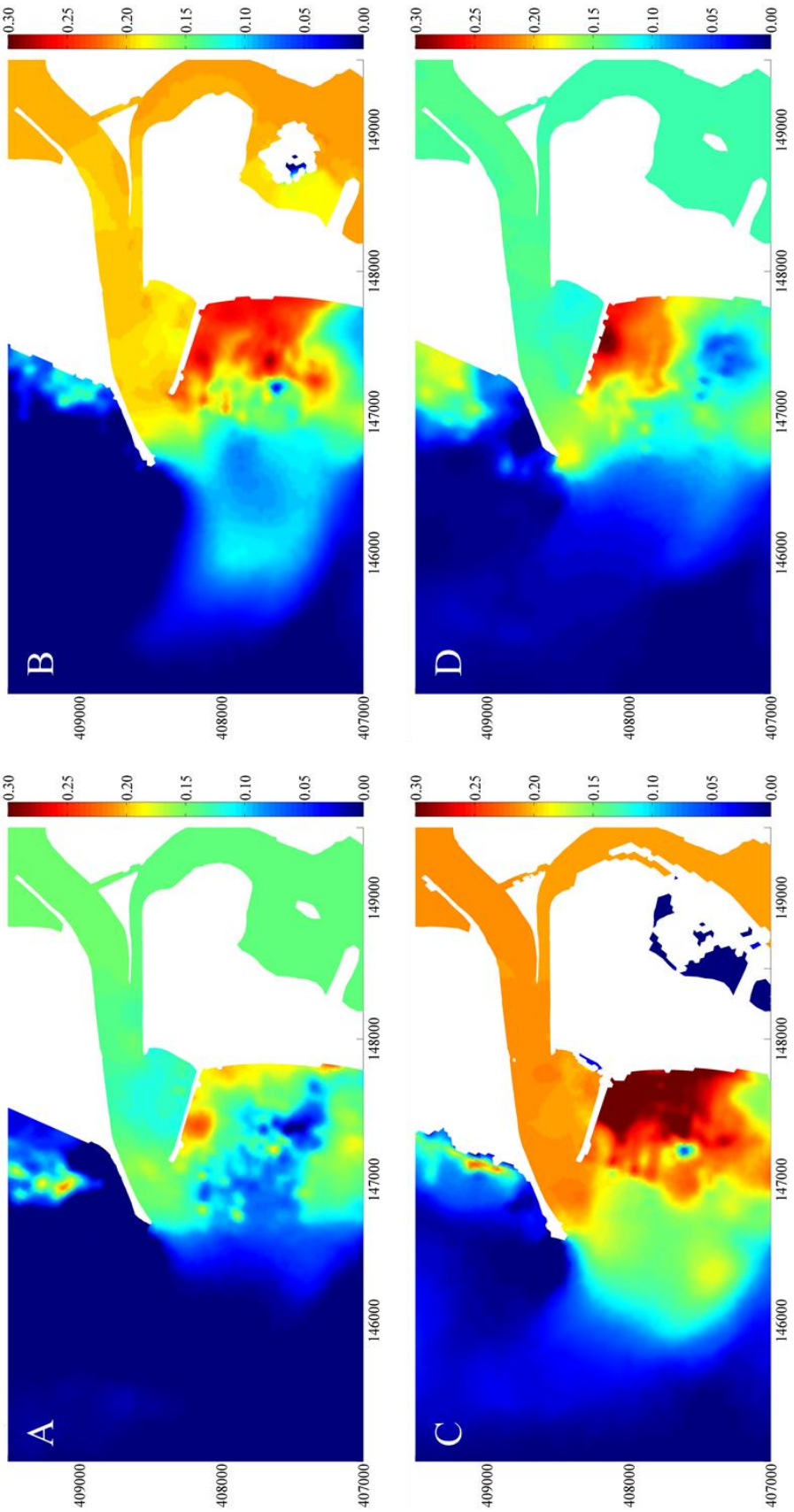

Figure 20. Horizontal fields of differences of sea surface elevation between scenarios 1 and 2 for spring tide condition, in meters. The letters correspond to the instants chosen to compute the horizontal fields, represented in Figure 18.

4.2.1.2. Intermediate Tide

The time series for the three scenarios mentioned before for the intermediate tidal condition are illustrated in Figure 21 for station 1 (upper panel). In order to better visualize the differences between the scenarios, the time series of the differences between all of them are illustrated in the lower panel.

Similarly to the spring tide condition, the normal wave climate (scenario 1) has no influence in the sea surface elevation while the storm regime scenario (scenario 2) shows a clear over-elevation of the sea surface elevation (wave set-up). The SSE differences are, once again, higher in low tide. In the station analysed, the difference between the scenarios 1 and 2 in high tide is about 13 cm, while in low tide is approximately 19 cm. As in the previous tidal condition, the differences between the scenario 0 and 1 are negligible, however there is a slight over-elevation in scenario 1. In the high tide, those differences are 1.8 cm, while in the low tide are 0.6 cm. These values are clearly visible in the low panel of the Figure 21.

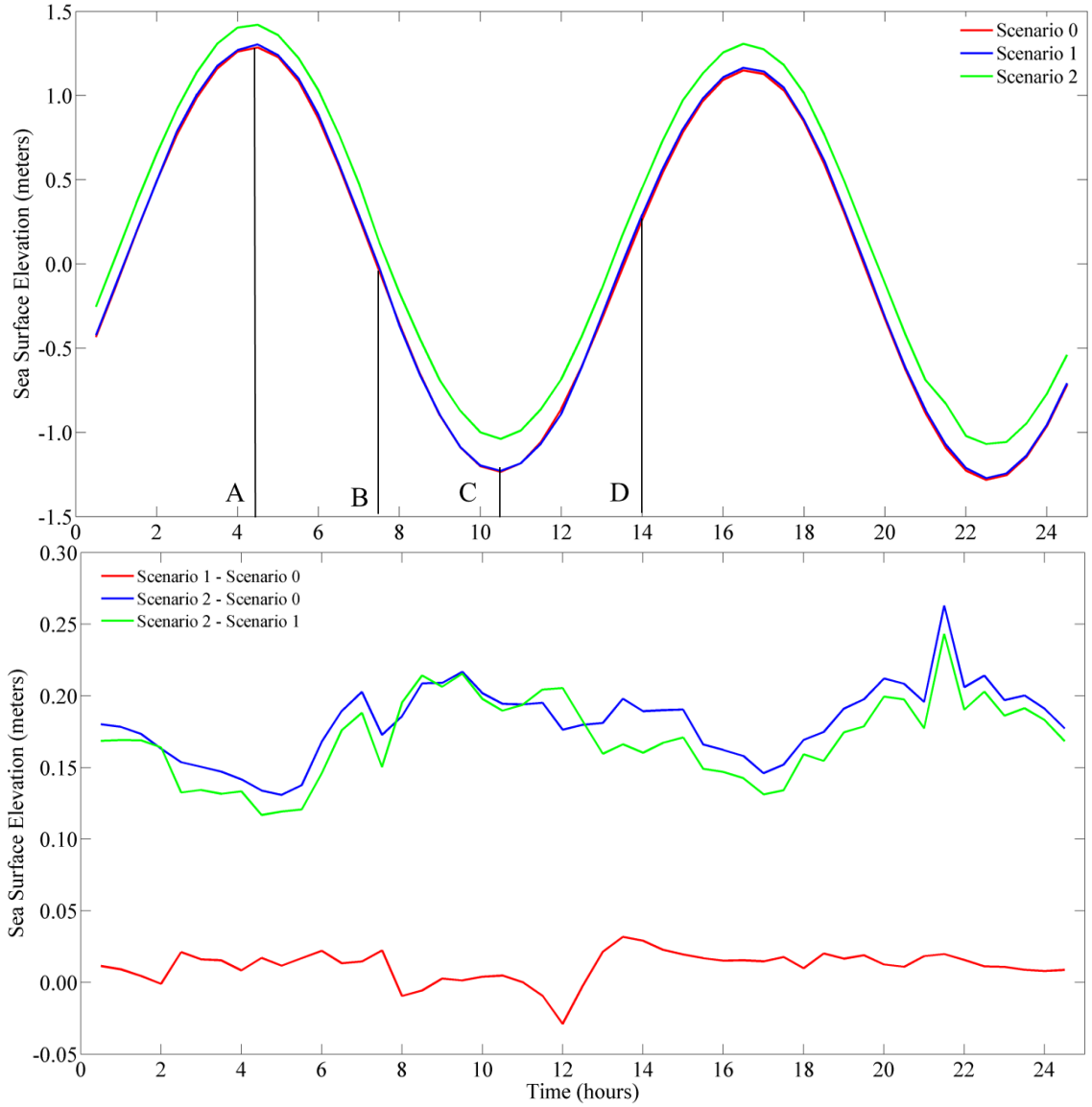

Figure 21. Comparison between normal and storm regimes as well as the reference scenario, for intermediate tide condition (upper panel). The vertical lines correspond to instants chosen to illustrate horizontal sea surface elevation fields. In the lower panel is represented the differences between all the scenarios.

The lower panel of Figure 21 lightens that the major differences are verified in scenario 2, because, as in spring tide condition, the differences between scenario 1 and 0 (red line) are close to 0, reaching a maximum of 3.2 cm. The blue and green lines corresponding to the differences between scenario 2 and 0, and between 2 and 1, respectively, reinforce the idea that there are no major differences between scenarios 0 and 1 (major differences between theses lines are 2.9 cm). Thus, it is possible to say that, for station 1, only the storm waves have influence in Sea Surface Elevation. In order to demonstrate that the differences between 0 and 1 are negligible in the entire inlet area, the horizontal fields of the differences between SSE for scenarios 0 and 1 are performed and are presented in Figure 22. Positive values mean that there is a wave set-up in the scenario 1 relatively to scenario 0. As before, the vertical lines and correspondent letters, represented in Figure 21, correspond to instants chosen to illustrate horizontal sea surface elevation fields. Similarly to the Spring tide condition, the differences in SSE between scenarios 0 and 1 never exceeds 3 cm in the entire inlet region, showing that the differences between scenarios 0 and 1 are negligible. Having this knowledge as a starting point, the horizontal fields of the SSE differences between scenarios 1 and 2 were performed and are presented in Figure 23. Positive values mean that there is a wave set-up in the scenario 2 relatively to scenario 1.

As referred in the analyses of time series (Figure 21), the wave set-up in the scenario 2 relatively to scenario 1 in the high tide (Figure 23 A) is about 13 cm. The difference between scenario 1 and 2 is constant in the entire inlet zone. In the ebb condition (image B), the patterns are similar to those obtained in the high tide, however the differences increase to values around 15 cm, reaching a maximum in the image C, corresponding to low tide condition. In this case, the differences between the scenarios are about 18 cm in most of the inlet area. However there are some places where the differences are higher, for example, between the jetties (location of the station previously analysed), with values close to 20 cm. In the flood condition, the wave set-up decrease again to values of about 14 cm, nevertheless in the region close to the North jetty the differences are 16 cm.

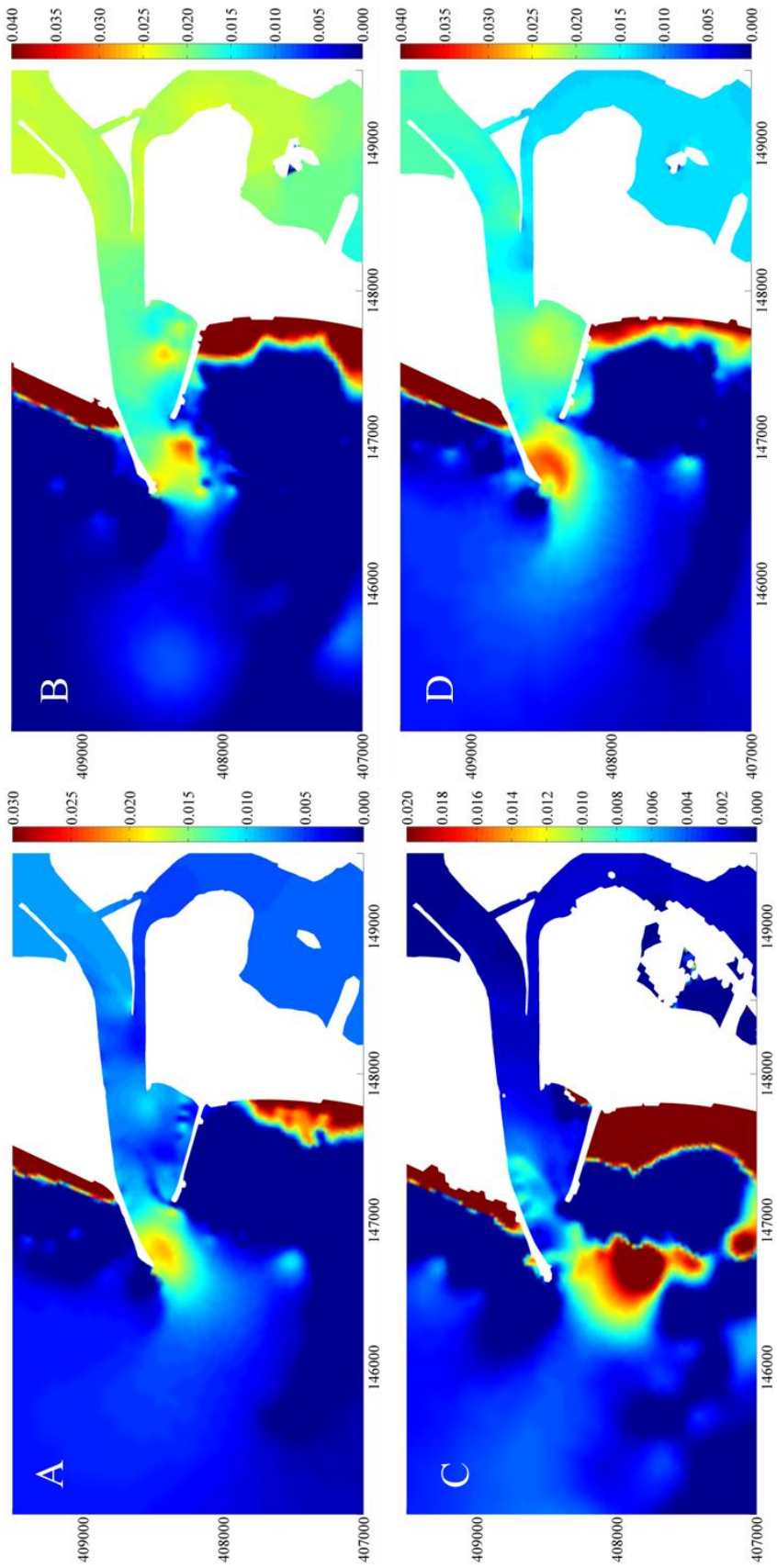

Figure 22. Horizontal fields of differences of sea surface elevation between scenarios 0 and 1 for intermediate tide condition, in meters. The letters correspond to the instants chosen to compute the horizontal fields, represented in Figure 21.

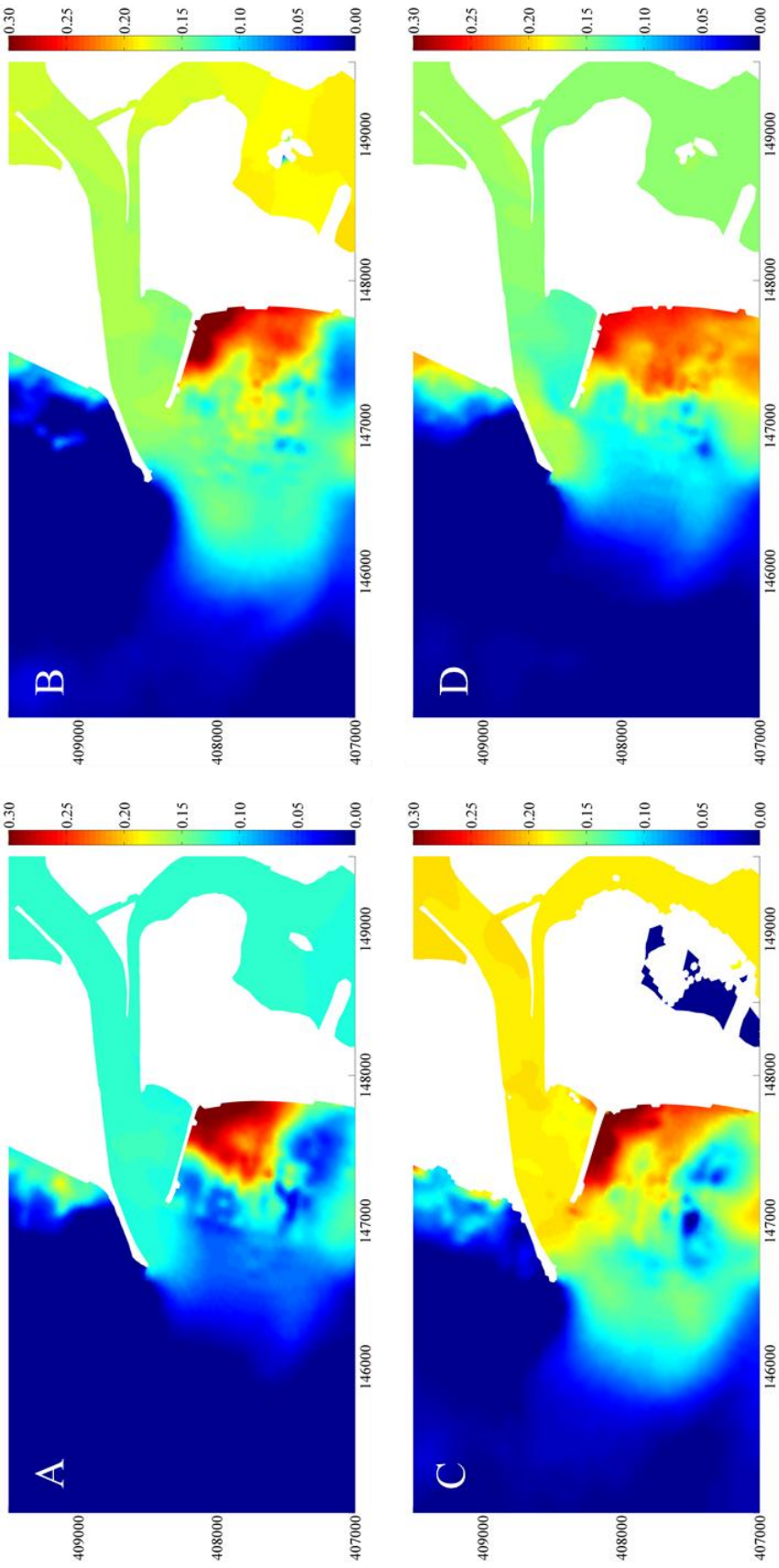

Figure 23. Horizontal fields of differences of sea surface elevation between scenarios 1 and 2 for intermediate tide condition, in meters. The letters correspond to the instants chosen to compute the horizontal fields, represented in Figure 21.

4.2.1.3. Neap Tide

The time series of SSE for the three scenarios under study for neap tide for station 1 is illustrated in Figure 24. Additionally, in order to get a better observation of the differences between the scenarios, the time series of the differences between all of them are illustrated in the lower panel.

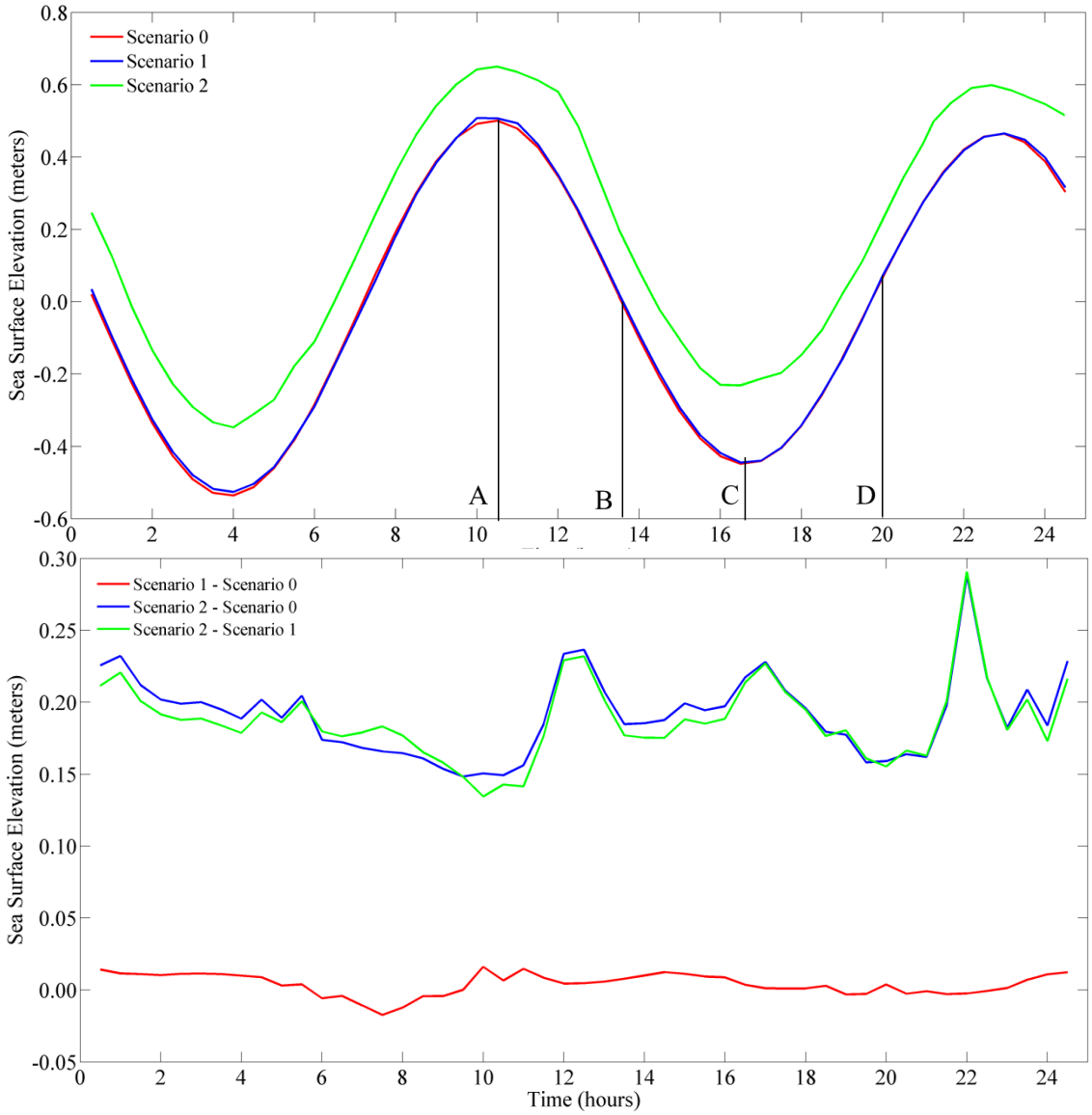

Figure 24. Comparison between normal and storm regimes as well as the reference scenario, for neap tide condition (upper panel). The vertical lines correspond to instants chosen to illustrate horizontal sea surface elevation fields. In the lower panel is represented the differences between all the scenarios.

As previously observed for the spring and intermediate tide conditions, the normal wave climate (scenario 1) has no influence in the sea surface elevation at the inlet and the storm regime scenario (scenario 2) shows a clear wave set-up. The difference between the scenarios 1 and 2 (visible in lower panel) in the high tide is 14.3 cm, while in the low tide is approximately 21.4 cm. As in the previous tidal regimes, the differences between the scenario 0 and 1 are negligible. In the high tide, those differences are 1 cm, while in the low tide are 0.65 cm. The lower panel of Figure 24 reinforces the idea that the

scenario 1 has no significant influence in SSE at the inlet, because the differences between scenarios 2 and 0 (blue line) are identical to the differences between scenarios 2 and 1 (green line). As expected, the differences between scenario 1 and 0 are close to 0, reaching a maximum of 1.6 cm. The analysis of Figure 24 shows, as in previous tidal conditions, that only the scenario 2 cause important changes in SSE. The influence of scenario 1 in the entire inlet area will be analysed, in more detail in Figure 25, that represents the horizontal fields of the differences of SSE between scenarios 0 and 1. Positive values mean that there is a wave set-up in the scenario 1 relatively to scenario 0.

As expected, the scenario 1 has no significant influence in SSE, because the difference between the scenarios never exceed 2 cm, being close to 0 in the majority of the instants studied. Taking this into account, the horizontal fields of the differences between scenarios 1 and 2 were computed and are presented in Figure 26. Positive values mean that there is a wave set-up in the scenario 2 relatively to scenario 1.

In high tide (image A), the SSE differences between the scenarios are minimal, revealing a wave set-up in scenario 2 of 13 cm relatively to scenario 1. In this case, the differences are higher in the Northern zone of the inlet, reaching a value of about 18.6 cm. In ebb condition (image B), the differences between the scenarios are approximately 18 cm in the inlet entrance, increasing gradually along the inlet channel, reaching values of 19.5 cm. As mentioned before, the maximum values are found in low tide (image C), where the differences are about 22 cm. In flood condition, the wave set-up decreases, presenting values of 14 cm for all the inlet area.

From the analysis performed for each tidal condition, was obtained the general pattern of the variations of SSE induced by the coastal waves. The results at the inlet reveal that the normal wave climate (scenario 1) has no influence in the sea surface elevation. For the storm regime scenario (scenario 2) was found a clear over-elevation of the sea surface (wave set-up). These results are consistent with the findings of Malhadas *et al*. [2009] for the Óbidos lagoon that concluded that there is a correlation between the wave height and the sea-level elevation only during high wave activity periods, when a significant wave set-up on lagoon sea level is observed.

The waves effect observed in the results obtained for the numerical model simulations are in agreement with the effect of waves found in the analysis of field data (section 4.1). The field data analysis shows a maximum of set-up induced by the waves of approximately 21 cm for a wave with *Hs* of 8 meters. The model results evidence results of the same order of magnitude, however in same instants, the over-elevation can reach values slightly higher than 25 cm.

The wave set-up found at the inlet in all the numerical results may be explained by the water gathering in the inlet zone caused by the constant wave propagation and consequently breaking inside the Ria de Aveiro inlet. The differences are higher during ebbing and consequently in the low tide, because in this case the waves propagation and tidal currents have opposing directions. In this circumstance there is a wave's compression, with a decrease in their wavelength and an increase in their amplitude. Thus, in the normal regime the tide acts almost as a single forcing agent, while in the storm regime scenario the constant wave propagation in the opposite direction of the tidal currents causes higher water retention in the inlet.

All the study area is exposed to the wave set-up, however the most affected zone is the *Barra* beach. This may be explained by the Southwestard direction of the storm waves, causing water retention between the South jetty and the beach, producing a constant wave set-up in that zone. Contrarily, the *Meia Laranja* beach located in a sheltered zone is characterized by a lower set-up.

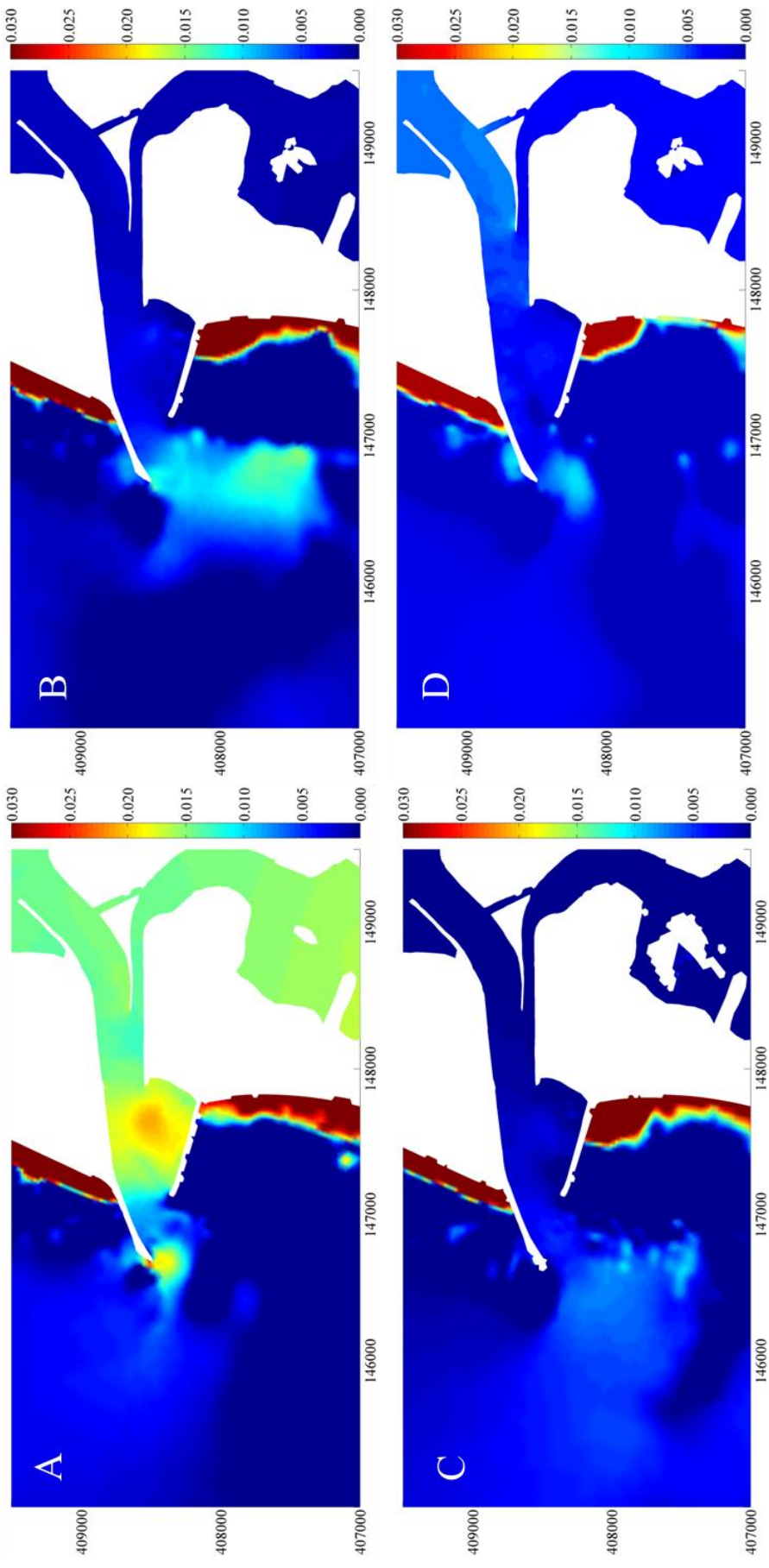

Figure 25. Horizontal fields of differences of sea surface elevation between scenarios 0 and 1 for neap tide condition, in meters. The letters correspond to the instants chosen to compute the horizontal fields, represented in Figure 24.

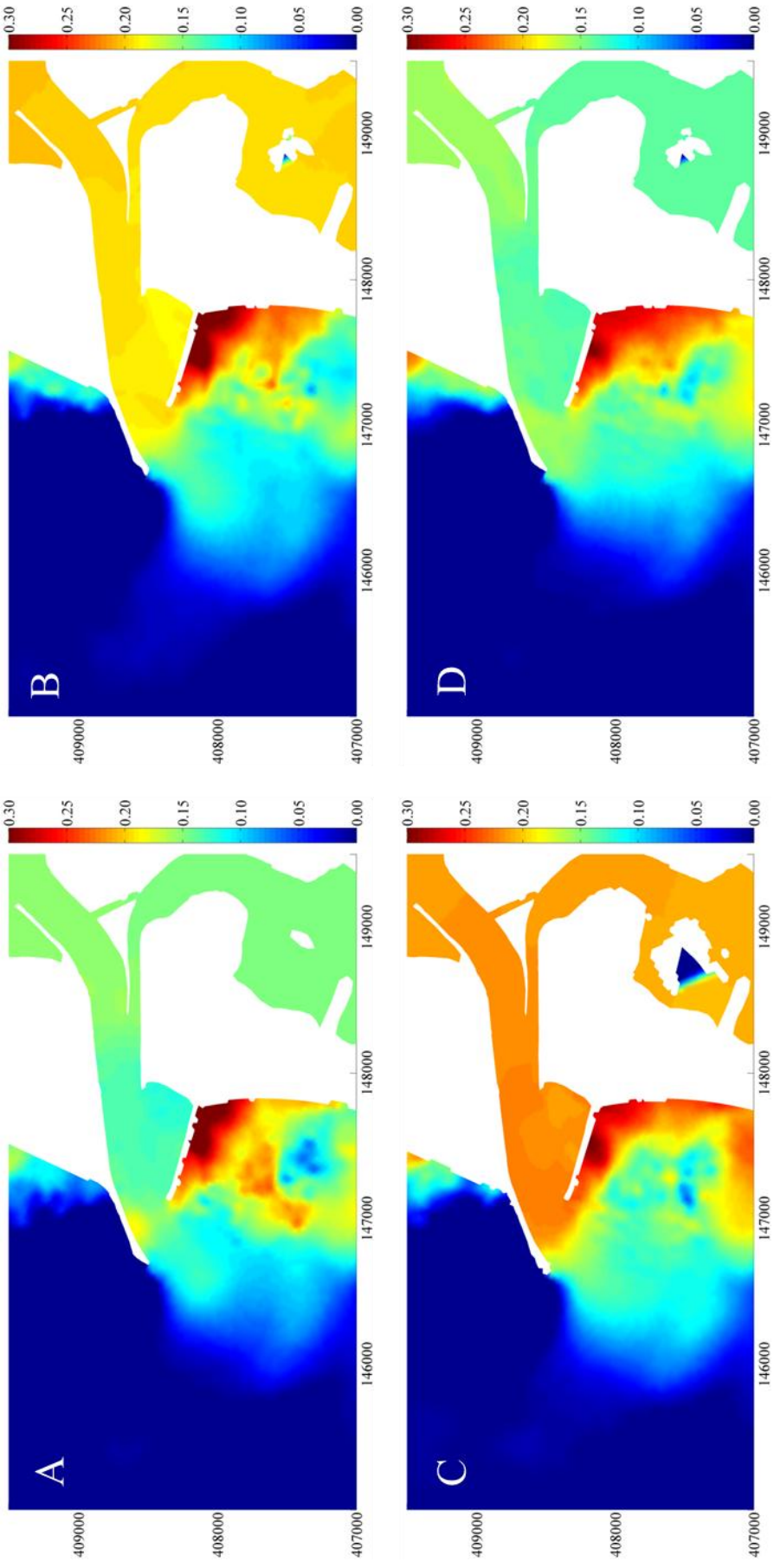

Figure 26. Horizontal fields of differences of sea surface elevation between scenarios 1 and 2 for neap tide condition, in meters. The letters correspond to the instants chosen to compute the horizontal fields, represented in Figure 24.

These results in SSE may have a considerable impact in Ria de Aveiro hydrodynamics. With the knowledge that the higher elevation induced by a storm surge registered in Ria de Aveiro was 1 meter, these values of wave set-up corresponds to approximately 20% of this value. Supposing that these wave set-up propagates into the lagoon, the margins of Ria de Aveiro may inundate. If the high wave climate coincides with a condition of spring tide, heavy rainfall and with the occurrence of a storm surge, the effects can be even higher.

It was also found that the effect of coastal waves at the Ria de Aveiro inlet is independent of tidal range, as there are no differences in the over-elevations determined for each tidal condition under study.

4.2.2. Current Velocity

In this section, the effect of the waves in the current velocity at Ria de Aveiro inlet is evaluated. Firstly, the velocities in the three scenarios are compared, through the representation of the horizontal fields in the same instants chosen to illustrate the horizontal SSE fields. Posteriorly, the horizontal fields of the differences between scenarios 1 and 2 are illustrated. All these analyses are performed for each tidal condition.

4.2.2.1. Spring Tide

The horizontal fields of the velocity intensity for the three scenarios, for the instants in study, are shown in Figure 27. To recall, the images A, B, C and D are illustrative of high tide, ebb condition, low tide and flood condition, respectively.

Starting with the comparison between scenario 0 (tide only) and scenario 1 (tide + normal wave climate), it was found that, in general, the waves considered in scenario 1 have no significant influence in the current velocity, due to the similarity between the patterns (in the inlet area) in scenario 0 and 1. The near shore zone is excluded of the analysis, because the goal of this study is focused in the inlet area. The other reason is that due to the waves breaking in the beaches, the velocity shows changes with chaotic patterns.

In images A of Figure 27, the current velocity has small values in the axis of the channel because this instant corresponds to a high tide period. The patterns and the order of magnitude of velocity in scenarios 0 and 1 are similar, however for high wave activity (scenario 2) a slight increase of the current velocity, reaching 1.3 ms^{-1} in the deeper areas of the inlet, is observed.

As expected, the current velocity in ebb condition (images B) is highest, reaching a value of 2.5 ms^{-1}. At the inlet area, the patterns and the order of magnitude of the current velocity are similar in scenarios 0 and 1. In scenario 0, the strong ebb current reaches the offshore zone, with velocities between 1.5 and 2 ms^{-1}. An identical pattern is observed in scenario 1, nevertheless with lower intensity, because the tide and waves act as opposite forces, minimizing the current velocity. In scenario 2, the waves coming from SW 'push' the ebb current to North, increasing its magnitude, to values between 2 and 2.5 ms^{-1}. Into the inlet, the velocity has a slight increase in scenario 2 when compared with scenario 1.

In low tide (images C), the current velocity is smaller when compared with ebb condition. The current patterns between scenario 0 and 1 are similar, with velocities of about 0.8 ms^{-1} in the axis of the channel. In the scenario 2, the patterns remain identical, with a slight increase of the velocity.

In the flood condition (images D), the comparison of current velocity between scenarios 0 and 1 in the interior of the inlet, show that the waves of scenario 1 have no influence in the current velocity. Thus, in scenarios 0 and 1, the velocity reaches maximum values of 1.8 ms^{-1} in the deeper areas of the inlet. In scenario 2, the velocity patterns are similar, however there is an increase of velocity, reaching 2.0 ms^{-1}. In this scenario, it are observed high velocities for all channel width, consequently the velocities in the inlet margins are higher when compared to those found for the scenarios 0 and 1.

From the analysis of Figure 27 it can be verified that in scenario 1 the tidal currents have more influence than the currents induced by waves. Nevertheless, in scenario 2 the presence of a combined effect of tidal currents and waves is observed. Then, the horizontal fields of the differences of current velocities between scenarios 1 and 2 are represented in Figure 28. Positive values represent higher velocities in the scenario 2, while negative values denote that the velocity is higher in the scenario 1.

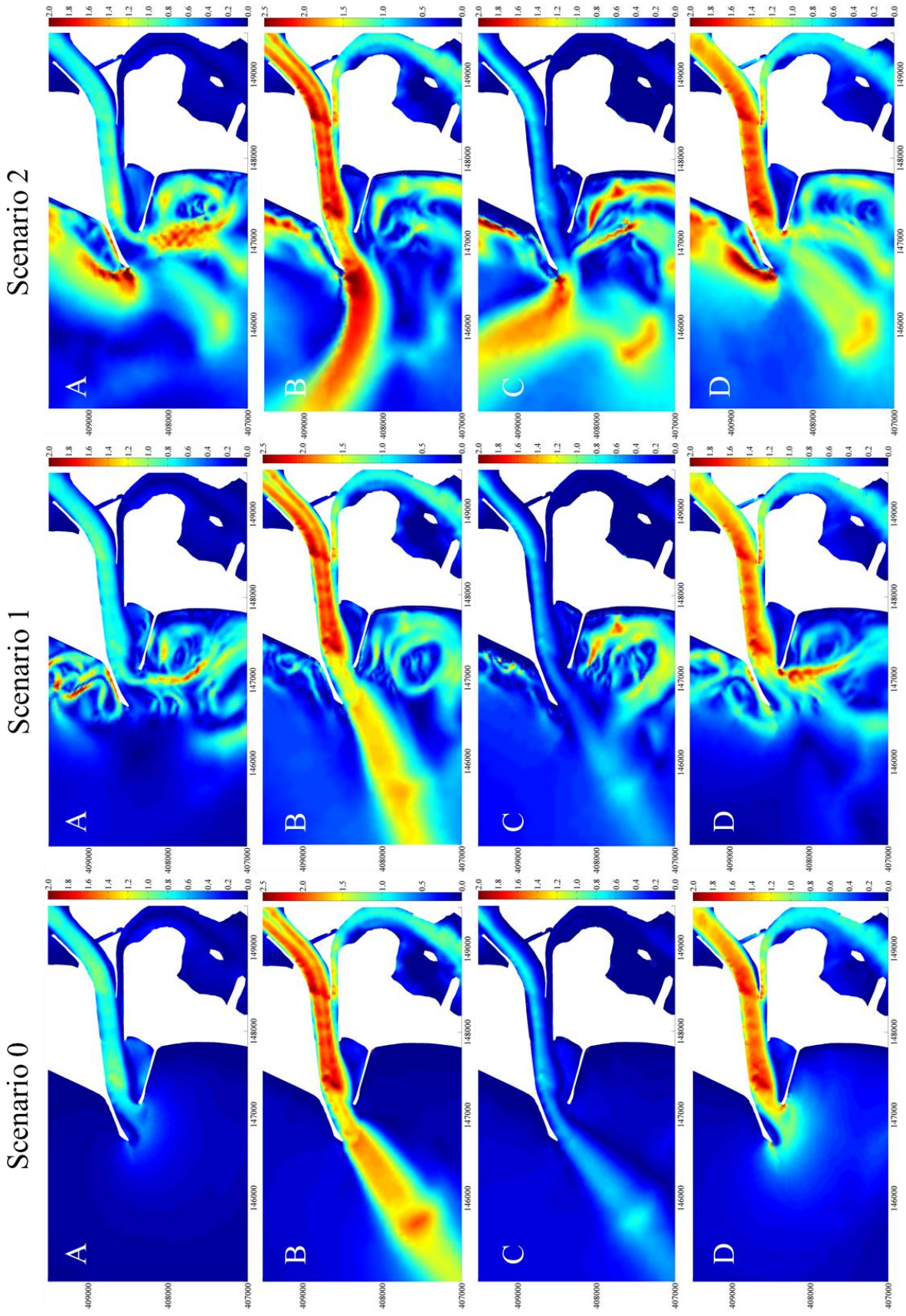

Figure 27. Representation of the velocity intensity in spring tide condition for the three scenarios, in m/s. The letters correspond to the instants chosen (presented in Figure 18) to represent the horizontal fields.

Figure 28 A represents the difference between the scenarios 1 and 2 in the high tide. In this condition, the storm waves coming from SW increases the current velocity close to the South jetty and in the axis of the channel (deeper areas), where the velocity differences reaches 0.35 ms^{-1}. Out of the central region of the inlet, the velocities are higher in the scenario 1, reaching a maximum difference of 0.33 ms^{-1}, close to the North jetty.

The horizontal field of the differences of current velocity at ebb condition represented in Figure 28 B, indicates that the currents induced by waves have lower importance when compared with the tidal currents, which in the ebb condition are very strong. Thus, in the offshore zone exists an area Northern of the inlet where the velocity is higher in scenario 2 (difference of 0.6 ms^{-1}), while Southern of the inlet the velocity is higher in scenario 1. This is justified by the ebb current that comes out the inlet. In scenario 1, the ebb current has the same orientation of the jetties, while in scenario 2 the waves coming from SW, 'push' the ebb current to North. Inside the inlet, the differences between the scenarios are constant, revealing an increase of velocity of 0.1 ms^{-1}, for scenario 2, in the entire study area. The exception is close to *Meia Laranja* beach, where the velocity is higher in scenario 1.

The image C (low tide) illustrates the same velocity patterns, inside the inlet, when compared to the ebb condition (image B). With exception to the area close to *Meia Laranja* beach, the velocity in scenario 2 is higher comparing with scenario 1. The difference value is uniform for all the inlet area (0.1 ms^{-1}).

In flood condition (image D), the differences are higher when compared to low tide. Close to the North jetty, the velocity is higher in scenario 2, revealing differences of 0.39 ms^{-1}. This may be explained due to the combined effect of flood current with the SW storm waves that break in the North jetty, leading to an increase of the velocity in this area. In most of the central channel of the inlet, the velocity increases about 0.15 ms^{-1} in scenario 2. On the other hand, in the region close to the South jetty, the velocity is higher in the scenario 1, because the waves coming to NW breaks in the South jetty, increasing the velocity in this zone.

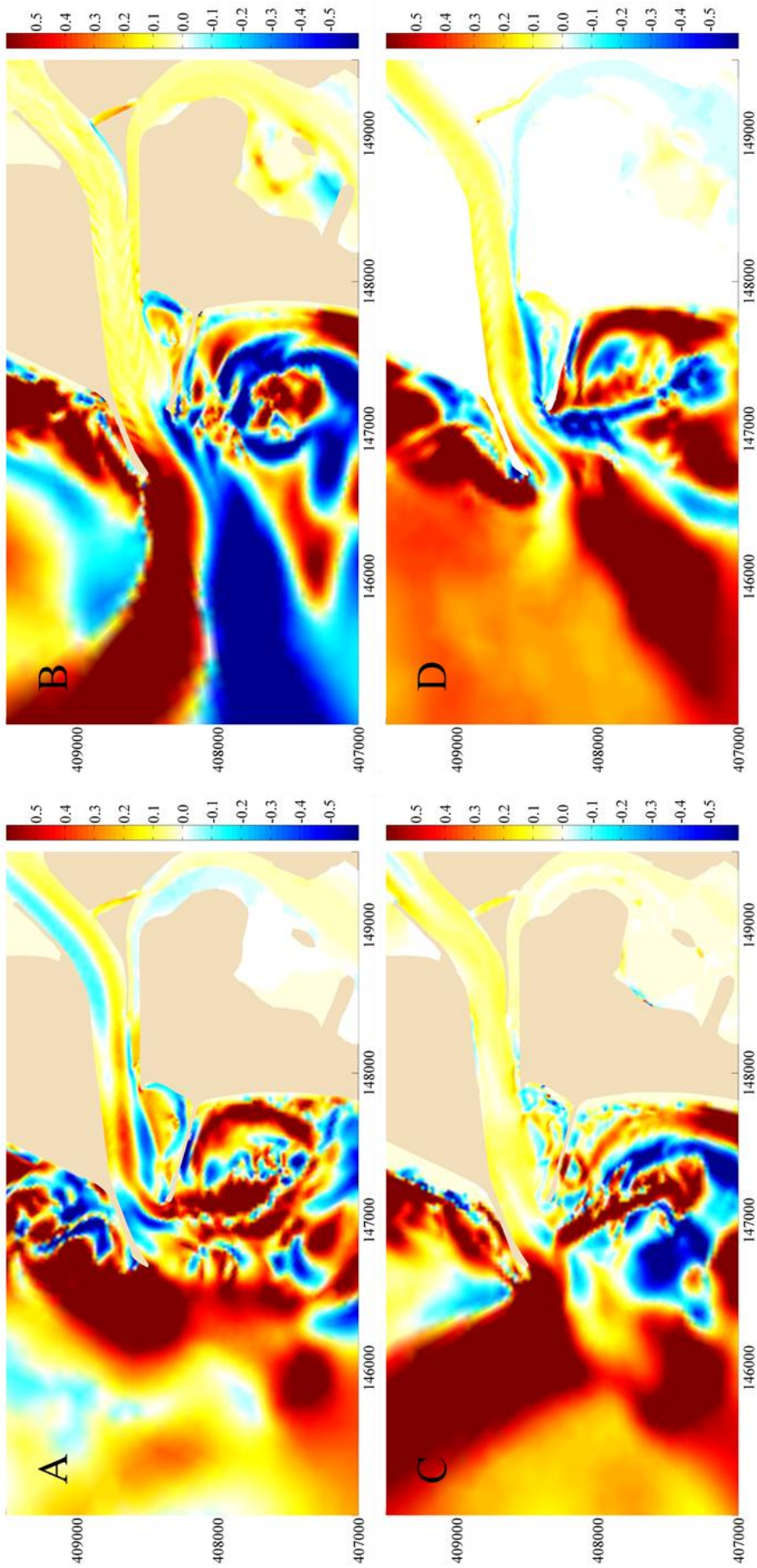

Figure 28. Horizontal fields of differences of the current velocity between scenarios 1 and 2 in spring tide condition, in m/s. The letters correspond to the instants chosen (presented in Figure 18) to represent the horizontal fields.

4.2.2.2. Intermediate Tide

The horizontal fields of the current velocity for the three scenarios are illustrated in Figure 29, for the instants in study. The images A to D correspond to the high tide, ebb condition, low tide and flood condition, respectively.

In general, comparing the three scenarios, it is verified that the velocity patterns found in scenario 0 (tide only) and in scenario 1 (tide + normal wave climate) are similar. Comparing the scenario 2 (tide + storm wave climate) with the other scenarios in study, some changes in the velocity patterns are observed, mainly in images B and D, corresponding to ebb and flood condition, respectively.

In high tide (images A), the difference between the three scenarios is negligible. Into the inlet area, in the central zone of the channel, the velocity is about 1.0 ms^{-1}, reaching values of 1.3 ms^{-1} in some restricted areas (deeper zones).

The image B shows, as in spring tide, a strong ebb current in the central channel, with velocities between 1.5 and 1.65 ms^{-1}, reaching 1.9 ms^{-1} in the deepest area of the inlet. Although inside the inlet there is a slight increase of the velocity in the scenario 2, what becomes evident is the ebb current being 'pushed' to North due the SW storm waves. This pattern was also observed in spring tide condition.

In low tide (images C), the current velocity is lower than the verified in the ebb condition. In the scenarios 0 and 1, the velocity in the axis of the inlet ranges between 0.47 and 0.61 ms^{-1}. The velocity patterns between these two scenarios are similar. The main difference is, due the NW waves, the tidal current in scenario 1 is pushed Southward, incrementing the velocities close to the South jetty (maximum of 1.06 ms^{-1}). The opposite pattern is observed in scenario 2, leading to high velocities near the North jetty (1.59 ms^{-1}). Into the inlet area the velocity is higher in scenario 2 (about 0.1 ms^{-1}).

In images D, corresponding to flood condition, the velocity pattern between scenarios 0 and 1 is similar. In most areas of the inlet, the velocity magnitude ranges between 1.01 and 1.21 ms^{-1}, with exception of the deepest zone of the inlet, where the velocity is 1.44 ms^{-1}. Comparing the scenario 2 with the scenarios 0 and 1, the differences are clear.

Thus, in order to study the differences between scenario 1 and 2, and since there are no considerable differences between scenarios 0 and 1, the horizontal fields of the current velocity differences between scenarios 1 and 2 is computed and illustrated in Figure 30. As in the previous tidal condition, positive values represent higher velocities in the scenario 2, while negative values denote that the velocity is higher in the scenario 1.

Figure 30 A shows small differences between scenarios 1 and 2, however in the upper region of the inlet, the velocities are higher in scenario 1. The magnitude of the difference is 0.07 ms^{-1}, reaching a maximum of 0.28 ms^{-1} between the jetties. In the Southest area of the inlet, the scenario 2 presents higher velocities (0.04 ms^{-1}).

In ebb condition (Figure 30 B), the velocity in scenario 2 is higher in all the inlet area, with differences ranging between 0.02 and 0.08 ms^{-1}. Close to the North jetty, the difference is about 0.45 ms^{-1}, while in the South jetty, the velocity is higher in scenario 1 (0.16 ms^{-1}). This might be justified by the inflection of the ebb current forced by the orientation of the storm waves.

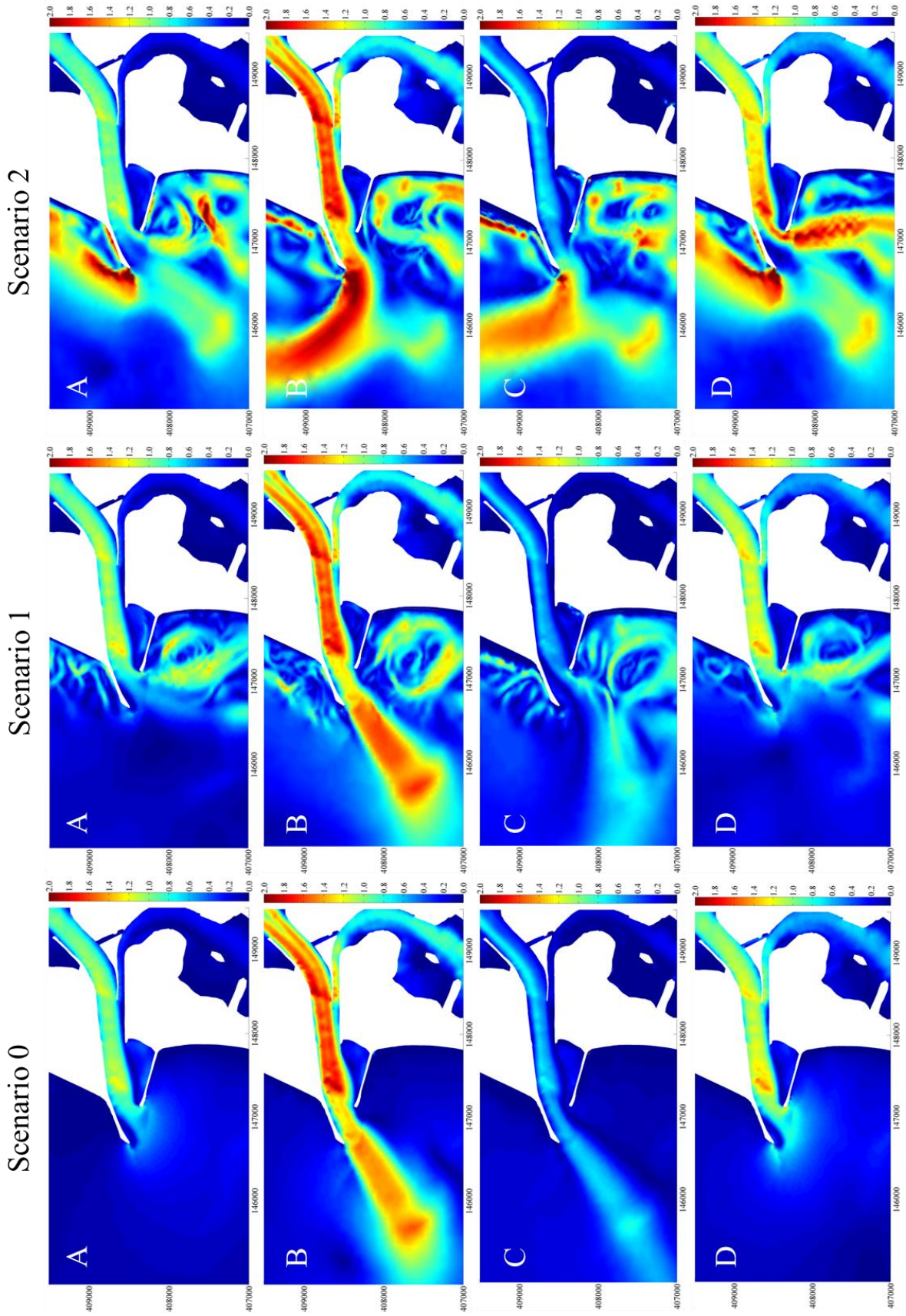

Figure 29. Representation of the velocity intensity in intermediate tide condition for the three scenarios, in m/s. The letters correspond to the instants chosen (presented in Figure 21) to represent the horizontal fields.

As mentioned and explained in the analysis of Figure 29, in low tide, the direction of the waves in scenarios 1 and 2 are very relevant. In scenario 1 the tidal current is pushed Southward, incrementing the velocities close to the South jetty, while in scenario 2 the opposite pattern is observed, leading to high velocities near the North jetty. Consequently, it is observed in Figure 30 C that the velocity close to North jetty is higher in scenario 2 (0.43 ms^{-1}) while in the South jetty, the velocity is higher in scenario 1 (0.47 ms^{-1}). In the remaining inlet region, the velocity is higher in the scenario 2, with differences ranging between 0.04 ms^{-1} and 1.1 ms^{-1}.

The differences between the scenarios in the flood condition (Figure 30 D) are considerable. In the axis of the inlet channel, the velocity is higher in scenario 2 with a magnitude difference of 0.53 ms^{-1} close to the South jetty, decreasing gradually into the inlet, achieving differences of about 0.18 ms^{-1} in its upstream zone. Close to the North jetty the velocity is higher in scenario 1, where the maximum differences reach 0.51 ms^{-1}.

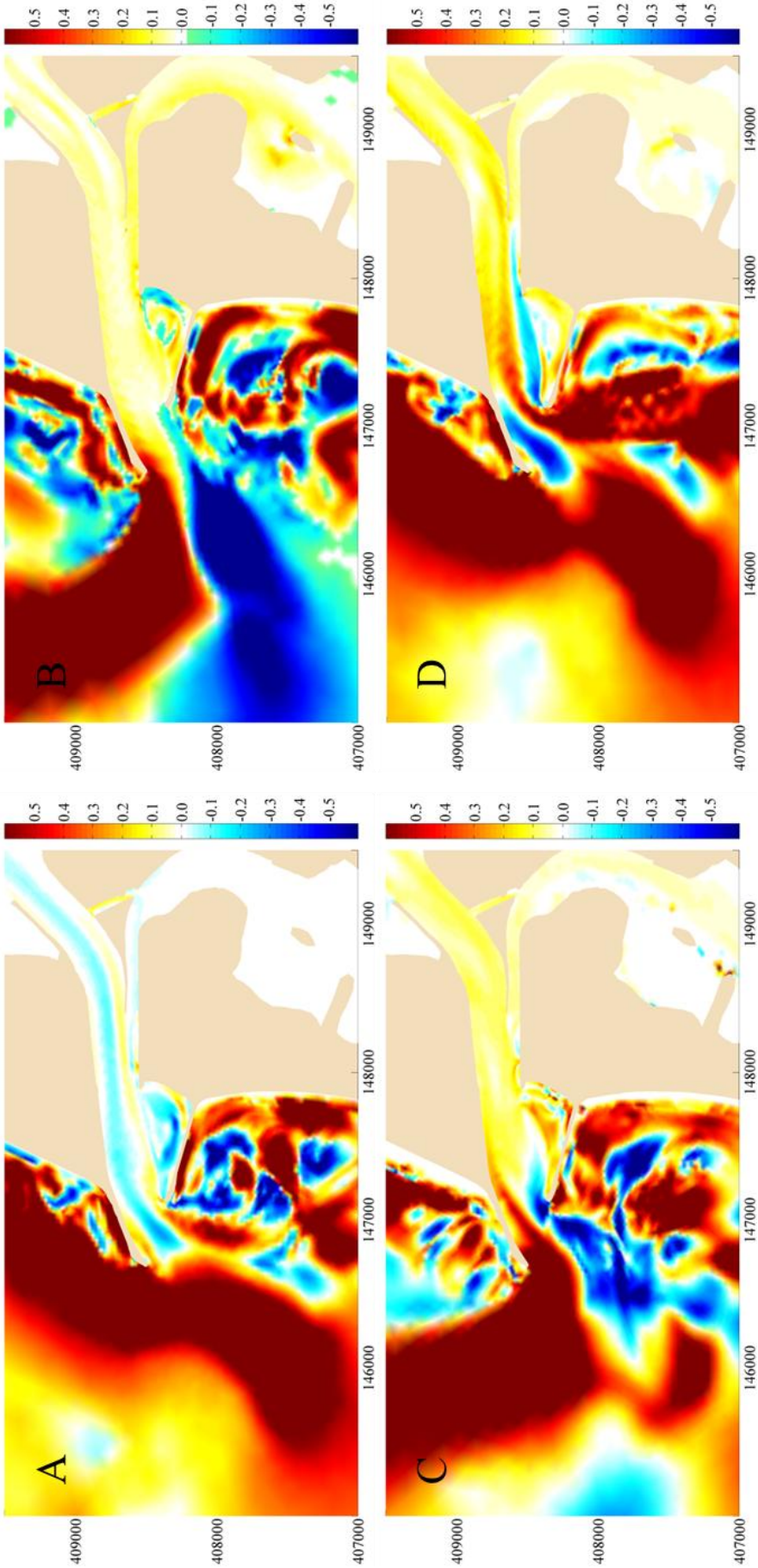

Figure 30. Horizontal fields of differences of the current velocity between scenarios 1 and 2 in intermediate tide condition, in m/s. The letters correspond to the instants chosen (presented in Figure 21) to represent the horizontal fields.

4.2.2.3. Neap Tide

The horizontal fields of the velocity for the three scenarios in study are computed and illustrated in Figure 31, for high tide (A), ebb condition (B), low tide (C) and flood condition (D).

The first analysis of the Figure indicates, as expected, that the current velocity in the neap tide is significantly lower when compared with spring and intermediate tidal conditions. It is important to note that the scale adopted in Figure 31 is different of the one used in Figures 27 and 29.

In Figure 31 A, is observed a slight increase of current velocity in scenario 1 when compared with scenario 0. However major differences are observed in scenario 2, in comparison with scenarios 0 and 1. In the central axis of the channel, in scenario 1, the velocity range between 0.41 and 0.46 ms^{-1}. In scenario 2, the region where the velocity is higher is in the Northern area of the inlet: 0.85 ms^{-1}, reaching a maximum of 0.96 ms^{-1}. In the central area, the velocity is close to 0 ms^{-1}, while in the Southern area, the velocity increases again to values around 0.62 ms^{-1}. Thus, the differences between scenario 2 and the reference scenario (0) seem clear.

In the ebb condition (images B), the patterns found in scenarios 0 and 1 are similar. In the central zone of the channel, the velocity range between 0.67 and 0.82 ms^{-1}, decreasing between the jetties, with values of about 0.48 ms^{-1}. In scenario 2, the current patterns are identical, however an increase of velocity is observed. In the axis of the channel, the velocity range between 0.72 and 0.84 ms^{-1}, while between the jetties the velocity is approximately 0.79 ms^{-1} close to the North jetty and 0.45 ms^{-1} near the South one.

In the low tide (images C), the velocity patterns inside the inlet for the three scenarios are similar. The velocities are lower when compared with the ebb condition, and are relatively constant in the central channel of the inlet, with values of about 0.30 ms^{-1}.

In the flood condition (images D), the velocity increases again. The velocity patterns between scenarios 0 and 1 are similar. However, in scenario 1, the velocity is higher when compared with reference scenario (scenario 0). In scenario 0, the velocity is about 0.55 ms^{-1} in the major part of the channel, reaching a maximum of 0.75 ms^{-1}. In scenario 1, the velocity in the central channel range between 0.57 and 0.65 ms^{-1}, reaching a maximum of 0.84 ms^{-1}. Nevertheless, the highest differences are observed in scenario 2. The waves coming from SW 'push' the flood current to the Northern zone of the inlet, leading to a substantial velocity increase in this area, reaching a value of 1.034 ms^{-1}. Consequently, the velocity in the Southern area of the inlet is smaller (close to 0.1 ms^{-1}) when compared with scenario 1.

Based on these results, the horizontal fields of the current velocity differences between scenarios 1 and 2 are represented in Figure 32. Positive values represent higher velocities in the scenario 2, while negative values means that the velocity is higher in the scenario 1.

As mentioned in the analysis of Figure 31 A, corresponding to the high tide, the scenario 2 reveals a considerable increase of the velocity Northern of the inlet channel, a decrease in the centre and an increase in the Southern area of the inlet. As expected, this pattern is observed in the horizontal fields of the current velocity differences between scenarios 1 and 2. In the Northern area of the channel, the velocity is higher in scenario 2 with values of 0.44 ms^{-1}, reaching a maximum of 0.72 ms^{-1}. In the central area, the velocity is higher in scenario 1 (maximum of 0.38 ms^{-1}), while in the Southern area of the channel, the velocity is higher in scenario 2, with a value of 0.41 ms^{-1}.

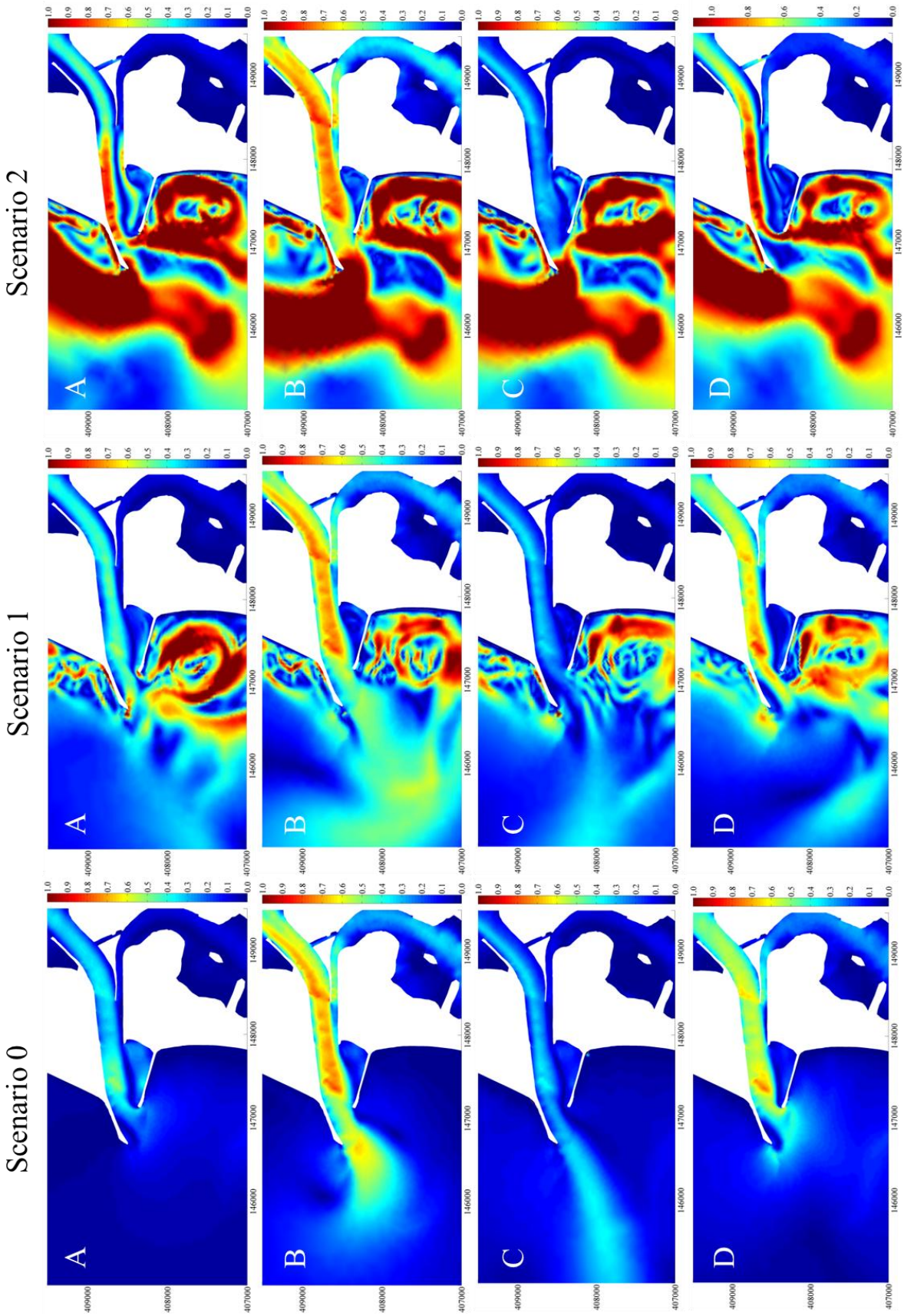

Figure 31. Representation of the velocity intensity in neap tide condition for the three scenarios, in m/s. The letters correspond to the instants chosen (presented in Figure 24) to represent the horizontal fields.

In ebb condition (Figure 32 B), the velocity, in scenario 2, is higher in the entire inlet area, with exception to the zone close to South jetty. In more detail, close to the North jetty major differences are observed (0.77 ms^{-1}). Close to the South jetty, the velocity is higher in scenario 1 (0.20 ms^{-1}). In the central channel of the inlet, the difference between the scenarios never exceeds 0.1 ms^{-1}, with the exception of the Southern zone, where the velocity difference can reach 0.21 ms^{-1}.

In Figure 32 C, corresponding to low tide, the difference between the scenarios inside the inlet is not significant. More specifically, as in previous tidal conditions, the velocity in the North jetty is higher in scenario 2 (0.57 ms^{-1}). On the other hand, in South jetty the velocity is higher in the normal wave climate scenario, with a difference of about 0.27 ms^{-1}. In the central area of the channel, the differences range between 0.02 (higher in scenario 2) and -0.02 ms^{-1} (higher in scenario 1). Then, it was found that, inside the inlet there are no important differences between the scenarios in this situation.

As mentioned before, in the flood tide situation (Figure 32 D), in scenario 2, the waves coming from SW 'push' the flood current to the Northern region of the inlet, with a significant increase of the velocity in this area (0.35 ms^{-1}). On the other hand, in scenario 1, the flood current enters in the lagoon in the central area, thus the velocity in this zone is higher in scenario 1 (maximum of 0.47 ms^{-1}). Close to the jetties, the velocity is higher in scenario 2. In the North jetty, the difference is about 0.35 ms^{-1}, although in the South one, the difference is 0.57 ms^{-1}. Between the jetties, the velocity is higher in scenario 1, reaching a maximum of 0.39 ms^{-1}.

From the analysis performed for each tidal condition, can be discussed the general patterns of the current velocity induced by the coastal waves. The pattern of the velocities difference between the scenarios is not as well defined as that found for the sea surface elevation. The regions with higher differences between the scenarios are offshore the inlet and near shore, Northward and Southward the inlet. This is justified considering that there are important differences in the current velocities in the breaking zone (where they show a chaotic pattern), which are dependent on the characteristics of the waves adopted for each scenario.

From the analysis of the previous results it was found that the currents in the Ria de Aveiro inlet are mainly tidal currents, however the currents induced by storm waves must be taken into account. In reality, it was verified that the currents induced by the waves interacts with the tidal currents, modifying its magnitude and direction. Therefore, the direction of the waves is an important factor, because it was observed that the waves can cause changes in the main flow direction.

In general, it was observed that, in the majority of situations analysed, the high wave climate (scenario 2) increases the velocity inside the inlet. This may be explained considering that the wave set-up caused by the storm waves (studied in subsection 5.2.1) creates a higher gradient pressure between the offshore sea level and the lagoon sea level, and consequently the velocity increases.

Other important pattern found in the majority of situations studied is that the velocity, in scenario 2, is higher close to the North jetty. On the other hand, in the South jetty, the velocity is higher in scenario 1. This happens because the waves in scenario 1 are Southward, breaking in the South jetty, whereas the waves coming from SW, in the high wave scenario breaks against the North jetty, increasing the velocity surrounding this zone.

In some shallow zones, for example in *Meia Laranja* beach, the velocity in some instants is higher for scenario 1. In this case, due the low depth of these areas, the velocity will be lower in scenario 2, since the increase in the total water column height is higher, and therefore by continuity the velocity will decrease.

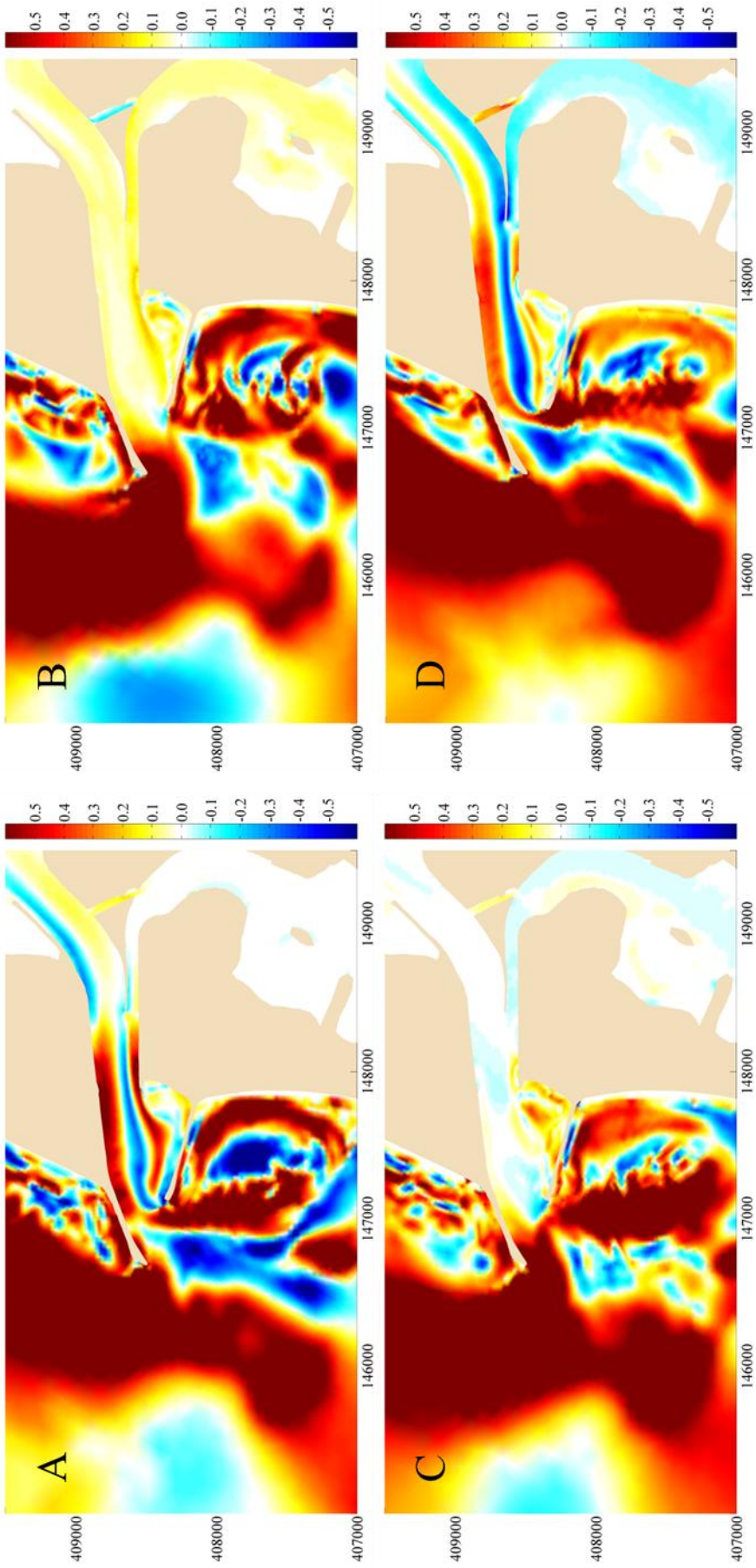

Figure 32. Horizontal fields of differences of the current velocity between scenarios 1 and 2 in neap tide condition, in m/s. The letters correspond to the instants chosen (presented in Figure 24) to represent the horizontal fields.

These results may have an important effect, for instance, in the sediment transport, because the changes in the current velocity may modify the patterns in its transport. In fact, the scientific community have it into regard. In Ria de Aveiro, the majority of the morphodynamics studies take into account the tidal forcing as well as the coastal waves. As example, Plecha *et al*. [2011], performed the evaluation of single waves effects on the morphologic evolution of a Ria de Aveiro lagoon inlet, concluding that the wave induced residual sediment fluxes in the cross sections upstream the lagoon mouth are smaller in magnitude than at the inlet, restricting the influence of the waves to the lagoon mouth and adjacent coastline.

5. Conclusions and Future Improvements

The main goal of this work was to study the influence of the wave regime on the hydrodynamics of Ria de Aveiro inlet through the analysis of field data and numerical modeling results. With this purpose, the 2DH morphodynamic modeling system MORSYS2D has been used. This modeling system integrates, in this study, the hydrodynamic model ELCIRC and the wave model SWAN, that was successfully applied to research the integrated effect of tidal and wave effects.

The hydrodynamic model ELCIRC was previously implemented in the Ria de Aveiro by Picado [2008], in order to understand the consequences of the partial salt pans walls destruction on the entire Ria de Aveiro lagoon hydrodynamics. The bathymetry used by the author was successfully updated with a recent bathymetry data set. Picado [2008] had also developed a horizontal grid which resolution was insufficient for the present work, because the grid had insufficient resolution in the offshore zone. For that reason and taking into account the main aim of this work the existing grid was improved, refining the offshore and the inlet zone, where this work is focused.

Several model runs were performed to calibrate the numerical model, by adjusting the bottom stress in order to reduce the differences between the available data and model results. According to the final results, the model was considered successfully calibrated for a very complex system as Ria de Aveiro. The results of the calibration in the inlet should be considered excellent. In the upstream channels, the agreement between the observations and model results is smaller when compared to the calibration results in the inlet. These differences are due to several factors, such as very narrow lagoon channels that are not well resolved by the horizontal model grid, and some possible uncertainties in the field data, as well as due to possible inaccuracies in the bathymetry. The temporal discrepancy between the data and predictions is also an important factor for the higher disagreement in the upper stations of the lagoon.

Once calibrated the ELCIRC component, the 2DH morphodynamic modeling system MORSYS2D was used to understand the effect of the coastal waves in Ria de Aveiro hydrodynamics. Different scenarios were defined: scenario with the absence of waves and wind; normal wave climate scenario and high wave climate scenario. In order to achieve the main goal of this study, the sea surface elevation and current velocity were analysed for all the scenarios in study.

The results found under the wave regime forcing show that for the low wave activity scenario (normal regime) the inlet hydrodynamics is mainly dominated by the tidal forcing. For the highest wave regime are found higher sea surface elevations at the inlet induced by the wave set-up when compared with simulations performed only with tidal forcing or with the normal regime. In fact, the modelling results show that the lagoon sea level remains above offshore sea level during storm wave periods. The wave set-up found at the inlet in all the numerical results may be explained by the gathering of water in the inlet zone caused by the constant wave propagation and consequently breaking inside the Ria de Aveiro inlet. The differences are higher during ebbing and consequently in the low tide, because in this case the waves propagation and tidal currents have opposing directions. In this case there is a wave's compression, with a decrease in their wavelength and an increase in their amplitude.

The currents induced by the waves interact with the tidal currents, modifying its characteristics such as the magnitude and the direction of the predominant flow. In summary, due to wave set-up, the waves cause a slight increase of the current velocity in the inlet area.

Although the dominant forcing of the Ria de Aveiro inlet hydrodynamics is the tide, it may be concluded that the sea level and current velocity fluctuations at the Ria de Aveiro inlet depend also on the wave regime. Consequently, the storm events induce important waves set-up that change the inlet

hydrodynamics, requiring that the coupling between waves and tides should be considered to represent accurately the processes which depend on the inlet dynamics.

As mentioned in introduction chapter, this is the first study that aims to research the influence of the waves in Ria de Aveiro hydrodynamics. For that reason, this work may constitute a starting point for further studies and improvements in the study of this subject. As example, it would be interesting to study how the over-elevation at the inlet caused by the waves propagates into the lagoon.

Dias and Mariano [2011] evaluated the hydrodynamic response of Ria de Aveiro to an extension by 200 meters of the north jetty, that is being presently implemented. Based on this study, it is of crucial importance to include the combined effect of tide and waves on modelling simulations in order to understand the influence of this coastal work in the hydrodynamics of the Ria de Aveiro inlet. Another important issue to research in the future consists in performing a sensitivity analysis in order to understand which is the most important wave component (*Hs*, direction or period) that causes the wave set-up in the lagoon, as well as what will be there relevant threshold values.

As referred in the introduction chapter (Section 1.1), the economic and environmental importance of tidal inlets has been growing worldwide. The Ria de Aveiro is an unmistakable example of this due to harbouring important commercial and fishing ports, and because many social and sportive activities are concentrated in the inlet area. Thus, the improvement of the knowledge of the processes that occur in the zone is crucial to the development of the economic activities surrounding these areas, as well as to the people who live around this region and enjoy its activities.

6. References

Ahmad, I., Mohmood, I., Coelho, J.P., Pacheco, M., Santos, M.A., Duarte, A.C., Pereira, E., 2012. Role of nonenzymatic antioxidants on the bivalves' adaptation to environmental mercury: Organ-specicities and age effect in Scrobicularia plana inhabiting a contaminated lagoon. *Environmental Pollution*, **163**, 218– 225.

Aldridge, J.N., 1997. Hydrodynamics model predictions of tidal asymmetry and observed sediment transport paths in Morecambe Bay. *Estuarine, Coastal and Shelf Science*, **44**, 39-56.

Alves, F. L., Silva, J. V., Pereira, C. A., Sousa L. P., 2011. Ten Years Assessment of ICZM Principles Applied at a Local Scale: Ria de Aveiro Case Study. *Journal of Coastal Research*, **SI 64**, 1311 – 1315.

Angwenyi, C. M., Rydberg, L., 2005. Wave-driven circulation across the coral reef at bamburi Lagoon, Kenya. Estuarine, *Coastal and Shelf Science,* **63**, 447–454.

Anjum, N.A., Ahmad I., Válega, M., Pacheco, M., Figueira, E., Duarte, A.C., Pereira, E., (in press). Salt marsh macrophyte Phragmites australis strategies assessment for its dominance in mercurycontaminated coastal lagoon (Ria de Aveiro, Portugal). *Environmental Science and Pollution Research.*

Araújo, I., 2005. Sea Level Variability: Examples from Atlantic Coast of Europe. PhD Thesis, School of the National Oceanography Centre, Southampton, UK, 216 p.

Araújo, I., Dias, J.M., Pugh, D., 2008. Model simulations of tidal changes in a coastal lagoon, the Ria de Aveiro (Portugal). *Continental Shelf Research*, **28**, 1010-1025.

Arora, C., Bhaskaran, P. K., 2012. Parameterization of bottom friction under combined wave-tide action in the Hooghly estuary, India. *Ocean Engineering,* **43,** 43–55.

Bertin, B., Fortunato, A., Oliveira, A., 2009. A modeling-based analysis of processes driving wave-dominated inlets. *Continental Shelf Research*, **29**, 819–834.

Booij, N., Ris, R., Holthuijsen, L., 1999. A third-generation wave model for coastal regions. 1. Model description and validation. *Journal of Geophysical Research*, **104(7)**, 7649-7666.

Casulli, V., Cattani, E., 1994. Stability, accuracy and efficiency of a semi-implicit method for 3D shallow water flow. *Computers & Mathematics with Applications,* **27**, 99-112.

Coli, A.B., 2003. Estimação de regimes de agitação marítima em locais onde não existam dados. 3as Jornadas Portuguesas de Engenharia Costeira e Portuária. Aveiro, Portugal.

Dias, J. M., 2001. Contribution to the Study of the Ria de Aveiro Hydrodynamics. PhD thesis, University of Aveiro, Portugal, 288 p.

Dias, J. M., Fernandes, E. H., 2006. Tidal and subtidal propagation in two atlantic estuaries: Patos lagoon (Brazil) and Ria de Aveiro lagoon (Portugal). *Journal of Coastal Research*, **SI 39**, 1422 – 1426.

Dias, J.M., Lopes, J.F., 2006a. Implementation and assessment of hydrodynamic, salt and heat transport models: the case of Ria de Aveiro Lagoon (Portugal). *Environmental Modelling & Software*, **21**, 1–15.

Dias, J.M, Lopes, J.F., 2006b. Calibration and Validation of Hydrodynamic, Salt and Heat Transport Models for Ria de Aveiro Lagoon (Portugal). *Journal of Coastal Research*, **SI 39**, 1680-1684.

Dias, J.M., Mariano, S.C., 2011. Numerical modelling of hydrodynamic changes induced by a jetty extension – the case of Ria de Aveiro (Portugal). *Journal of Coastal Research*, **SI 64**, 1008-1012

Dias, J.M., Picado, A., 2011. Impact of morphologic anthropogenic and natural changes in estuarine tidal dynamics. *Journal of Coastal Research*, **SI 64**, 1490-1494.

Dias, J.M., Lopes, J.F., Dekeyser, I., 1999. Hydrological characterisation of Ria de Aveiro, Portugal, in early Summer. *Oceanologica Acta*, **22**, 473–485.

Dias, J. M., Lopes, J. F., Dekeyser, I., 2000. Tidal propagation in Ria de Aveiro lagoon, Portugal. *Phys Chem Earth (B),* **25**, 369-374.

Dias J.M., Lopes J.F., Dekeyser I., 2003. A Numerical Model System Application to the Study of the Transport Properties in Ria de Aveiro Lagoon, *Ocean Dynamics*, **53**, 220-231.

Dias, J. M., Sousa, M. C., Bertin, X., Fortunato, A. B., Oliveira, A., 2009. Numerical modeling of the impact of the Ancão Inlet relocation (Ria Formosa, Portugal). *Environmental Modelling & Software*, **24**, 711–725.

Dias, J.M., Vaz, L., Plecha, S., 2011a. Plano de Ordenamento da Orla Costeira, Caracterização Climática: Orla Costeira Ovar – Marinha Grande, Universidade de Aveiro, Aveiro, Portugal, 39 p.

Dias, J.M., Lopes, C.L., Vaz, L., Plecha, S., 2011b. Plano de Ordenamento da Orla Costeira, Caracterização da Dinâmica Costeira: Orla Costeira Ovar – Marinha Grande, Universidade de Aveiro, Aveiro, Portugal, 36 p.

Dunn, S.L., 2001. Wave set up in River entrances. PhD Thesis, Department of Civil Engineering, University of Queensland. Brisbane, Australia,191 p.

Dunn, S. L., Nielsen, P. Nielsen., Madsen, A. P., Evans, P., 2000. Wave set up in Rivers. ASCE International Conference on Coastal Engineering, Sydney, Australia, 3432–3445.

FitzGerald, D.M., 1996. Geomorphologic variability and morphodynamic and sedimentologic controls on tidal inlets. *Journal of Coastal Research*, **23**, 47–71.

Fortunato, A.B., Oliveira, A., 2004. Um modelo morfodinâmico para estuários baseado em malhas não-estruturadas. *Applied Computing Engineering Journal*, **3(2),** 87-93.

Fortunato, A. B., Pinto, L., Oliveira, A., Ferreira, J. S., 2002. Tidally generated shelf waves off the western Iberian coast. *Continental Shelf Research*, **22**, 1935-1950.

Fry, V., Aubrey, D. G., 1990. Tidal velocity asymmetries and bedload transport in shallow embayments. *Estuarine, Coastal and Shelf Science,* **30**, 453-473.

Guza, R.T., Thorton, E. B., 1981. Wave set-up on a natural beach. *Journal of Geophysical Research*, **86**, 4133–4137.

Hanslow, D. J., Nielsen, P., 1992. Wave set up on beaches and in River entrances. In: Proceedings of 23rd International Conference on Coastal Engineering, 240–252.

Hanslow, D. J., Nielsen, P., Hibbert, K., 1996. Wave set up in River entrance. In: Proceedings of 25th International Conference on Coastal Engineering, 2244–2257.

Leendertse, J. J., Gritton, E. C., 1971. A Water-Quality Simulation Model for Well-Mixed Estuaries and Coastal Seas. Volume II, Computation Procedures. Memorandum R-708-NYC. The Rand Corporation, New York, USA.

Li, M., Zhong, L., Boicourt , W. C., 2005. Simulations of Chesapeake Bay estuary: Sensitivity to turbulence mixing parameterizations and comparison with observations. *Journal of Geophysical Research*, **110**, C12004.

Longuet-Higgins, M.S., Stewart, R.W., 1964. Radiation stress in water waves; a physical discussion, with applications. *Deep-Sea Research*, **11**, 529-562.

Lopes, C., 2009. Impacts of sea level rise in Ria de Aveiro lagoon during 21st century. MSc Thesis, Physical Department, University of Aveiro, 48 pp.

Lopes, J. F., Dias, J. M., Dekeyser, I. 2006. Numerical modelling of cohesive sediments transport in the Ria de Aveiro lagoo, Portugal. *Journal of Hydrology*, **319**, 176-198.

Lopes, J. F., Almeida M. A., Cunha M. A., 2010. Modelling the ecological patterns of a temperate lagoon in a very wet spring season. *Ecological Modelling*, **221**, 2302-2322.

Lopes, C.L., Silva, P., Dias, J.M., Rocha, A., Picado, A., Plecha, S., Fortunato, A.B., 2011a. Local sea level changes scenarios for the end of the 21st century and potential physical impacts in the lower Ria de Aveiro (Portugal). *Continental Shelf Research*, **31**, 1515-1526.

Lopes, C.L., Silva, P.A., Rocha, A., Dias, J.M., 2011b. Sensitivity analysis of Ria de Aveiro hydro-morphodynamics to the sea level rise integration period. *Journal of Coastal Research*, **SI 64**, 230-234.

Malhadas, M. S., Leitão, P. C., Silva, A., Neves, R., 2009. Effect of coastal waves on sea level in Óbidos Lagoon, Portugal. *Continental Shelf Research*, **29**, 1240–1250.

Mendes, R., 2010. Numerical modeling of the Ria de Aveiro plume: a preliminary study. MSc Thesis, Physical Department, University of Aveiro, 50 pp.

Mendes, R., Vaz, N., Dias, J.M., 2011. Numerical modeling changes induced by the low lying areas adjacent to Ria de Aveiro. *Journal of Coastal Research*, **SI 64**, 1125.1129.

Miranda, L. B., Castro, B. M., Kjerfve, B., 2002. Princípios de Oceanografia Física de Estuários. *Edusp – Editora da Universidade de São Paulo,* 424 pp.

Moreira, M. H., Queiroga, H., Machado, M. M., Cunha, M. R., 1993. Environmental gradients in a southern estuarine system: Ria de Aveiro, Portugal, implication for soft bottom macrofauna colonization. *Netherland Journal of Aquatic Ecology*, **27 (2-4)**, 465–482.

Morgado, F., Queiroga, H., Melo, F., Sorbe, J. C., 2003. Zooplankton abundance in a coastal station of the Ria de Aveiro inlet (north-western Portugal): relations with tidal and day/night cycles. *Acta Oceanologica,* **24**, 175-181.

Nguyen, X., Tanaka, H., Nagabayashi, H., 2007. Wave set up at River and Inlet Entrances Due to an Extreme Event. To appear in Proceedings of International Conference on Violent Flows, Kyushu University, Fukuoka, Japan.

Nielsen, C., Apelt, C. ,2003. The application of wave induced forces to two- dimensional finite element long wave hydrodynamic model. *Ocean Engineering*, **30**, 1233–1251.

Oliveira, A., Fortunato, A. B., Rego, J. R. L., 2006a. Effect of morphological changes on the hydrodynamics and flushing properties of the Óbidos lagoon (Portugal). *Continental Shelf Research*, **26(8)**, 917–942.

Oliveira, A., Fortunato, A. B., Dias, J. M., 2006b. Numerical modelling of the Aveiro inlet dynamics. *Coastal Engineering*, 3282-3294.

Oshiyama, S., Lee, H., Tanaka, H., 2001. Fluctuation characteristics of water level in medium-and small scale River mouths. In:Proceedings of 25th International Conference on Coastal Engineering, JSCE, Vol.48, 411–415 pp.

Pawlowicz, R., Beardsley, B., Lentz, S., 2002. Classical tidal harmonic analysis including error estimates in MATLAB using T_TIDE. *Computers and Geosciences*, **28**, 929–937.

Pereira, C., Salvador S., Arrojado C., Silva Y.J., Santos A.L., Cunha A., Gomes N.C.M., Almeida A., 2011. Evaluating seasonal dynamics of bacterial communities in marine fish aquaculture: a preliminary study before applying phage therapy. *Journal of Environmental Monitoring*, **13** (4), 1053 – 1058.

Phillips, O.M., 1977. The Dynamics of the Upper Ocean. 2nd ed, Cambridge University Press.

Picado, A., 2008. Degradation of the salt pans in Ria de Aveiro: An Hydrodynamical Study. MSc Thesis, Physical Department, University of Aveiro, 50 pp.

Picado, A., Dias, J.M., Fortunato, A. B., 2010. Tidal changes in estuarine systems induced by local geomorphologic modifications. *Continental Shelf Research*, **30**, 17, 1854-1864.

Picado, A., Silva, P.A., Fortunato, A.B., Dias, J.M., 2011. Particle tracking-modeling of morphologic changes in the Ria de Aveiro. *Journal of Coastal Research*, **SI 64**, 1560-1564.

Plecha, S., 2011. Contribution to the Study of the Ria de Aveiro Inlet Morphodynamics. pHD Thesis, Physical Department, University of Aveiro, 163 pp.

Plecha, S., Silva, P.A., Oliveira, A., Dias, J.M., 2011. Evaluation of single waves effects on the morphology evolution of a coastal lagoon inlet. *Journal of Coastal Research*, **SI 64**, 1155-1159.

Plecha, S., Silva, P.A., Oliveira, A., Dias, J.M., 2012. Establishing the Wave Climate Influence on the Morphodynamics of a Coastal Lagoon Inlet. *Ocean Dynamics*, **62**, 799-814.

Pires, H. N. O., 1985. Alguns aspectos do clima de agitação marítima de interesse para a navegação na costa de Portugal. *O Clima de Portugal*, **37**, 34 pp.

Pires, A., Quintino V., Gentil F., Freitas R., Rodrigues A.M., (in press). Reproductive biology of a brooding Diopatra species: Diopatra marocensis. *Estuarine, Coastal and Shelf Science*.

Prandle, D., 1982. The vertical structure of tidal currents and other oscillatory flows. *Continental Shelf Research*, **2**, 191–207.

Pugh, D.T., 1996. Tides, Surges and Mean Sea-Level (reprinted with corrections). John Wiley & Sons Ltd, Chichester, UK, 486 pp.

Short, A. D., 2007. Beaches of the New South Wales coast: a guide to their nature, characteristics, surf and safety. 2nd ed. Sydney University Press, Sydney, 398p.

Silva J., Duck R.W., 2001. Historical changes of bottom topography and tidal amplitude in the Ria de Aveiro, Portugal - trends for future evolution. *Climate Research*, **18**, 17-24.

Tanaka, H., Nagabayashi, H., Yamauchi, K., 2000.Observations of wave set-up height in a River mouth. In: Proceedings of 27th International Conference on Coastal Engineering, 3458–3471 pp.

Tanaka, H., Lee, H. S., Furumichi, K., 2003.Influence of morphological change on water level rise at the Shiribetsu River mouth. *Journal of Hydroscience and Hydraulic Engineering*, **21(1)**, 71–78.

Teixeira, S., 1994. Dinâmica Morfossedimentar da Ria de Aveiro (Portugal). PhD Thesis. Faculdade de Ciências da Universidade de Lisboa, Portugal, 397 p.

Troussellier, M., Gattuso, JP., 2007. Coastal Lagoons. In:Encyclopedia of Earth. Eds. Cutler J. Cleveland Washington, D.C.: Environmental Information Coalition, National Council for Science and the Environment.

Vaz, N., 2007. Study of heat and salt transport processes in the Espinheiro Channel (Ria de Aveiro). PhD Thesis, Physical Department, University of Aveiro, Portugal, 151 pp.

Vaz, N., Dias, J.M., 2008. Hydrographic characterization of an estuarine tidal channel. *Journal of Marine Systems*, **70**, 168-181.

Vaz, N., Dias, J. M., Leitão, P., Martins, I., 2005. Horizontal patterns of water temperature and salinity in an estuarine tidal channel: Ria de Aveiro. *Ocean Dynamics*, **55**, 416-429.

Vaz, N., Dias, J. M., Leitão, P. C., Nolasco, R., 2007. Application of the Mohid-2D model to a mesotidal temperate coastal lagoon. *Computers & Geosciences*, **33**, 1204-1209.

Vila-Concejo, A., Hughes, M. G., Short, A. D., Ranasinghe, R., 2010. Estuarine shoreline processes in a dynamic low energy system. *Ocean Dynamics*, **60**, 285-298.

Vitorino, J., Oliveira, A., Jouanneau, J.M., Drago, T., 2002. Winter dynamics on the northern Portuguese shelf. Part 1: physical processes. *Progress in Oceanography*, **52**, 129–153.

Warner, J. C., Geyer, W. R., Lerczak, J. A., 2005. Numerical modelling of an estuary: a comprehensive skill assessment. *Journal of Geophysical Research*, **110**, C05001.

Wilmott, C.J., 1981. On the validation of models. *Physical Geography*, **2**, 184–194.

Zang, Y., Baptista, A., Meyers, E., 2004. A cross-scale model for 3D baroclinic circulation in estuary-plume-shelf systems: I. Formulation and skill assessment. *Continental Shelf Research*, **24**, 2187-2214.